Neuroscience

Specific presynaptic functions require distinct Drosophila Ca_V2 splice isoforms

Reviewed Preprint
v2 • January 6, 2025
Revised by authors

Reviewed Preprint
v1 • August 14, 2024

Christopher Bell, Lukas Kilo, Daniel Gottschalk, Jashar Arian, Lea Deneke, Hanna Kern, Christof Rickert, Oliver Kobler, Julia Strauß, Martin Heine, Carsten Duch, Stefanie Ryglewski

Johannes Gutenberg University Mainz, Institute of Developmental Biology and Neurobiology, Biocenter 1, Mainz, Germany • RWTH Aachen University, Aachen, Germany • Leibniz Institute for Neurobiology Magdeburg, Combinatorial NeuroImaging Core Facility, Magdeburg, Germany

eLife Assessment

Cav2 voltage-gated calcium channels play key roles in regulating synaptic strength and plasticity. In contrast to mammals, invertebrates like Drosophila encode a single Cav2 channel, raising questions on how diversity in Cav2 is achieved from a single gene. Here, the authors present **solid** evidence that two alternatively spliced Cac isoforms enable **important** changes in Cav2 expression, localization, and function in synaptic transmission and plasticity at the Drosophila neuromuscular junction. How the isoforms affect synaptic calcium channel levels remains less clear. This study provides insights into the roles of voltage-gated calcium channel splice isoforms in synaptic transmission.

https://doi.org/10.7554/eLife.100394.2.sa3

Abstract

The multiplicity of neural circuits that accommodate the sheer infinite number of computations conducted by brains requires diverse synapse and neuron types. At many vertebrate synapses release probability and other aspects of presynaptic function are tuned by different combinations of $Ca_V2.1$, $Ca_V2.2$, and $Ca_V2.3$ channels. By contrast, most invertebrate genomes contain only one *Ca_V2* gene. The one Drosophila Ca_V2 homolog, cacophony (cac), localizes to presynaptic active zones (AZs) to induce synaptic vesicle release. We hypothesize that Drosophila cac functional diversity is enhanced by two specific exon pairs that are mutually exclusively spliced and not conserved in vertebrates, one in the voltage sensor and one in the intracellular loop containing the binding site(s) for Ca_β and G-protein βγ subunits. We test our hypothesis by combining opto– and electrophysiological with neuroanatomical approaches at a fast glutamatergic model synapse, the Drosophila larval neuromuscular junction. We find that alternative splicing in the voltage sensor affects channel activation voltage and is imperative for normal synapse function. Only the isoform with the higher activation voltage localizes to the presynaptic AZ and mediates evoked release. Removal of these cac splice isoforms renders fast glutamatergic synapses non-functional. By contrast, alternative splicing at the other alternative exon that encodes the

intracellular loop between the first and the second homologous repeats does not affect cac presynaptic AZ localization, but it tunes multiple aspects of presynaptic function. While expression of one exon yields normal transmission, expression of the other exon reduces channel number in the AZ and thus release probability. This also abolishes presynaptic homeostatic plasticity. Moreover, reduced channel number upon selective exon excision increases paired pulse ratios and the variability of synaptic depression during low frequency stimulation trains (1 and 10 Hz), and thus affects short term plasticity. Effects on short term plasticity can be rescued by increasing the external calcium concentration to match release probability to control. In sum, in Drosophila alternative splicing provides a mechanism to regulate different aspects of presynaptic functions with only one *Ca_V2* gene.

Introduction

Information transfer at fast chemical synapses requires action potential triggered calcium influx through voltage gated calcium channels (VGCCs) into the presynaptic terminal, which in turn initiates synaptic vesicle (SV) release through a complex cascade of biophysical and biochemical reactions (Südhof 2013; 2014; Dittman, Ryan 2019). The millisecond temporal precision of SV release upon the arrival of an action potential in the axon terminal requires clustering of the VGCCs in a spatially restricted presynaptic specialization, named the presynaptic active zone (AZ; Eggermann et al. 2011; Südhof 2012; Van Vactor, Sigrist 2017; Dolphin, Lee 2020; Emperador-Melero, Kaeser 2020). At the AZ, protein-protein interactions ensure a nanoscale coupling of VGCCs to SVs in the readily releasable pool (Kittel et al. 2006), an arrangement that supports efficient and fast neurotransmission (Eggermann et al. 2011).

Despite these common organizational principles, fast chemical synapses are highly heterogeneous to accommodate the diverse computational requirements of different types of neurons and brain circuits (Moser et al. 2023; Zhang et al. 2022). One means of synapse diversification is to organize VGCCs heterogeneously at the AZ to modify either their nanoscale spatial relation to the SVs ready for release (Dittman, Ryan, 2019; Rebola et al. 2019), or the profiles of the calcium dynamics that shape release probability (P_r; Zhang et al. 2022). The calcium dynamics in nano- or microdomains are affected by VGCC number, clustering, and properties, and are thus strongly dependent on calcium channel subtype.

The vertebrate genome contains 10 genes encoding the α_1-subunit of VGCCs that fall into three families (Ca_V1, Ca_V2, Ca_V3; Dolphin, 2009). With the exception of Ca_V1 triggering release at retinal ribbon and auditory brain stem synapses (Moser et al. 2020), Ca_V2 usually mediates evoked release at other mammalian synapses. The three subtypes of Ca_V2 exhibit different biophysical properties (Sheng et al. 2012), which may explain their different contribution to SV release at a given synapse (Li et al. 2007). $Ca_V2.1$ and $Ca_V2.2$ trigger SV release at most synapses and $Ca_V2.3$ likely make only a small contribution (Dietrich et al. 2003). However, all three Ca_V2 subtypes may co-localize to the same synapse and contribute to SV release (Takahashi, Momiyama 1993; Wheeler et al. 1994; Wu et al. 1998), and different types of mammalian synapses can utilize either only one subtype or combinations of Ca_V2 subtypes (reviewed in Zhang et al. 2022).

The Drosophila genome contains only 3 genes encoding α_1-subunits of VGCCs, each one homologous to one vertebrate Ca_V family (Littleton, Genetzky 2000). Therefore, the joint functions of mammalian $Ca_V2.1$, $Ca_V2.2$, and $Ca_V2.3$ are covered by only one Drosophila gene, namely *Dmca1A* (also named *cacophony* or *nightblindA*, Smith et al. 1996; 1998). Cacophony (cac) is, in fact, essential for fast synaptic transmission in Drosophila (Kawasaki et al. 2002) and loss of cac cannot be compensated for by the Drosophila counterparts of Ca_V1 or Ca_V3 (Krick et al. 2021). This suggests that Drosophila lacks the combinatorial logic of employing different blends of $Ca_V2.1$, $Ca_V2.2$, and $Ca_V2.3$ for fine-tuning of P_r as present in mammals. However, the Drosophila

cac locus contains two mutually exclusive alternative splice sites that are not present in the vertebrate Ca_v2 gene family, one in the voltage sensor in the fourth transmembrane domain of the first homologous repeat (IS4) and one in the intracellular linker between the first and the second homologous repeats (I-II). Alternative splicing at these mutually exclusive sites may provide mechanisms to fine tune action potential triggered calcium dynamics at presynaptic AZs by adjusting the numbers, nanoscale localization and properties of presynaptic cacophony VGCCs. We test this hypothesis by employing the CRISPR-Cas9 technology to remove mutually exclusive exons at either the *IS4* or the *I-II* site and test the resulting functional consequences at the Drosophila neuromuscular junction (NMJ), a well-established model for presynaptic function of a fast glutamatergic synapse (Atwood, Karunanithi 2002; Harris, Littleton 2015).

We find that alternative splicing at the *IS4* site affects cac voltage activation and only one of both mutually exclusive splice events allows for presynaptic AZ localization and thus evoked synaptic transmission at a fast glutamatergic synapse. By contrast, alternative splicing at the *I-II* site does not affect presynaptic AZ localization, but it affects P_r, short term plasticity, and presynaptic homeostatic plasticity.

Results

Cacophony (*cac*) is located on the X-chromosome and contains multiple alternative splice sites but only two that are mutually exclusive (**Fig. 1A**, see also enlarged schematic of the cac regions housing these two mutually exclusive exon pairs (green boxes); cac schematic in **Fig. 1B**). The first one is located in the fourth transmembrane domain of the first homologous repeat (IS4), and thus affects the voltage sensor. Both alternative *IS4* exons are 99 bp long and encode 33 amino acids (AAs). The polypeptide encoded by *IS4A* (first alternative exon of the *IS4* locus) differs from that of *IS4B* in 13 AAs and contains one additional positively charged AA. The second mutually exclusive exon pair encodes part of the intracellular linker between homologous repeats I and II (*I-II*; **Fig. 1B**), and is thus predicted to affect binding sites for calcium channel β subunits (Ca_β) and G-protein βγ subunits ($G_{\beta\gamma}$). Both alternative *I-II* exons are 117 bp long and encode 39 AAs. The polypeptide encoded by *I-IIA* (first alternative exon of the *I-II* locus) differs from that of *I-IIB* in 23 AAs. Sequence analysis strongly suggests that I-IIB contains both, a Ca_β as well as a $G_{\beta\gamma}$ binding site (AID: α-interacting domain) because the binding motif QXXER is present. In mouse $Ca_v2.1$ and $Ca_v2.2$ channels the sequence is QQIER, while in Drosophila cacophony I-IIB it is QQLER. In the alternative I-II linker I-IIA, this motif is not present, strongly suggesting that $G_{\beta\gamma}$ subunits cannot interact at the AID. However, as already suggested by Smith et al. (1998), also based on sequence analysis, Ca_β should still be able to bind, although possibly with a lower affinity. We employ CRISPR-Cas9 to excise one of both alternative exons either at the *IS4* or the *I-II* loci (**Fig. 1C**). Genomic removal of *IS4A* results in fly strains that contain only the *IS4B* exon and are named *ΔIS4A* (**Fig. 1C**). Accordingly, genomic removal of the *I-IIA* exon results in flies with *I-IIB* only that are named *ΔI-IIA* (**Fig. 1C**). To analyze the functions of mutually exclusive exon variants, we create exon-out fly strains with removal of one exon at a time of each of the four exons (*IS4A*, *IS4B*, *I-IIA*, *I-IIB*). Excision of the respective exon is always confirmed by sequencing (see methods). Fly strains with first chromosomes that carry exon excisions are cantonized by 10 generations of backcrossing into Canton S wildtype flies. Exon-out strains are produced from either wildtype (Canton S) or white mutant flies (w^{1118}, see methods) as well as from fly strains with previously introduced N-terminal fluorophore tagging of the *cac* gene (Gratz et al. 2019). Neither on-locus super folder GFP (sfGFP) tagging, nor on-locus tagging of the endogenous cacophony channel with mEOS4b (Ghelani et al. 2023) impairs cac localization at presynaptic AZs or synaptic function at the larval Drosophila NMJ. In this study, sfGFP-tagged (**Fig. 1B**) exon-variants serve analysis of channel localization and mEOS4b tagged (**Fig. 1B**) ones serve to count channel number in AZs, and untagged fly strains serve to control for possible effects of the fluorescent tags.

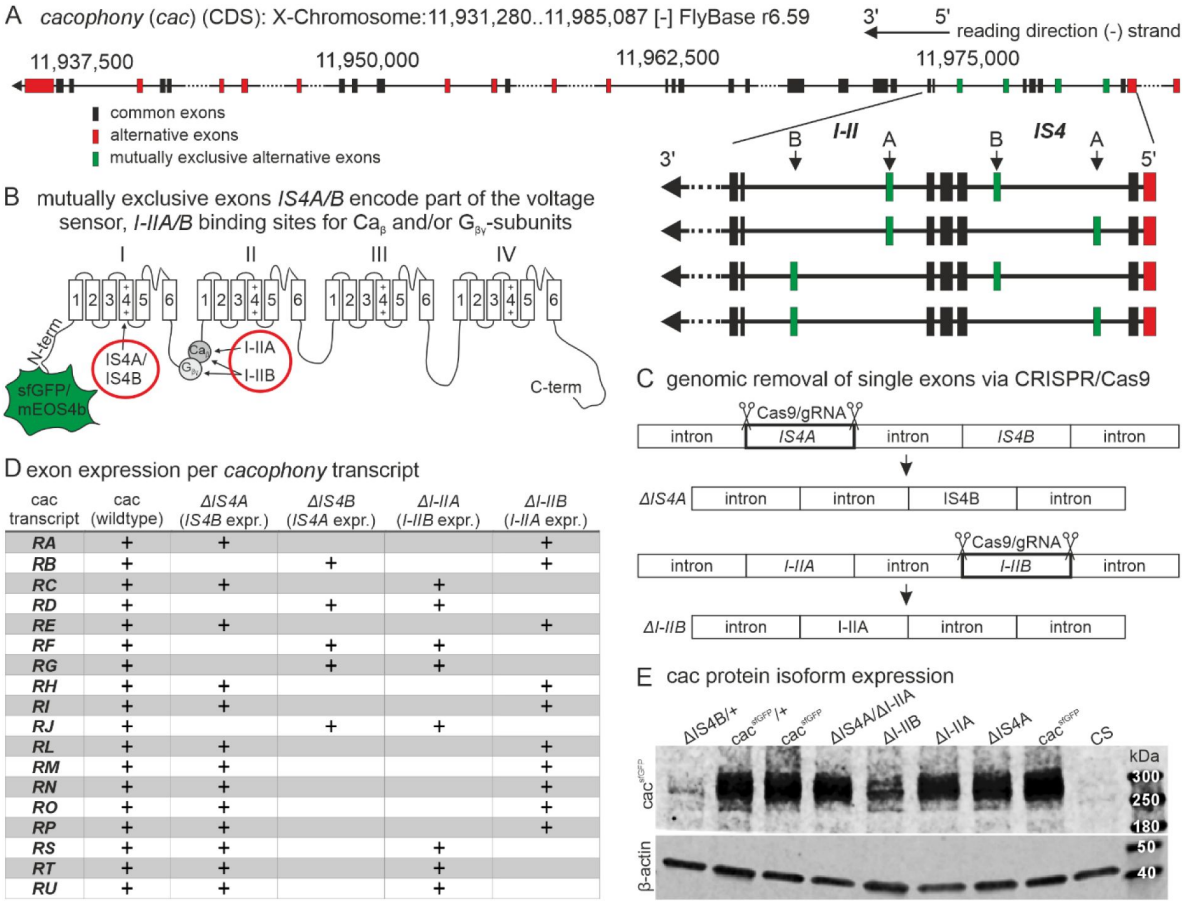

cac transcript	cac (wildtype)	ΔIS4A (IS4B expr.)	ΔIS4B (IS4A expr.)	ΔI-IIA (I-IIB expr.)	ΔI-IIB (I-IIA expr.)
RA	+	+			+
RB	+		+		+
RC	+	+		+	
RD	+		+	+	
RE	+	+			+
RF	+		+	+	
RG	+		+	+	
RH	+	+			+
RI	+	+			+
RJ	+		+	+	
RL	+	+			+
RM	+	+			+
RN	+	+			+
RO	+	+			+
RP	+	+			+
RS	+	+		+	
RT	+	+		+	
RU	+	+		+	

Figure 1.

Cacophony alternative splicing gives rise to different protein isoforms.

(A) *Cacophony* is located on the non-coding strand of the X-chromosome between positions 11,931,280 and 11,985,087 (Flybase version r6.59). Reading direction is indicated on the top right (arrow). Horizontal black lines indicate introns, larger introns are broken by dots. Black boxes indicate exons shared by all *cacophony* splice variants, red boxes indicate alternative exons, green boxes represent exons that are mutually exclusively spliced. Enlarged area on the right emphasizes mutually exclusive exon pairs *IS4A/B* and *I-IIA/B*. **(B)** Schematic of cacophony with N-terminal sfGFP or mEOS4b tag and two exon pairs that are spliced mutually exclusively. *IS4A* and *IS4B* exons encode isoforms of the 4th transmembrane domain (S4) and thus part of the voltage sensor of the first homologous repeat (I) of the calcium channel, while *I-IIA* and *I-IIB* give rise to two versions of the intracellular linker between homologous repeats I and II. I-IIA contains a non-well conserved binding site for voltage gated calcium channel β-subunits (Ca_β) whereas I-IIB gives rise to a conserved Ca_β-binding site as well as a binding site for G-protein βγ-subunits ($G_{\beta\gamma}$). **(B)** Genomic removal of one of the mutually exclusively spliced exons of one or two exon pairs by CRISPR/Cas9 mediated double strand breaks in the germ line results in exon out mutants by imprecise excision of the cut exons and cell-intrinsic DNA repair. **(C)** *Cacophony* gives rise to 18 annotated transcripts (RA-RU, left). Multiple variants express the same mutually exclusive exons but differ with respect to expression of other alternatively spliced but not mutually exclusive exons. Removal of the mutually exclusive exons *IS4A/IS4B* and/or *I-IIA/I-IIB* allows expression of fewer *cacophony* splice variants. Transcript variants that are possible upon exon excision are marked by +. **(D)** Western Blots reveal expression of GFP-tagged cacophony protein (cac^{sfGFP}) for all excision variants at the expected band size of ~240 kDa (cacophony) plus ~30 kDa (sfGFP, top), while no band can be detected in the Canton S wildtype (CS, top, right) that does not express cac^{sfGFP}. 10 adult brains were used of hemizygous males for all genotypes except for *ΔIS4B* which is homo-/hemizygous lethal. For *ΔIS4B* 20 brains of heterozygous females and a heterozygous cac^{sfGFP} control were used (F1 females from cross with Canton S wildtype flies(+)). β-actin was used as loading control (bottom). *ΔIS4B* shows weak expression (top, left), while all other exon out variants express strongly, although *ΔI-IIB* shows somewhat weaker expression (top, middle).

Of the 18 annotated *cacophony* transcripts in Drosophila (Flybase, r6.59), 13 remain upon removal of *IS4A*, 5 upon removal of *IS4B*, 8 upon removal of *I-IIA*, and 10 upon removal of *I-IIB* (**Fig. 1D**). For each mutually exclusive exon, we have created multiple exon-out fly strains. Each exon removal induces reproducible phenotypes (see methods). Removal of *IS4B* is embryonic lethal as confirmed in all CRISPR-Cas9 mediated excisions (n=12), both before and after crossing out into a wildtype background. Removal of each of the three other mutually exclusive exons results in viable fly strains, Drosophila larvae without any obvious deficits, before and after crossing out into a wildtype background, but with distinct behavioral phenotypes in adult flies (the latter are not further addressed in this study). Western blots with GFP tagged cac channels test whether the channel protein is expressed in the CNS of all exon-out fly strains (**Fig. 1E**). *ΔIS4B* flies are homozygous lethal and are thus used heterozygously over untagged wildtype channels that contain all exons for Western blot analysis. Brain homogenate from sfGFP tagged controls and from all exon-out fly strains with sfGFP tagged cac channels yield a band at roughly the expected size of 250-270 kDa (Drosophila cac isoforms range from 212 to 242 kDa and sfGFP is 27 kDa), whereas no band is detected in control brains without tagged cac (**Fig. 1E**, right lane). Protein level in *ΔIS4B* flies (first band from left, **Fig. 1E**) is lower as compared to heterozygous controls with all isoforms (second band from left, **Fig. 1E**). Similarly, protein level in *ΔI-IIB* flies (fifth band from left, **Fig. 1E**) is lower as compared to homozygous controls with all isoforms (third and eighth band from left, **Fig. 1E**), thus indicating that cac isoforms containing IS4B and I-IIB are normally abundantly expressed. By contrast, homozygous removal of *IS4A* or of *I-IIA* does not cause obvious differences in expression levels as compared to homozygous sfGFP tagged controls (**Fig. 1E**). Taken together, CRISPR-Cas9 is successfully employed to produce all possible distinct exon excisions at the mutually exclusive splice sites of Drosophila *cacophony*. This now allows for analysis of *cac* exon specific functions.

We next analyze the functional consequences of the removal of each of the mutually exclusive exons at the *IS4* and at the *I-II* loci for cac channel localization, channel number, and channel function at motoneuron presynaptic terminals of the larval Drosophila neuromuscular junction (NMJ).

IS4B localizes to presynaptic active zones and is required for evoked synaptic transmission

Drosophila cac channels interact with the scaffold protein bruchpilot (brp) to localize to presynaptic AZs (Kittel et al. 2006; Ghelani et al. 2023). Immunohistochemical triple label at the larval Drosophila NMJ tests whether either one of the mutually exclusive exons at the *IS4* locus is required for correct presynaptic cac localization. On the level of CLSM, we define correct cac localization in presynaptic AZs at the larval NMJ as cac puncta that overlap with brp puncta but no cac label anywhere else in the presynaptic bouton. Motoneuron axon terminals on larval muscles 6 and 7 (M6/7) are labeled with HRP (**Figs. 2A-C**, right column, blue), cac^{sfGFP} by α-GFP immunolabel (**Figs. 2A-C**, left column, green), and AZs by α-brp immunohistochemistry (**Figs. 2A-C**, second column, magenta). For a better visualization of label in AZs, **figures 2Ai**-Ci show selective enlargements of single boutons with all labels. In controls, cac^{sfGFP} channels with full isoform diversity strictly co-localize with brp in presynaptic AZs (**Fig. 2A**, cac and brp overlay, 3rd column) as previously reported (Gratz et al. 2019). The same is the case for cac channels that contain IS4B but lack IS4A *(ΔIS4A*, **Fig. 2B**). By contrast, cac channels that contain IS4A but lack IS4B (*ΔIS4B*) do not localize to presynaptic AZs (**Fig. 2C**). On the level of CLS microscopy we define strict AZ localization as cac puncta clearly overlapping with brp puncta but no cac label anywhere else in the synaptic bouton. Importantly, upon excision of *IS4B*, cac channels are not only absent from AZs, but immunolabel for tagged IS4A channels cannot be detected above background anywhere in the axon terminals (**Fig. 2Ci**, see also below **Fig. 3A**, bottom). Since *ΔIS4B* is homozygous lethal, heterozygous animals are used for triple labels of tagged IS4A channels, the AZ marker brp, and motoneuron terminals on M6/7. Axon terminal shape and brp label in AZs are qualitatively normal, but the label for cac^{IS4A} (=*ΔIS4B*) channels is absent (**Fig.**

2Ci). Accordingly, the Pearson's correlation coefficient of IS4A and brp is ~0.2 (**Fig. 2D**), which is considered negligible (Mukaka 2012), whereas cac and IS4B (=*ΔIS4A*) channels show a significant Pearson's correlation coefficient as previously reported for controls (Krick et al. 2021). In addition, quantification of brp labeling intensity did not show any difference between genotypes, not even in the absence of cac upon excision of *IS4B* (data not shown). These data indicate that the *IS4B* exon is required for targeting/localizing cac channels within the AZ.

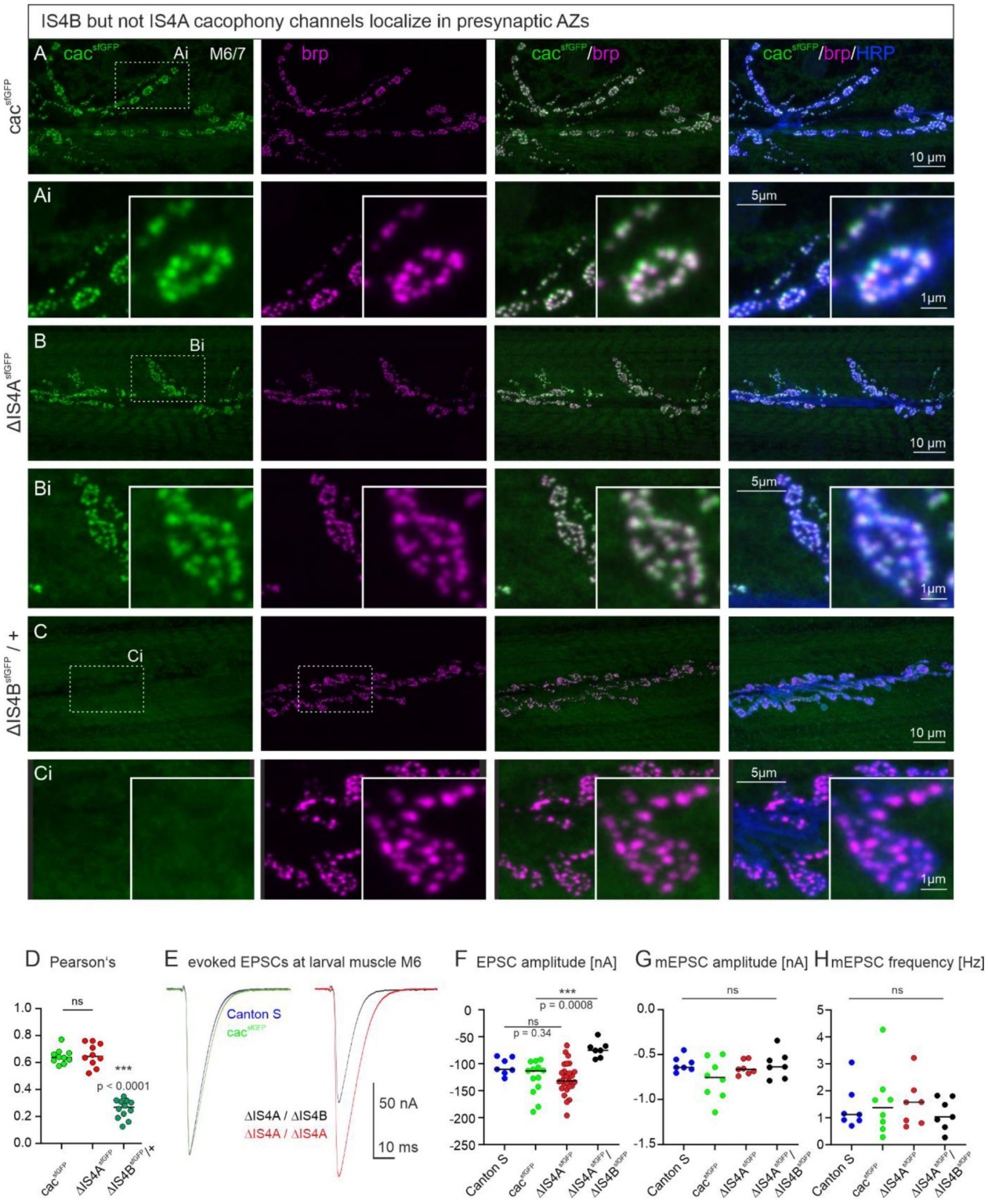
IS4B but not IS4A cacophony channels localize in presynaptic AZs
A cacsfGFP Ai M6/7
brp
cacsfGFP/brp
cacsfGFP/brp/HRP
10 µm
Ai
5µm
1µm
B Bi
ΔIS4AsfGFP
10 µm
Bi
5µm
1µm
C Ci
ΔIS4BsfGFP / +
10 µm
Ci
5µm
1µm
D Pearson's
ns
***
p < 0.0001
cacsfGFP
ΔIS4AsfGFP
ΔIS4BsfGFP/+
E evoked EPSCs at larval muscle M6
Canton S
cacsfGFP
ΔIS4A / ΔIS4B
ΔIS4A / ΔIS4A
50 nA
10 ms
F EPSC amplitude [nA]
***
p = 0.0008
ns
p = 0.34
Canton S
cacsfGFP
ΔIS4AsfGFP
ΔIS4AsfGFP/ ΔIS4BsfGFP
G mEPSC amplitude [nA]
ns
H mEPSC frequency [Hz]
ns

Figure 2.

The IS4B exon is required for cacophony localization to AZs and for evoked synaptic transmission.

(A-C) Representative confocal projection views of triple labels for GFP tagged cac channels (green), the AZ marker brp (magenta), and HRP to label axonal membrane (blue) as well as enlargements of the area marked by dotted rectangles (Ai-Ci). Label was done in control animals with all cac exons (cac^{sfGFP}, top row, **A, Ai**), in animals with selective excision of either the alternative exon *IS4A* ($\Delta IS4A^{sfGFP}$, middle rows, **B, Bi**), or the alternative exon *IS4B* ($\Delta IS4B^{sfGFP}$, bottom row, **C, Ci**). Excision of *IS4B* is embryonic lethal, so that localization analysis was conducted in heterozygous animals ($\Delta IS4B^{sfGFP}$/+). The gross morphology of the neuromuscular junctions (muscle fibers, bouton numbers and sizes, AZ numbers) was similar in all three genotypes. GFP tagged cac channels localize to AZs **(A, Ai)** as previously reported (Gratz et al. 2019; Krick et al. 2021). Excision of the *IS4A* exon does neither impact cac AZ localization nor labeling intensity **(B, Bi)**. By contrast, upon excision of the *IS4B* exon, no cac label is detected **(C, Ci)**. **(D)** Pearson's correlation analysis of cac and brp in cac^{sfGFP} (green), *ΔIS4A* (red), and heterozygous *ΔIS4B* (dark green) animals reveals correlation coefficients of ~0.6 for cac^{sfGFP} and *ΔIS4A* but not for *ΔIS4B* (Pearson's correlation coefficient ~0.26, which is significantly different from cac^{sfGFP} control ($p<0.001$, ANOVA with Dunnett's post hoc test, comparison only against control) and considered negligible. This is in line with absent label in *ΔIS4B* animals (C, Ci). **(E, F)** Representative traces of evoked synaptic transmission as recorded in TEVC from muscle fiber 6 upon extracellular stimulation of the motor nerve from a wildtype control animal (CS, blue), an animal cac^{sfGFP} (green), and animals with cac^{sfGFP} and either *IS4A* exon excision (*ΔISA4*, red) or transheterozygous female animals with *IS4B* excision over *IS4A* excision (*ΔISAB/ΔISA4*, black). **(E)** Excitatory postsynaptic currents (EPSCs) are similarly shaped between CS control (blue) and animals expressing cac^{sfGFP} (green), and **(F)** EPSC amplitudes are not statistically different ($p=0.34$, two sided Tukey's multiple comparison test). In animals with homozygous *IS4A* exon excision (red), EPSC amplitude is slightly but not significantly increased ($p=0.18$, two sided Tukey's multiple comparison test). In transheterozygous animals with *IS4A* excision on one chromosome and *IS4B* excision on the other one, EPSC amplitude is significantly decreased ($p=0.0008$), two sided Tukey's multiple comparison test). **(G)** Quantal size (mEPSC amplitude) and spontaneous release frequency **(H)** show no significant difference between genotypes.

Previous studies showed that presynaptic cac channels are required for normal evoked synaptic transmission at the Drosophila NMJ (Kawasaki et al. 2002). Reduced cac label in presynaptic AZs goes along with reduced synaptic transmission (Kittel et al. 2006), whereas increased cac channel numbers during presynaptic homeostatic plasticity are effective to increase mean quantal content (Ghelani et al. 2023; Medeiros et al. 2024). If cac presynaptic AZ localization requires *IS4B* but not the *IS4A* exon, removal of *IS4B* but not *IS4A* should impair evoked synaptic transmission. Two electrode voltage clamp recordings from larval muscle 6 in abdominal segment 3 indicate that excitatory postsynaptic currents (EPSCs) as evoked by single presynaptic action potentials are similar in wildtype (Canton S, **Figs. 2E**, F, blue) and in animals with sfGFP tagged cac channels (**Figs. 2E**, F, green). Upon removal of *IS4A*, EPSC amplitude is slightly but not significantly increased (**Fig. 2E, F**, *ΔIS4A*, red). In transheterozygous animals (*ΔIS4B/ΔIS4A*) with removal of *IS4A* on one chromosome and *IS4B* on the other, EPSC amplitude is significantly reduced (**Figs. 2E**, F, black). Spontaneous synaptic vesicle (SV) release as characterized by the amplitude (**Fig. 2G**) and the frequency (**Fig. 2H**) of miniature excitatory postsynaptic currents (mEPSCs) is not affected in *ΔIS4B/ΔIS4A* transheterozygotes. Together, these data indicate that *IS4A* is neither required for AZ localization of channels, nor for evoked synaptic transmission, whereas *IS4B* is required for normal AZ localization and synaptic transmission.

A limitation of these experiments is that homozygous removal of *IS4B* is embryonic lethal, so that presynaptic terminals that are devoid of cac^{IS4B} channels can only be studied in mosaic animals that are heterozygous for *IS4B* excision at most synapses but hemizygous *ΔIS4B* at few synapses of interest. Employing the FlpStop method (see methods, Fisher et al. 2017), mosaic animals with motoneurons to muscle 12 (M12) that are *ΔIS4B*/cac^{null} can be produced in otherwise heterozygous

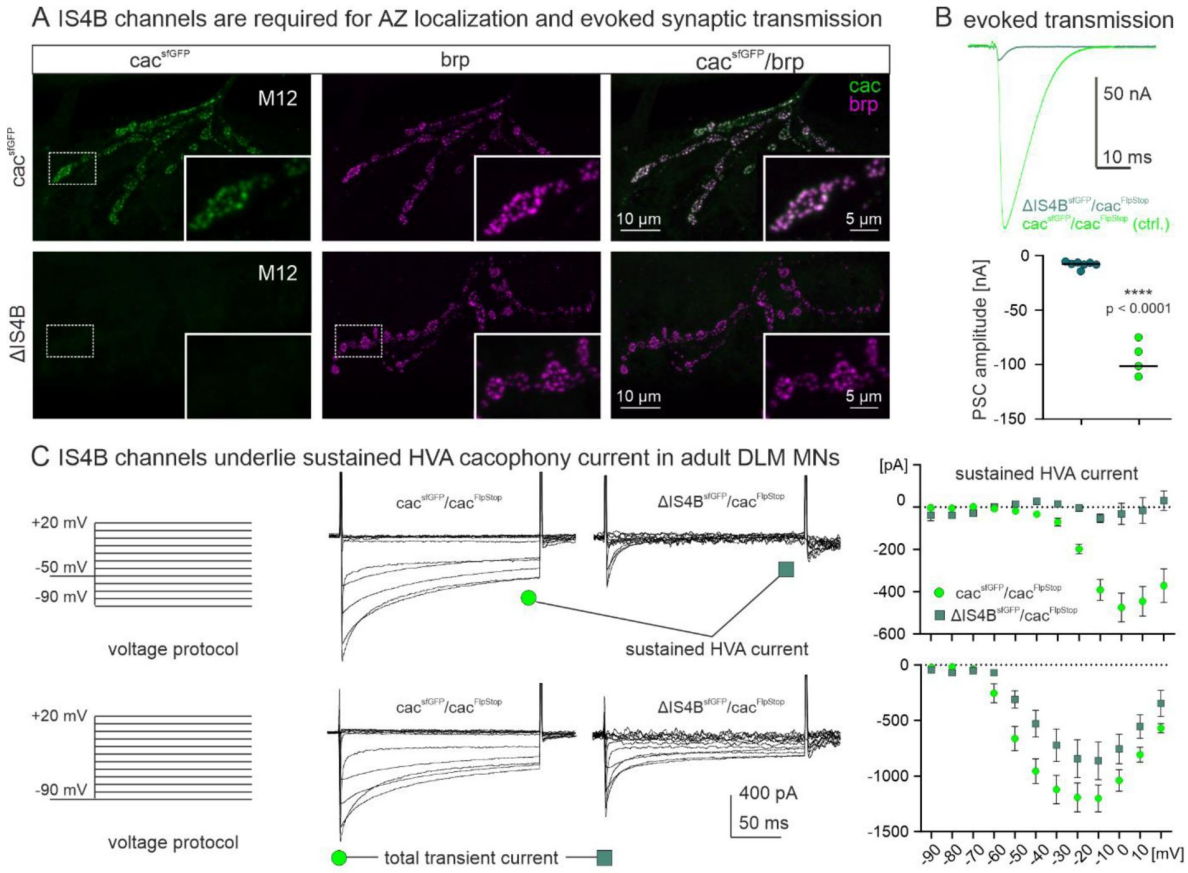

Figure 3.

The IS4B exon is required for cacophony localization to AZs and for evoked synaptic transmission

(A, B) Since animals homozygous for *IS4B* exon excision are lethal, we created mosaic animals that were heterozygous for cac in most neurons but hemizygous for either cac^{sfGFP} or *ΔIS4B* in motoneurons innervating muscle M12 (see methods, $cac^{FlpStop}$). In controls with all cac exons (cac^{sfGFP}, green, top row), cac^{sfGFP} colocalizes with brp (magenta) in presynaptic AZs on M12 **(A,** enlargements of area indicated by dotted white rectangle in bottom right corner of each image**)** and evoked synaptic transmission induces EPSCs of about 100 nA amplitude **(B)**. By contrast, upon deletion of *IS4B* (**A**, bottom row, see also enlargement in bottom right corner) in motoneurons to M12 no cac label is found throughout the motor terminals that are marked by brp (magenta) and evoked synaptic transmission is reduced by more than 90%, Student's T-test, $p < 0.0001$ **(B)**. **(C)** Cacophony mediates HVA as well as LVA calcium currents in adult flight motoneurons. All currents are recorded from the somata of adult flight motoneurons in mosaic animals with only one copy of the cac locus in flight motoneurons (see methods). HVA currents (upper traces) are measured by starting from a holding potential of −50 mV (LVA inactivation) followed by step command voltages from −90 mV to +20 mV in 10 mV increments (left, top row), while total cac current (lower traces) is elicited by step commands in 10 mV increments from a holding potential of −90 mV allowing activation of LVA currents (left, bottom row). In GFP-tagged controls (cac^{sfGFP} / $cac^{FlpStop}$) this reveals transient and sustained HVA current components (middle, top traces). However, following excision of the *IS4B* exon ($ΔISAB^{sfGFP}$ / $cac^{FlpStop}$), the sustained HVA current is absent. By contrast, upon excision of IS4B, the total cac current that also contains cac LVA currents is only partially decreased (middle, bottom traces). Current-voltage (IV) relation of sustained HVA and for total cac current for controls with all cac exons (cac^{sfGFP}, green circles, n = 7) and following excision of *IS4B* ($ΔIS4B^{sfGFP}$, dark green squares, n = 4).

animals (*ΔIS4B*; **Fig. 3A**, bottom row). In control animals, cac^{sfGFP} channels localize to brp positive AZs in motoneuron axon terminals on M12 (**Fig. 3A**, top row and selective enlargement). By contrast, cac^{IS4A} do not localize to brp positive AZs in motoneuron axon terminals on M12 (**Fig. 3A**, bottom row and selective enlargement). Therefore, *IS4B* is indeed required for cac AZ localization in excitatory glutamatergic axon terminals at the Drosophila NMJ. Consequently, evoked synaptic transmission is nearly abolished in motoneuron terminals that lack IS4B (**Fig. 3B**). Please note that even upon *IS4B* excision, and thus without any cac channels in AZs, the intensity of brp puncta remained unchanged as compared to control ($p = 0.81$; Mann Whitney U-test). We conclude that *IS4B* is required for evoked synaptic transmission from chemical presynaptic terminals, whereas *IS4A* has no essential function for action potential induced neurotransmitter release from presynaptic terminals.

The IS4B exon is required for sustained HVA cac mediated calcium current

Technical constraints prohibit a voltage clamp characterization of IS4B containing cac channels at the larval motoneuron presynaptic terminal, and the somatodendritic calcium current in larval motoneurons is mediated by the Drosophila Ca_V1 homolog *DmCa1D* (Worrell, Levine 2008; Kadas et al. 2017). However, Drosophila cac currents have previously been shown in somatodendritic voltage clamp recordings from pupal and adult motoneuron somata (Ryglewski et al. 2012; 2014a; b). Although these recordings are not representative for cac currents at larval presynaptic terminals, they show that Drosophila cac channels can in principle contribute to transient and sustained as well as high (HVA) and low (LVA) voltage activated currents (Ryglewski et al. 2012). Given that mutually exclusive splicing at the *IS4* site affects the voltage sensor (**Fig. 1B**) and that only the *IS4B* exon is required for evoked synaptic transmission, we next tested whether *IS4B* makes a significant contribution to a specific sub-type of cac mediated calcium current. The comparison of voltage clamp recordings from adult flight motoneuron somata in animals with full cac isoform diversity and mosaic animals with *IS4B* excision in only these motoneurons (see methods) shows that *IS4B* is required for sustained HVA cac current. Following electrical inactivation of LVA currents with prepulses to –50 mV (**Fig. 3C**, top left), HVA with an activation voltage of ∼-30 mV shows a sustained component that is reliably recorded with full cac isoform diversity (**Fig. 3C**, top left current traces and top IV diagram) but the sustained HVA component is absent in *ΔIS4B* motoneurons (**Fig. 3C**, top right current traces and top IV diagram). By contrast, total cac current (bottom traces) that contains LVA and HVA components is not abolished but only reduced by the excision of *IS4B* (**Fig. 3C**, bottom). Somatodendritic calcium current as recorded in neurons without the IS4B exon prove that cac^{IS4A} channel isoforms are expressed and functional (**Fig. 3C**) although cac^{IS4A} isoforms are not present in presynaptic terminals at the NMJ (**Figs. 2C**, **3A**). Therefore, the *IS4B* exon is vital for evoked synaptic transmission and promotes sustained HVA calcium current, whereas the *IS4A* exon is not sufficient for evoked synaptic transmission but mediates somatodendritic cacophony current in adult flight motoneurons.

Alternative splicing at the I-II site does not affect active zone localization but channel number and release probability

Immunohistochemical triple label at the larval Drosophila NMJ tests whether either one of the mutually exclusive exons at the *I-II* locus is required for correct presynaptic cac localization. Motoneuron axon terminals on larval muscles 6 and 7 (M6/7) are labeled with HRP (**Fig. 4A-C**, right column, blue), sfGFP tagged cac channels by α-GFP immunolabel (**Fig. 4A-C**, left column, green), and AZs by α-brp immunocytochemistry (**Fig. 4A-C**, second column, magenta). For a better visualization of brp and cac puncta, selective enlargements are shown for each genotype in **Figs. 4Ai-Ci**. In controls, sfGFP tagged cac channels with full isoform diversity co-localize with brp in presynaptic AZs (**Figs. 4A**, Ai) as also shown above (**Figs. 2A**, Ai). The same is the case for both mutually exclusive variants at the *I-II* locus. Cac channels that contain I-IIB but lack I-IIA

(*ΔI-IIA*, **Figs. 4B**, Bi), and *vice versa*, cac channels that contain I-IIA but lack I-IIB (*ΔI-IIB*, **Fig. 4C**, Ci) show AZ localization (see overlays of brp and cac^{sfGFP} in **Figs. 4B, Bi, C, Ci**, third column). For all cac isoforms that are targeted to presynaptic AZs, quantification reveals similar Pearson's correlation coefficients of ~0.65 (**Fig. 4D**), which corresponds to previous reports (Krick et al. 2021). Moreover, the Manders 1 and 2 co-localization coefficients are similar for control, cac^{IS4B}, and both I-II locus isoforms $cac^{I\text{-}IIB}$ and $cac^{I\text{-}IIA}$ (**Figs. 4E**, F). In sum, alternative splicing at the *I-II* site does not affect cac expression in presynaptic AZs.

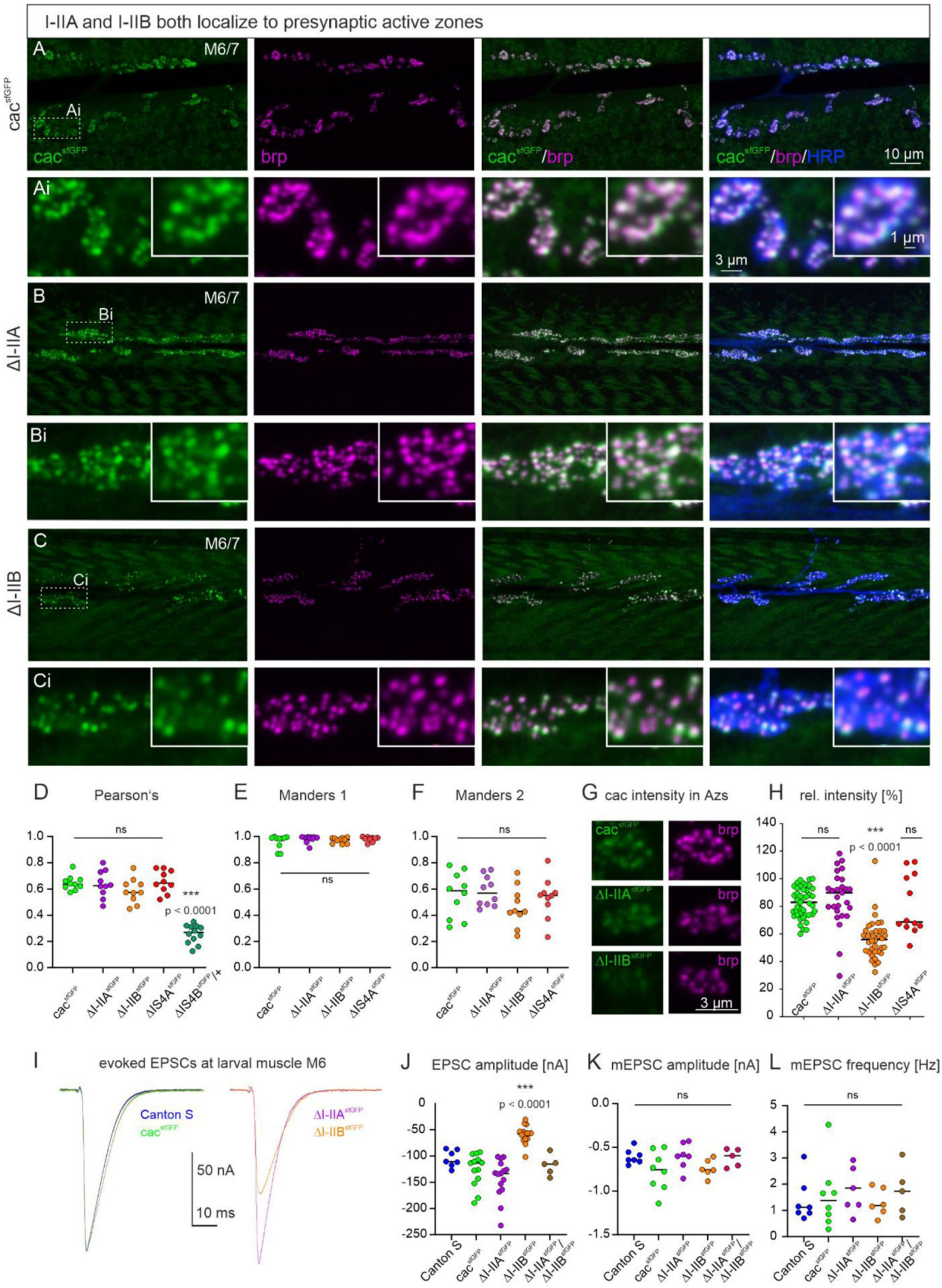
I-IIA and I-IIB both localize to presynaptic active zones
A
M6/7
Ai
cacsfGFP
brp
cacsfGFP/brp
cacsfGFP/brp/HRP
10 µm
3 µm
1 µm
B
M6/7
Bi
ΔI-IIA
C
M6/7
Ci
ΔI-IIB
D Pearson's
E Manders 1
F Manders 2
G cac intensity in Azs
H rel. intensity [%]
ns
***
p < 0.0001
I evoked EPSCs at larval muscle M6
Canton S
50 nA
10 ms
J EPSC amplitude [nA]
K mEPSC amplitude [nA]
L mEPSC frequency [Hz]

Figure 4.

Excisions at the I-II exon do not affect AZ cacophony localization but can alter cac^{sfGFP} label intensity in AZs and EPSC amplitude.

(A-C) Representative confocal projection views of triple labels for GFP tagged cac channels (green), the AZ marker brp (magenta), and HRP to label axonal membrane (blue) with enlargements that are indicated by white dotted rectangles in A-C (Ai-Ci). Label in control animals with all cac exons (cac^{sfGFP}, top two rows, **A, Ai**), with selective excision of either the alternative exon *I-IIA* (*ΔI-IIA^{sfGFP}*, middle two rows, **B, Bi**), or the alternative exon *I-IIB* (*ΔI-IIB^{sfGFP}*, bottom two rows, **C, Ci**). The gross morphology of the neuromuscular junctions (muscle fibers, bouton numbers and sizes, AZ numbers) was similar in all three genotypes (not shown). Excision of the *I-IIA* exon does neither impact cac AZ localization nor labeling intensity **(B, Bi, H)**. Excision of *I-IIB* does not impact cac AZ localization but labeling intensity seems lower **(C, Ci, H)**. **(D-F)** Quantification of cac co-localization with the AZ marker brp yields a similar Pearson's colocalization coefficient **(D)** as well as similar Manders 1 **(E)** and Manders 2 **(F)** coefficients for controls (green) and both exon-out variants of the *I-II* locus (ΔI-IIA purple, ΔI-IIB orange) as well as for *ΔIS4A* (red) but not for *ΔIS4B* (dark green, ANOVA with Dunnett's post hoc test, $p < 0.0001$). **(G)** ΔI-IIB^{sfGFP} shows fainter immunofluorescence signals in the AZ as compared to control (cac^{sfGFP}) and *ΔI-IIA^{sfGFP}*. **(H)** Quantification confirms a significant reduction in *ΔI-IIB^{sfGFP}* labeling intensity (Kruskal Wallis ANOVA with Dunn's post hoc test, $p < 0.0001$) and no differences between *ΔI-IIA^{sfGFP}* and control ($p > 0.99$). **(I)** Evoked synaptic transmission as recorded in TEVC from muscle fiber 6 upon extracellular stimulation of the motor nerve. Excitatory postsynaptic currents (EPSCs) are of similar shape and amplitude for CS control (blue) and animals with GFP-tagged cac channels (cac^{sfGFP}, green, p=0.34, two sided Tukey's multiple comparison test). Excision of *I-IIA* (*ΔI-IIA^{sfGFP}*, purple) has no effect on evoked release amplitude (p=0.52, two sided Tukey's multiple comparison test), but excision of *I-IIB* (*ΔI-IIB^{sfGFP}*, orange) reduces evoked release significantly ($p < 0.0001$). **(J)** Quantification of EPSC amplitude reveals a highly significant reduction in *ΔI-IIB^{sfGFP}* (orange) as compared cac^{sfGFP} controls (green), but neither animals with excision of the *I-IIA* exon (purple), nor transheterozygous animals with excision of *I-IIA* on one and *I-IIB* on the chromosome (brown) show differences to control (p=0.97, two sided Tukey's multiple comparison test). **(K)** Quantal size (mEPSC amplitude) and spontaneous release frequency **(L)** show no significant difference among genotypes.

However, removal of the *I-IIB* exon reduces the intensity of cac immunolabel in AZs as compared to control or *ΔI-IIA* highly significantly by ~50% (**Figs. 4G**, H). These data indicate that *I-IIB* excision may result in fewer cac channels per presynaptic AZ. We employ two electrode voltage clamp recordings from the postsynaptic cell (M6) to test for the resulting consequences on synaptic transmission (**Figs. 4I-L**). The amplitude of the postsynaptic current (EPSC) as evoked by an action potential in the presynaptic motor axon is similar in Canton S with untagged cac and animals expressing cac^{sfGFP} channels (**Figs. 4I, J, see** also above, **Figs. 2E**, F). Removal of the *I-IIA* exon (*ΔI-IIA*, **Fig. 4I**, purple trace) does not result in significant differences of EPSC amplitude as compared to tagged or untagged controls (**Figs. 4I**, J). By contrast, removal of the *I-IIB* exon (*ΔI-IIB*, **Fig. 4I**, orange trace) results in a reduction in EPSC amplitude by ~50% (**Fig. 4J**), which matches the reduced channel immunofluorescence signal in AZs (**Fig. 4H**) upon removal of the *I-IIB* exon. By contrast, neither removal of the *I-IIA* exon nor removal of the *IS4A* exon reduces tagged cac channel intensity in AZs (**Fig. 4H**), and neither of these manipulations affect EPSC amplitude (**Figs. 2F**, **4J**). The differences or similarities between genotypes in EPSC amplitude also hold when analyzing EPSC charge instead of amplitude (significantly smaller EPSC charge in *ΔI-IIB*, $p < 0.0001$, ANOVA with Dunnet post hoc comparison). In contrast to different cac puncta intensities in I-IIA versus I-IIB containing cac channels the intensity of brp puncta remains control like across the exon excision mutants (Kruskal Wallis ANOVA, $p = 0.1$, data not shown).

It seems unlikely that presynaptic cac channel isoform type affects glutamate receptor types or numbers, because the amplitude of spontaneous miniature postsynaptic currents (mEPSCs, **Fig. 4K**) and the labeling intensity of postsynaptic GluRIIA receptors are not significantly different

between controls, I-IIA, and I-IIB junctions (see suppl. Fig. 2, p = 0.48, ordinary one-way ANOVA, mean and SD intensity values are 61.0 ± 6.9 (control), 55.8 ± 8.5 (*ΔI-IIA*), 61.1 ± 17.3 (*ΔI-IIB*)). However, we cannot exclude altered GluRIIB numbers and have not quantified GluR receptor field sizes. Similarly, the frequency of miniature postsynaptic currents (mEPSCs) remains unaltered (**Fig. 4L**). Since mEPSC frequency has been related to RRP size at some synapses (Pan et al., 2009; Ralowicz et al., 2024), this indicates unaltered RRP size upon *I-IIB* excision, but we have not directly measured RRP size. In sum, these data show that neither exon at the *I-II* locus is required for cac localization to AZs, but *I-IIB* is required for normal evoked synaptic transmission amplitude. A reduced amplitude of evoked synaptic transmission along with less intensive presynaptic cac immunolabel in *ΔI-IIB* animals (**Figs. 4H**, J) is indicative for fewer calcium channels in AZs. Alternatively, the nanoscale localization of cac could be affected by alternative splicing.

We assess the latter by dual color STED microscopy of the AZ marker brp and cac^{sfGFP} in different exon excision mutants (**Figs. 5A-E**). Collecting STED image stacks of synaptic boutons on muscle 6 (**Fig. 5A**) reveals numerous AZs in various spatial orientations relative to the focal plane (**Fig. 5A-C**). In a strict top view (**Fig. 5C** 1) the orientation of the synapse is planar so that the central cac cluster (magenta) is surrounded by four brp puncta (green) all in the same plane. If the AZ lies tilted relative to the focal plane, the same arrangement is viewed from different angles (side views, **Figs. 5C** 2-6). The localization of cac relative to brp in different exon-out variants (**Figs. 5D**, E) is quantified by measuring the distance between the center of the cac cluster and the center of the nearest brp punctum in top and side views within the same optical sections (see methods). There is no difference in the cac to brp distance between different views/synapse orientation in relation to the focal plane. In all cac exon-out variants that are expressed in AZs (control, *ΔIS4A*, *ΔI-IIA* and *ΔI-IIB* but not *ΔIS4B*) the median distance ranges between 103 and 109 nm and reveals no significant differences (Kruskal-Wallis test, p = 0.62) between control (median distance, 106.1 nm) and any of the exon-out variants shown *(ΔIS4A*, *ΔI-IIA* and *ΔI-IIB*, **Fig. 5E**). Alternative splicing at the *I-II* locus does therefore neither affect targeting of cac to AZs (**Figs. 4A-F**), nor cac localization within the brp scaffold of the AZ (**Figs. 5A-E**).

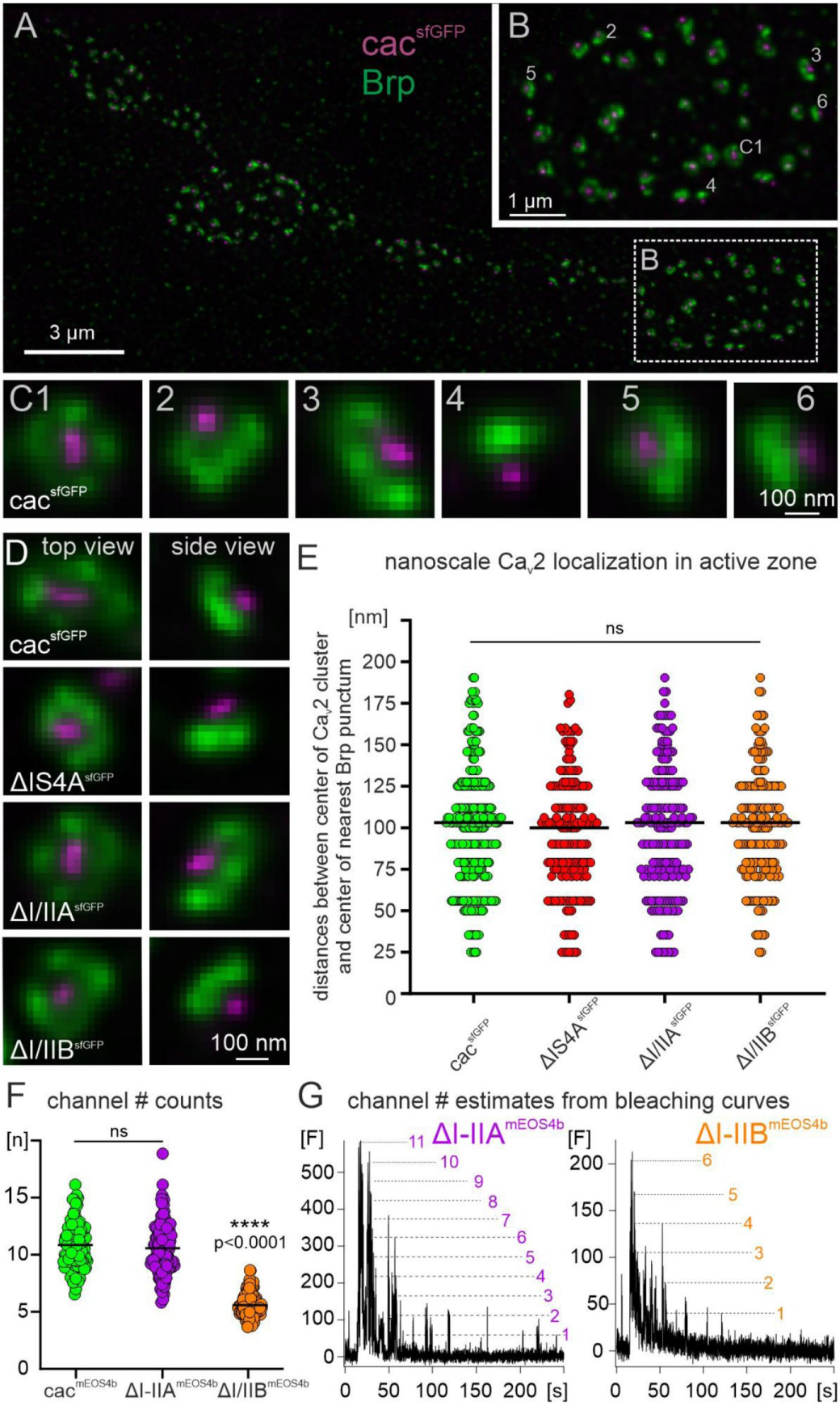
A
cac^sfGFP
Brp
3 µm
B
2
3
5
6
C1
4
1 µm
B
C1
2
3
4
5
6
cac^sfGFP
100 nm
D
top view
side view
cac^sfGFP
ΔIS4A^sfGFP
ΔI/IIA^sfGFP
ΔI/IIB^sfGFP
100 nm
E
nanoscale Ca_v2 localization in active zone
[nm]
distances between center of Ca_v2 cluster and center of nearest Brp punctum
ns
200
175
150
125
100
75
50
25
0
cac^sfGFP
ΔIS4A^sfGFP
ΔI/IIA^sfGFP
ΔI/IIB^sfGFP
F
channel # counts
[n]
ns
****
p<0.0001
15
10
5
0
cac^mEOS4b
ΔI-IIA^mEOS4b
ΔI/IIB^mEOS4b
G
channel # estimates from bleaching curves
[F]
ΔI-IIA^mEOS4b
11
10
9
8
7
6
5
4
3
2
1
500
400
300
200
100
0
0 50 100 150 200 [s]
[F]
ΔI-IIB^mEOS4b
6
5
4
3
2
1
200
150
100
50
0
0 50 100 150 200 [s]

Figure 5.

Dual color STED imaging reveals equal nanoscale channel localization in AZs of cacophony for all exon-out variants, and live sptPALM imaging reduced channel numbers in AZs for ΔI-IIB.

(A) Representative intensity projection image of the AZ marker bruchpilot (labeled with anti-brp, green) and cac clusters (cac^{sfGFP} labeled with anti-GFP, magenta) as imaged with dual color STED at motoneuron axon terminal boutons on larval muscle M6. The dotted white box demarks one bouton that is enlarged in **(B)**. Each cac cluster (magenta) is in close spatial proximity to the AZ marker brp (green) and depending on AZ orientation, cac and brp is viewed from different angles. Top views (= planar views, see C1 in B and in selective enlargement) show 4 brp puncta that symmetrically surround the central cac cluster. Viewing AZs at the edge of the bouton shows the cac cluster facing to the outside and the brp puncta in close proximity (see 2-6). **(C)** Selective enlargements of each AZ that is numbered in B. **(D)** Top views (left column) and side views (right column) of the cac/brp arrangement in AZs in controls with cac^{sfGFP} (top row), with excision of exon *IS4A* ($\Delta ISA4^{sfGFP}$, second row), with excision of exon *I/IIA* ($\Delta I/IIA^{sfGFP}$, third row), and with excision of exon *I/IIB* ($\Delta I/IIB^{sfGFP}$, bottom row). **(E)** Quantification of the distances between the center of each cac punctum to the nearest brp punctum in the same focal plane. **(F-G)** Live sptPALM imaging of mEOS4b tagged cac channels from AZs of MN terminals on muscle 6 in controls with full isoform diversity ($cac^{mEOS4b,}$ green) and following the removal of either *I-IIA* ($\Delta I\text{-}IIA^{mEOS4b}$, purple) or *I-IIB* ($\Delta I\text{-}IIB^{mEOS4b}$, orange). **(F)** Quantification of channel numbers from bleaching curves **(G)** reveals ~ 9-11 cacophony channels per AZ for tagged controls, which matches previous reports (Ghelani et al. 2023). Counts for *ΔI-IIA* reveal no significant differences (Kruskal-Wallis test with Dunn's posthoc comparison, p=0.94), but cac number in AZs is reduced by ~50 % in *ΔI-IIB* (p<0.0001). **(G)** Bleaching curves of single AZs were illuminated after ~10 s and then imaged under constant illumination for another 240 s. Discrete bleaching steps (dotted lines) indicate the bleaching of single cac^{mEOS4b} channels. Comparing the amplitudes of single events and their integer multiples (dotted lines) to the maximum fluorescence at illumination start allows estimates of the total channel number per AZ.

This leaves changes in cac properties or channel number in AZs as plausible causes for the reduction in evoked synaptic transmission upon removal of the *I-IIB* exon (**Figs. 4I**, J). As previously reported, channel number in presynaptic AZs can be estimated by live sptPALM imaging of mEOS4b tagged cac channels at the NMJ (cac^{mEOS4b}, Ghelani et al. 2023). To estimate channel number in AZs of axon terminals on larval muscle M6 in controls, *ΔI-IIA*, and *ΔI-IIB* (**Fig. 5F**), the bleaching behavior of cac^{mEOS4b} signals in individual AZs is imaged during steady illumination. Discrete bleaching steps (**Fig. 5G**, dotted lines) indicate bleaching events of individual cac^{mEOS4b} molecules, and thus the fluorescence intensity of a single cac^{mEOS4b} channel. Larger channel numbers produce integer multiple fluorescence intensity amplitudes. Dividing the full fluorescence amplitude that is measured at the illumination onset of all channels in the AZ by the fluorescence intensity from a single channel yields total channel number per AZ. Quantification from three animals per genotype with at least 30 AZs per animal confirms a previous study (Ghelani et al. 2023) showing that control animals with full cac channel isoform diversity express ~10 cac channels per AZ (**Fig. 5F**, green, 10.8 ± 2 channels). Removing the alternative exon *I-IIA* does not affect channel number per AZ (**Fig. 5F**, purple, 10.5 ± 2 channels), but excision of *I-IIB* reduces channel number to ~50 % (**Fig. 5F**, orange, 5.6 ± 1 channels). A ~50% reduction in channel number counts in AZs (**Fig. 5F**) is in line with ~50 % reduction in cac immunofluorescence in AZs (**Fig. 4H**) and evoked synaptic transmission (**Figs. 4I**, J) upon excision of *I-IIB*. In sum, these data indicate that the reduction of evoked synaptic transmission amplitude in *ΔI-IIB* is a consequence of reduced channel number.

Functional consequences of I-II site alternative splicing during repetitive firing

In addition to reducing the numbers of SVs that are released upon one presynaptic action potential (quantal content), removal of the *I-IIB* exon has significant effects on synaptic transmission during repetitive stimulation and on synaptic plasticity. First, the paired pulse ratio (PPR) is affected. In 0.5 mM calcium, controls with sfGFP-tagged cac channels show slight paired pulse (PP) depression at interpulse interval (IPI) durations below 20 ms (**Fig. 6A**). Similarly, upon removal of the *I-IIA* exon ($\Delta I\text{-}IIA^{sfGFP}$) PP depression is observed for IPIs below 20 ms (**Fig. 6B**). By contrast, upon removal of the *I-IIB* exon, some animals show PP depression and others PP facilitation, so that the average PPR is close to 1 for all IPIs, but the variance is large, in particular for short IPIs (**Fig. 6C**). To test whether increased PPRs and increased PPR variance can be fully explained by reduced channel numbers upon excision of *I-IIB*, or whether additional factors were required to explain these findings, we increased the external calcium concentration to 1.8 mM so that the first pulse amplitude in *ΔI-IIB* animals matched that of control animals in 0.5 mM calcium. This fully rescued the effect of *I-IIB* excision. In fact, mean and variance of PPRs as recorded from *ΔI-IIB* in 1.8 mM external calcium were similar to the PPRs as observed in controls and in *ΔI-IIA* in 0.5 mM external calcium across all interpulse intervals (**Fig. 6D**). Considering the variance at 0.5 mM external calcium, for control and for excision of *I-IIA* the coefficient of variation is ~5-10 % across IPIs whereas upon excision of *I-IIB* it reaches 15-20% for short IPIs (**Fig. 6E**). However, increasing external calcium to 1.8 mM in recordings in *ΔI-IIB* animals increases the first EPSC amplitude to that observed in controls in 0.5 mM external calcium (**Fig. 6D**) and eliminates altered PPRs as well as increased variance (**Figs. 6D**, E).

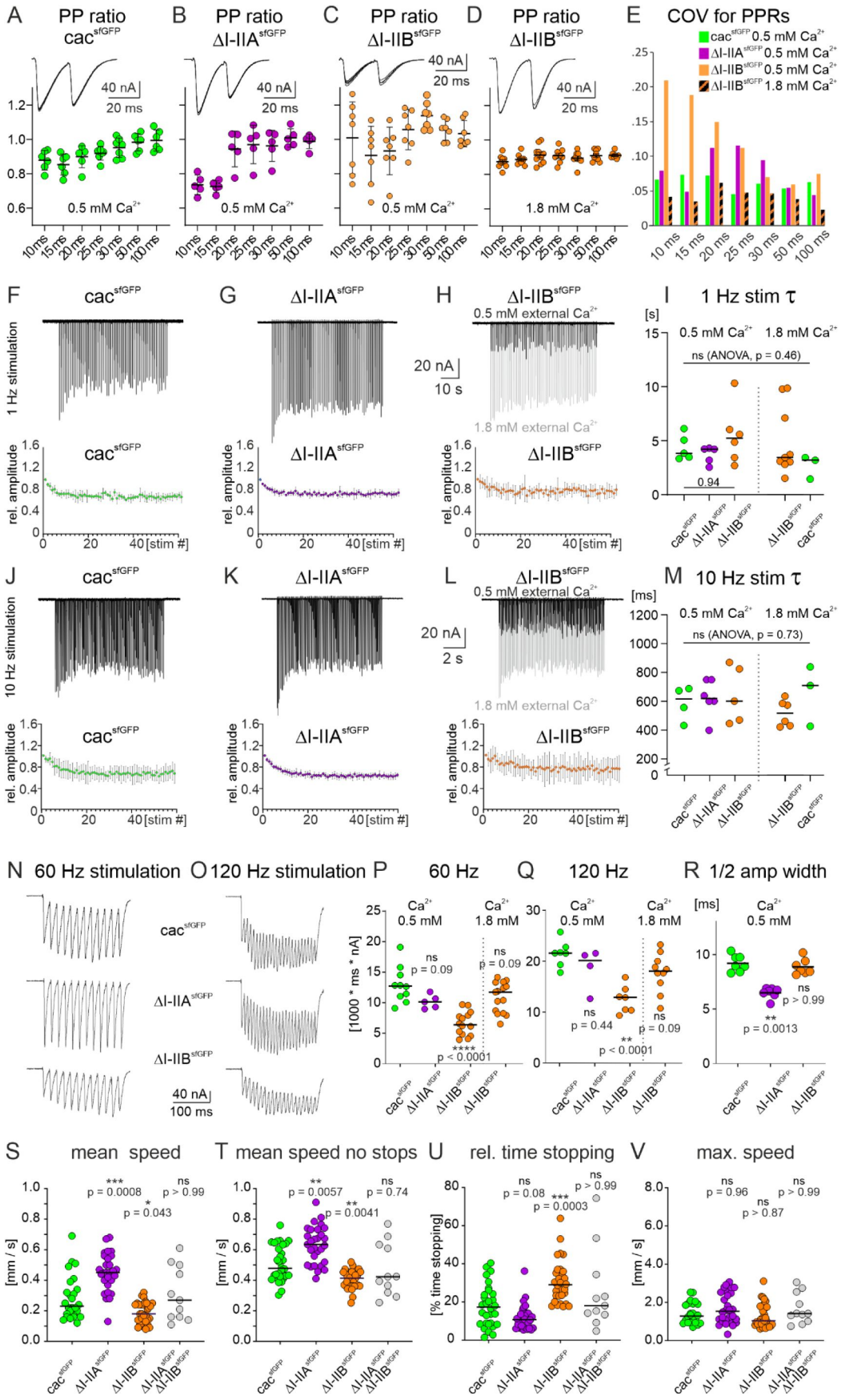
A PP ratio cac^sfGFP
B PP ratio ΔI-IIA^sfGFP
C PP ratio ΔI-IIB^sfGFP
D PP ratio ΔI-IIB^sfGFP
E COV for PPRs
cac^sfGFP 0.5 mM Ca2+
ΔI-IIA^sfGFP 0.5 mM Ca2+
ΔI-IIB^sfGFP 0.5 mM Ca2+
ΔI-IIB^sfGFP 1.8 mM Ca2+
40 nA
20 ms
0.5 mM Ca2+
1.8 mM Ca2+
10ms 15ms 20ms 25ms 30ms 50ms 100ms
F cac^sfGFP
G ΔI-IIA^sfGFP
H ΔI-IIB^sfGFP
I 1 Hz stim τ
1 Hz stimulation
0.5 mM external Ca2+
1.8 mM external Ca2+
20 nA
10 s
rel. amplitude
[stim #]
[s]
0.5 mM Ca2+ 1.8 mM Ca2+
ns (ANOVA, p = 0.46)
0.94
J cac^sfGFP
K ΔI-IIA^sfGFP
L ΔI-IIB^sfGFP
M 10 Hz stim τ
10 Hz stimulation
20 nA
2 s
[ms]
ns (ANOVA, p = 0.73)
N 60 Hz stimulation
O 120 Hz stimulation
P 60 Hz
Q 120 Hz
R 1/2 amp width
40 nA
100 ms
[1000 * ms * nA]
Ca2+ 0.5 mM
Ca2+ 1.8 mM
ns p = 0.09
ns p = 0.09
**** p < 0.0001
ns p = 0.44
** p < 0.0001
ns p = 0.09
[ms]
ns p > 0.99
** p = 0.0013
S mean speed
T mean speed no stops
U rel. time stopping
V max. speed
[mm / s]
[% time stopping]
*** p = 0.0008
ns p > 0.99
* p = 0.043
** p = 0.0057
ns p = 0.74
** p = 0.0041
ns p = 0.08
*** p = 0.0003
ns p > 0.99
ns p = 0.96
ns p > 0.99
ns p > 0.87

Figure 6.

Alternative splicing in the I-II linker affects short term plasticity due to decreased calcium influx and motor behavior.

(A-D) Paired pulse ratio (PPR, ratio of second EPSC amplitude divided by first EPSC amplitude) as measured in 0.5 mM external calcium (**A-C**) or in 1.8 mM external calcium (**D**) at different interpulse intervals (IPIs ranging from 10 ms to 100 ms) in control animals (cac^{sfGFP}, **A**), in animals with removal of *I-IIA* ($\Delta I\text{-}IIA^{sfGFP}$, **B**), and in animals with removal of *I-IIB* ($\Delta I\text{-}IIB^{sfGFP}$) either in 0.5 mM calcium (**C**) or 1.8. mM calcium (**D**). The large variance in PPR upon excision of I-IIB (**C**) is rendered control-like if the first EPSC amplitude of the twin pulse is adjusted to 0.5 mM external calcium control level (**D**; comp. with **A**). This is also reflected in the coefficient of variation (COV) for PPRs (**E**, 0.5 mM calcium: cac^{sfGFP} green, *ΔI-IIA* purple, *ΔI-IIB* orange; 1.8 mM calcium: *ΔI-IIB* orange/black pattern). **(F-I)** Synaptic depression as measured in 0.5 mM external calcium in response to stimulus trains of 1 minute duration at 1 Hz frequency for animals with GFP-tagged cac (cac^{sfGFP}, **F**), following removal of *I-IIA* ($\Delta I\text{-}IIA^{sfGFP}$, **G**), and with removal of *I-IIB* ($\Delta I\text{-}IIB^{sfGFP}$, **H**). The top traces show representative TEVC recordings from the postsynaptic muscle cell, and the diagrams mean values (n=5 for F and G, N=6 for H, error bars are SD). (**H**) The light gray trace shows *ΔI-IIB* in 1.8 mM external calcium, while the black trace shows *ΔI-IIB* in 0.5 mM calcium. For all 3 genotypes, depression reaches steady state at ~ 80 % of the original EPSC amplitude, but upon excision of *I-IIB* it is more variable **(H)**. Depression time courses do not differ between genotypes but are more variable in *ΔI-IIB,* independent of external calcium concentration (**H, I**). **(J-M)** Synaptic depression in response to stimulus trains at 10 Hz frequency for animals with GFP-tagged cac (cac^{sfGFP}, **J**), following removal of *I-IIA* ($\Delta I\text{-}IIA^{sfGFP}$, **K**), and with removal of *I-IIB* ($\Delta I\text{-}IIB^{sfGFP}$, **L**: black in 0.5 mM calcium, gray trace in 1.8 mM calcium). Again, depression is most variable between animals upon excision of *I-IIB* **(L, M)** but time courses do not differ between genotypes. However, time course variation decreases in 1.8 mM calcium in animals with excision of *I-IIB* (**M**). Motoneuron stimulation at 60 **(N)** or 120 Hz **(O)** frequency, both for durations of 200 ms in animals with GFP-tagged cac (cac^{sfGFP}, top traces), following removal of *I-IIA* ($\Delta I\text{-}IIA^{sfGFP}$, middle traces), and with removal of *I-IIB* ($\Delta I\text{-}IIB^{sfGFP}$, bottom traces). To compare charge transfer across the NMJ during high frequency bursts the total EPSC area below baseline (prior to stimulation) was measured during each 200 ms burst and plotted for each genotype for 60 Hz stimulation in **(P)** and for 120 Hz stimulation in **(Q).** Decreased charge transfer in animals with excision of the *I-IIB* exon is rescued to control level if external calcium is increased to 1.8 mM so that the first EPSP matches control amplitude in 0.5 mM external calcium (**P, Q,** far right data points *ΔI-IIB* in 1.8 m calcium). **(R)** shows single evoked EPSC half amplitude width. (**S-V**) show different measurements during larval crawling for control animals with GFP-tagged cac (cac^{sfGFP}), removal of *I-IIA* ($\Delta I\text{-}IIA^{sfGFP}$), removal of *I-IIB* ($\Delta I\text{-}IIB^{sfGFP}$), and in transheterozygous animals with removal of *I-IIA* on one and removal of *I-IIB* on the other chromosome ($\Delta I\text{-}IIA^{sfGFP}/\Delta I\text{-}IIB^{sfGFP}$). The measured parameters are mean speed during 10 minutes of crawling **(S)**, mean speed without any stops **(T)**, the relative time spent stopping **(U)** and the maximum speed reached **(V)**. In all diagrams each dot demarks a measurement from a different animal and horizontal bars the medians. For statistics, non-parametric Kruskal Wallis ANOVA with planned Dunn's posthoc comparison to control was conducted.

We next tested whether the time course of synaptic depression during low frequency repetitive stimulation at 1 Hz is affected upon removal of either *I-II* exon. In 0.5 mM external calcium, repetitive stimulation of the NMJ to muscle M6/7 at 1 Hz frequency for 1 minute causes synaptic depression that reaches steady state at about 80 % of the initial transmission amplitude with a time constant of about 5 s (Krick et al. 2021). The same is observed for cac^{sfGFP} controls (**Figs. 6F**, I) and upon removal of *I-IIA* (**Figs. 6G**, I). Removal of *I-IIB* does not affect the magnitude and time course of depression at 1 Hz stimulation (**Fig. 6H**), but it increases the variability of the time constant until steady state depression is reached (**Fig. 6I**). Again, we triturated the external calcium concentration (1.8 mM) so that the first EPSC amplitude in the train in Δ*I-IIB* matched the first one in controls recorded in 0.5 mM external calcium (gray trace in **Fig. 6H** is *ΔI-IIB* in 1.8 mM calcium and black trace in 0.5 mM calcium). This did neither affect the mean time constant of depression nor the larger variance observed in *ΔI-IIB* (**Fig. 6I**), indicating that these parameters do not depend on calcium influx into AZs. At 10 Hz stimulation neither removal of *I-IIA* nor of *I-IIB* affects the time course or amplitude of synaptic depression (**Figs. 6J-M**). Increasing the external

calcium concentration (1.8 mM) so that the first EPSC amplitude in the train in *ΔI-IIB* matches the first one in controls recorded in 0.5 mM external calcium (gray trace in **Fig. 6L** is *ΔI-IIB* in 1.8 mM calcium and black trace in 0.5 mM calcium) does not affect magnitude or time course of depression (**Fig. 6M**). Similarly, increasing external calcium to 1.8 mM in controls does not affect the time constant of synaptic depression, in line with the findings at 1 Hz that these parameters do not depend on the amount of calcium influx into AZs.

Taken together removal of *I-IIA* does not alter channel number and does not affect PPRs or the time course of synaptic depression. By contrast, removal of *I-IIB* reduces channel number. This in turn is the cause for altered PPRs at short interpulse intervals (**Figs. 6C**, E) and can be rescued by increasing external calcium. Neither excision of *I-IIA*, nor of *I-IIB* has significant effects on the magnitude or time course of synaptic depression at low stimulation frequencies.

However, motoneuron firing frequencies as previously measured during tethered crawling (Kadas et al. 2017) reach ~120 Hz during bursts of about 200 ms duration. Given that the main function of excitatory synaptic transmission to larval muscles is locomotion, it seems important to test stimulation protocols that reflect behaviorally relevant motoneuron firing patterns. Applying motoneuron stimulation for 200 ms duration at either 60 Hz (**Fig. 6N**) or 120 Hz frequency (**Fig. 6O**) in 0.5 mM external calcium reveals summation of the EPSCs in control animals with GFP-tagged cac channels (**Figs. 6N, O, top** traces) as well as in animals without the *I-IIB* exon (*ΔI-IIB*, **Figs. 6N**, O, bottom traces). By contrast, upon excision of *I-IIA*, summation of EPSCs is absent at 60 Hz but present at 120 Hz stimulation frequency (*ΔI-IIA*, **Figs. 6N**, O, middle traces). The reason why EPSP summation occurs only at very high motoneuron firing frequencies (120 Hz) in *ΔI-IIA*, but already at 60 Hz in controls and in *ΔI-IIB* animals is a significantly smaller EPSP half-width upon excision of the *I-IIA* exon (**Fig. 6R**). This might be an indication for an effect of *I-IIA* exon excision on cac channel biophysical properties (see discussion). At both high frequency stimulation protocols (60 and 120 Hz) charge transfer is significantly reduced upon excision of *I-IIB* (**Figs. 6P**, Q). We measure charge transfer as the total area under the postsynaptic response traces during 200 ms long stimulation bursts at either 60 Hz (**Figs. 6N**, P) or 120 Hz (**Figs. 6O**, Q). To test whether this is caused by reduced calcium influx during an EPSC in *ΔI-IIB* (**Figs. 6N**, O), we again increased the external calcium concentration to 1.8 mM so that the first EPSC of the train matches the first EPSC amplitude observed in controls in 0.5 mM external calcium (see **Figs. 6N**, O, bottom gray overlay traces). This increased median total charge in *ΔI-IIB* to control values for both 60 Hz and 120 Hz stimulation (**Figs. 6P**, Q), thus indicating that the reduced charge transfer in *ΔI-IIB* at 0.5 mM external calcium can be explained by reduced presynaptic calcium channel number and concomitant reduced calcium influx.

Although crawling speed of Drosophila larvae is mainly adjusted by varying the duration between subsequent peristaltic waves of motoneuron bursting (peristaltic wave period duration, Liu et al. 2023), differences in cac mediated neuromuscular synaptic transmission may also play an important role. In accordance with reduced charge transfer to the postsynaptic muscle cell upon excision of the *I-IIB* exon (**Figs. 6N-R**), mean crawling speed is significantly reduced in *ΔI-IIB* animals (**Fig. 6S**). The mean crawling speed (including stops) of cac^{sfGFP} control larvae is roughly 0.2 mm per second and not significantly affected in transheterozygous *ΔI-IIA* over *ΔI-IIB* larvae that contain full cac isoform diversity (**Figs. 6T**, U). Removal of *I-IIB* (*ΔI-IIB*) causes a significant decrease in mean locomotion speed (**Fig. 6S**, orange) whereas removal of *I-IIA* significantly increases speed (*ΔI-IIA*, **Fig. 6S**, purple). Alterations in locomotion speed upon alternative cac exon removal could either be caused by changes in mean ground speed (mean speed excluding stops), or by changes in the duration of stopping, or by both. Mean ground speed in controls is about 0.5 mm per second (**Fig. 6T**), which is slightly slower but within the range previously reported (0.65-0.8 mm per second, Wang et al. 1997; Guo et al. 2016). The decreased net locomotion speed in *ΔI-IIB* larvae is caused by significant reductions in the mean ground speed (**Fig. 6T**) paired with significant increases in the duration of stopping (**Fig. 6U**). By contrast, the net locomotion speed increase as observed in *ΔI-IIA* larvae is caused by significant

increases in mean ground speed (**Fig. 6T**) without significant changes in the duration of stopping (**Fig. 6U**). However, the maximum locomotion speed observed does not differ significantly between controls and any of the test groups (Kruskal Wallis test, p=0.14; **Fig. 6V**), although *ΔI-IIB* neuromuscular junctions show significantly reduced charge transfer at 120 Hz motoneuron bursting (**Fig. 6Q**). This may indicate a safety plateau of charge transfer at maximum speed.

I-IIB is required for presynaptic homeostatic plasticity

Chemical synapses are subject to various forms of short-term (Fioravante, Regehr 2011), Hebbian (Nicoll, Schmitz 2005) and homeostatic plastic adjustments (Turrigiano 2008). The Drosophila larval NMJ has become a prominent model to analyze the mechanisms underlying presynaptic homeostatic potentiation (PHP, Frank et al., 2006; Davis, Müller 2015). PHP is a compensatory increase in the number of SVs that are released upon one presynaptic action potential (quantal content) in response to reduced postsynaptic receptor function. Consequently, EPSC amplitude is restored to its original setpoint despite reduced mEPSC amplitudes. Quantal content can be increased by a larger size of the readily releasable pool (RRP) of SVs, or by elevated release probability (P_r). A recent study has shown that the induction of PHP at the Drosophila NMJ requires an increase in P_r that is mediated by increasing the number of cac channels in the presynaptic AZ (from ~10 to ~12, Ghelani et al, 2023; see also Gratz et al. 2019). Our data show that exclusion of *IS4B* impairs cac localization to the AZ (**Figs. 2C**, Ci and 3A), whereas exclusion of *I-IIB* reduces cac number in the presynaptic AZ (**Fig. 5F**), raising the question whether homeostatic plasticity is affected by *I-II* exon splicing. Acute pharmacological blockade of postsynaptic glutamate receptors with the bee wolf toxin, philanthotoxin (PhTx), is a well-established means to induce PHP within minutes at the Drosophila larval NMJ (Frank et al. 2006; Davis, Müller 2012; 2015; Gratz et al. 2019; Ghelani et al. 2023). In control animals with GFP-tagged cac channels as well as upon excision of the *I-IIA* exon (normal channel numbers, **Fig. 5F**), bath application of PhTx reliably reduces the amplitude of spontaneously occurring minis (mEPSCs; data are presented as % of baseline without PhTx within genotype: cac^{sfGFP} control: **Figs. 7A**, E, green; *ΔI-IIA*: **Figs. 7B**, E, purple), but evoked EPSC amplitude is not reduced as compared to control (data are presented as % of baseline without PhTx; cac^{sfGFP} control: **Figs. 7A**, D, green; *ΔI-IIA*: **Figs. 7B**, D, purple). Normal EPSC amplitudes at reduced mEPSC amplitudes are caused by a compensatory increase in mean quantal content (data are presented as % of baseline without PhTx; **Fig. 7F**; cac^{sfGFP} control: green; *ΔI-IIA*: purple). By contrast, PHP is not observed upon removal of the *I-IIB* exon (**Figs. 7C-F**). As in controls and in *ΔI-IIA* animals, PhTx application reduces mEPSC amplitude by ~0.2 nA as expected (**Figs. 7C**, E), but in *ΔI-IIB* no compensatory increase in mean quantal content is observed (**Fig. 7F**), so that EPSC amplitude is not restored to its original setpoint (**Fig. 7D**). Similarly, in *ΔI-IIB* animals, PHP is also not possible in response to a permanent reduction of glutamate receptor function in *GluRIIA* mutants, which has been named PHP maintenance and is genetically separable from PHP induction (James et al. 2019). In *GluRIIA* mutants, compensatory upregulation of mean quantal content is observed in animals with GFP-tagged cac and upon excision of *I-IIA*, but not following excision of the *I-IIB* exon (**Fig. 7G**). Therefore, the lack of the *I-IIB* exon causes fewer cac calcium channels in the AZ and impairs both PHP initiation and maintenance.

Given that synapses that contain only cac isoforms without the *I-IIB* exon show a lower release probability, more variable paired pulse ratios and synaptic depression, and an inability for compensatory increases in mean quantal content, the question arises whether normal synapses contain the $cac^{I\text{-}IIA}$ channels at all. This can be tested in transheterozygous $\Delta I\text{-}IIA^{GFP}/\Delta I\text{-}IIB^{mEOS4b}$ animals, which show normal EPSC amplitudes as well as mEPSC amplitudes and frequencies (**Figs. 4J-L**). Co-labeling of AZs with anti-brp (**Fig. 7H**, blue) in animals that contain cac channels without I-IIB but with GFP-tagged I-IIA (**Fig. 7H**, green) on one chromosome and cac channels without I-IIA but with mEOS4b-tagged I-IIB (**Fig. 7H**, magenta) indicates that all AZs contain cac with I-IIB, some AZs contain only I-IIB channel (**Fig. 7H**1, H2, white arrow heads), most contain both I-IIB and I-IIA, but very few AZs contain cac channels with only I-IIA (**Fig. 7H**2, asterisk).

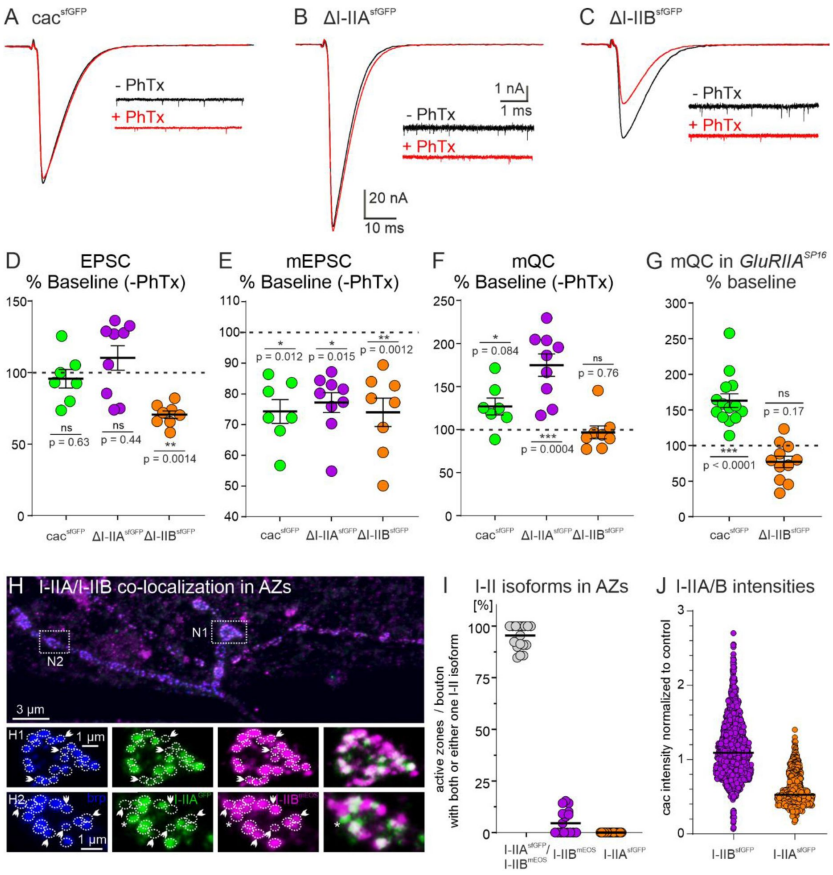

Figure 7.

Removal of I-IIB impairs presynaptic homeostatic potentiation.

(A-C) Acute presynaptic homeostatic potentiation (PHP) can be induced in control (cac^{sfGFP}) and *ΔI-IIA* but not in *ΔI-IIB* animals by bath application of the glutamate IIA receptor (GluRIIA) blocker philanthotoxin (PhTx) (A-C; black traces: without PhTx, red traces after PhTx application). **(D-F)** Quantification of EPSC amplitude, mEPSC amplitude, and mean quantal content (mQC) is shown as % change in PhTx treated animals to untreated control within genotypes (% Baseline (−PhTx). Untreated controls are set to 100 % (dotted line in **D-F**). EPSC amplitudes in cac^{sfGFP} and *ΔI-IIA* animals are not significantly affected (**D**, cac^{sfGFP}, green p=0.63, *ΔI-IIA*, purple p=0.44), while the EPSC amplitude in *ΔI-IIB* animals is significantly reduced after PhTx treatment (**D**, orange, p=0.0014). However, reduction of mEPSC amplitude in all genotypes shows successful block of GluRIIA compared to the respective control (**E**, % change to untreated control within genotype; cac^{sfGFP}, green p=0.012; *ΔI-IIA*, purple p=0.0015, *ΔI-IIB*, orange p=0.0012). Accordingly, mean quantal content (mQC) is increased in cac^{sfGFP} and *ΔI-IIA* animals but not in *ΔI-IIB* animals (**F**, cac^{sfGFP}, green p=0.084; *ΔI-IIA*, purple p=0.0004, *ΔI-IIB* p=0.76). **(G)** PHP maintenance is typically assessed in *GluRIIA* mutants. PHP maintenance is observed in cac^{sfGFP} animals because mQC is increased in a *GluRIIA^{SP16}* mutant background (*GluRIIA^{SP16}*; green, p<0.0001). By contrast, in *ΔI-IIB* animals the *GluRIIA* mutant background does not cause an increase in mQC (orange p=0.17). All pairwise comparisons in **(D-G)** use unpaired Student's T-test between untreated and treated condition within each genotype. **(H)** In animals that are transheterozygous for the removal of *I-IIA* and the removal of *I-IIB*, and carry GFP-tagged I-IIA and mEOS4b-tagged I-IIB cacophony channels (I-IIA^{sfGFP}/I-IIB^{mEOS}), triple immunolabel for the AZ marker brp, GFP, and mEOS4b show that most AZs (blue) but not all (white arrow heads in H1, H2 and asterisk in H2) contain both, GFP-tagged I-IIA (green) and mEOS4b-tagged I-IIB (magenta) channels. Magenta label in the overlay (H1, H2, right column, arrow heads) indicates AZs with only I-IIB channels, green label in the overlay (H2, right column, asterisk) indicates one AZ with only I-IIA channels. **(I)** Quantification shows that >95 % of all brp positive AZs contain I-IIA and I-IIB channels (gray dots), few AZs (~5 %) contain only I-IIB (= *ΔI-IIA*; purple), and almost no AZ contains only I-IIA (= *ΔI-IIB*; orange). **(J)** Relative fluorescence intensity of sfGFP-tagged I-IIB channels (= *ΔI-IIA*; purple) and sfGFP-tagged I-IIA channels (= *ΔI-IIB*; orange). For assessment of I-IIB channels, tagged channels were expressed transheterozygously over untagged I-IIA channels (*ΔI-IIA^{sfGFP}/ΔI-IIB$^{no\ tag}$*; purple) and *vice versa* (*ΔI-IIB^{sfGFP}/ΔI-IIA$^{no\ tag}$*; orange). Quantification of relative fluorescence intensity compared to transheterozygous control (*cac^{sfGFP}/cac$^{no\ tag}$*) reveals an expression ratio of I-IIB to I-IIA channels of 2:1.

Quantification reveals that ~95 % of all AZs contain cac channels with both, the I-IIA and the I-IIB exon, less than 5 % of the AZs contain only cac with the I-IIB exon and almost no AZ contains only cac with the I-IIA exon (**Fig. 7I**). These data show that the vast majority of presynaptic AZs house a mixture of I-IIA and I-IIB cac. To test whether there is a consistent average ratio of I-IIA and I-IIB channels in presynaptic AZs we measured the cac puncta fluorescence intensities for heterozygous cac^{sfGFP}/cac, $cac^{I\text{-}IIAsfGFP}$/$cac^{I\text{-}IIB}$, and $cac^{I\text{-}IIBsfGFP}$/cacI-IIA animals. This way intensity is always measured from cac puncta with the same GFP tag. Normalizing all values to the intensities obtained in AZs from heterozygous cac^{sfGFP}/cac controls reveals a consistent ratio 2:1 in the relative intensities of I-IIB and I-IIA across junctions and animals (**Fig. 7J**). This is consistent with the counts in our spt-PALM analysis (see **Fig. 5F**) and indicates on average roughly twice as many I-IIB as compared to I-IIA channels across AZs.

Discussion

The Drosophila *Ca_v2* homolog is named *cacophony* and contains two mutually exclusive splice sites that do not exist in vertebrate *Ca_v2* VGCC genes. Our data show that alternative splicing at these sites substantially increases Drosophila cac functional heterogeneity. We report that the first mutually exclusive exon, that is located in the fourth transmembrane domain of the first homologous repeat (*IS4*), affects cac biophysical properties and is decisive as to whether the channels localize to presynaptic active zones (AZs) and thus participate in fast synaptic transmission. By contrast, mutually exclusive splicing at the second site encoding the intracellular linker between the first and the second homologous repeat (I-II) does not affect cac presynaptic AZ localization, but instead, fine-tunes multiple different aspects of presynaptic function. In vertebrates, substantial functional synaptic heterogeneity can result from different combinations of $Ca_v2.1$, $Ca_v2.2$, and/or $Ca_v2.3$ in the presynaptic AZ (reviewed in Zhang et al. 2022). In Drosophila, the collective functions of mammalian $Ca_v2.1$, $Ca_v2.2$, and $Ca_v2.3$ must be portrayed by one *Ca_v2* gene. Mutually exclusive splicing at the *IS4* and *I-II* sites might have been a different evolutionary strategy to create cac mediated functional synaptic heterogeneity. However, alternative splicing increases functional diversity also in mammalian Ca_v2 channels. Although the mutually exclusive splice site in the S4 segment of the first homologous repeat (IS4) is not present in vertebrate Ca_v channels, alternative splicing in the extracellular linker region between S3 and S4 is at a position to potentially change voltage sensor properties (Bezanilla 2002). Alternative splice sites in rat $Ca_v2.1$ exon 24 (homologous repeat III) and in exon 31 (homologous repeat IV) within the S3-S4 loop modulate channel pharmacology, such as differences in the sensitivity of $Ca_v2.1$ to Agatoxin. Alternative splicing is thus a potential cause for the different pharmacological profiles of P– and Q-channels (both $Ca_v2.1$; Bourinet et al. 1999). Moreover, the intracellular loop connecting homologous repeats I and II is encoded by 3-5 exons and provides strong interaction with $G_{\beta\gamma}$-subunits (Herlitze et al. 1997). In $Ca_v2.1$ channels, binding to $G_{\beta\gamma}$ –subunits is potentially modulated by alternative splicing of exon 10 (Bourinet et al. 1999). Moreover, whole cell currents of splice forms α1A-a (no Valine at position 421) and α1A-b (with Valine) represent alternative variants for the I-II intracellular loop in rat $Ca_v2.1$ and $Ca_v2.2$ channels. While α1A-a exhibits fast inactivation and more negative activation, α1A-b has delayed inactivation and a positive shift in the IV-curve (Bourinet et al. 1999). This is phenotypically similar to what we find for the mutually exclusive exons at the IS4 site, in which IS4B mediates high voltage activated cacophony currents while IS4A channels activate at more negative potentials and show transient current (**Fig. 3**; see also Ryglewski et al. 2012). Furthermore, altered Ca_β interaction have been shown for splice isoforms in loop I-II (Bourinet et al. 1999), similar to what we suspect for the I-II site in cacophony. Finally, in mammalian VGCCs, the C-terminus presents a large splicing hub affecting channel function as well as coupling distance to other proteins. Taken together, Ca_v2 channel diversity is greatly enhanced by alternative splicing also in vertebrates, but the specific two mutually exclusive exon pairs investigated here are not present in vertebrate *Ca_v2* genes. Below, we will discuss the consequences of Drosophila *cac* splicing at these sites for presynaptic function.

Exon IS4B is required for sustained HVA current and presynaptic AZ localization

Mutually exclusive splicing in the 4th transmembrane domain of the first homologous repeat (*IS4*) yields either *IS4A* or *IS4B*. Our data show that the *IS4B* exon is required for presynaptic AZ localization of cac and for evoked synaptic transmission at a fast glutamatergic synapse, the Drosophila NMJ. Accordingly, excision of the *IS4B* exon is embryonic lethal. This is in accordance with the finding that the only cac knock-in construct that has ever been reported to rescue lethality of Drosophila *cac* null mutants contains the *IS4B* exon (*UAS-cac1*; Kawasaki et al. 2004). The other alternative exon at the *IS4* site, *IS4A*, is not sufficient to mediate presynaptic AZ localization, does not contribute to evoked synaptic transmission at fast synapses, but it gives rise to functional cacophony channels that localize to other neuron types and neuronal compartments. Therefore, the absence of cac^{IS4A} isoforms from presynaptic AZs at the NMJ is not a consequence of general channel degradation upon excision of *IS4B*, but of exon specific channel localization. In fact, cac^{IS4A} isoforms are expressed sparsely but in stereotypical patterns in the larval brain and VNC (see suppl. Fig. 1). Moreover, in the absence of IS4B isoforms, cac^{IS4A} channels mediate somatodendritic calcium current in adult motoneurons. By contrast, cac^{IS4A} isoforms are not detectable in presynaptic boutons at the larval NMJ. Accordingly, animals with excision of *IS4A* show normal neuromuscular transmission.

Our voltage clamp recordings from motoneuron somata show that splicing in the 4th transmembrane domain, where the voltage sensor is located, affects cac activation voltage. Removing the *IS4B* exon virtually abolishes fast activating, sustained cac mediated HVA current. We infer that *IS4B* containing cac mediate fast activating, sustained HVA current also in presynaptic AZs, although we cannot exclude the possibility that cac^{IS4B} interacts with different accessory calcium channel subunits or with different other proteins to give rise to macroscopically different calcium currents, depending on whether the cac α_1-subunit localizes to presynaptic AZs, or to other subcellular compartments. However, fast activating, sustained HVA current is in accordance with the demands of the Drosophila larval NMJ that transmits burst of ~200 ms duration with action potential frequencies of ~120 Hz during crawling (Kadas et al. 2017). Fast voltage gated activation of sustained HVA calcium current with fast inactivation upon repolarization is useful at large intraburst firing frequencies without excessive cac inactivation. Our somatic voltage clamp recordings further demonstrate that *IS4B* is not only essential for evoked synaptic transmission, but cac with the *IS4B* exon can also give rise to somatodendritic HVA current. Therefore, the *IS4B* exon is essential for presynaptic function but it can also give rise to cac currents in other neuronal compartments and it is abundantly expressed throughout VNC neuropils. By contrast, the cac^{IS4A} channels are not expressed in NMJ presynaptic terminals, but they show a reproducible sparse expression pattern in some VNC regions, thus likely mediating some distinctly different functions that are yet uncharacterized. An abundant function of IS4B channels in presynaptic AZs of fast chemical synapses is in line with strong protein detection in Westerns from brains, whereas the sparse expression of IS4A in distinct sub-regions of the CNS is in line with a faint band in Western Blots.

I-II exon alternative splicing fine-tunes presynaptic function

In contrast to the *IS4* exon, mutually exclusive splicing in the intracellular loop between the first and the second homologous repeats (I-II) does not affect cac localization in AZs at the NMJ. In fact, >95 % of all presynaptic AZs contain both, cac isoforms with I-IIA and cac isoforms with I-IIB. Single on-locus alternative exon removal at the *I-II* site allows the study of presynaptic cac channel function with only one of the mutually exclusive I-II exons. Removal of *I-IIA* (*ΔI-IIA*) leaves 8 isoforms that contain *I-IIB*. This does not affect cac localization or channel number in presynaptic AZs as compared to control. However, half amplitude width of evoked EPSCs is significantly decreased whereas median amplitude of evoked EPSCs is increased from ~115 nA to ~130 nA, although the amplitude increase is statistically just not significant (one sided Mann Whitney U-test,

p = 0.078). Together a slight amplitude increase and a decreased half width likely cancel out changes in EPSC charge. Similar channel numbers and localizations but altered EPSC amplitudes and shapes could potentially be caused by different cac properties in the absence of *I-IIA* as compared to control. Specifically, decreased EPSC half width could be caused by significantly faster channel inactivation kinetics, and slightly increased single channel conductance may increase EPSC amplitude. Alternatively, altered EPSC width and amplitude could also be caused by changes in presynaptic action potential shape or postsynaptic glutamate receptor properties or compositions. Although we found no difference in GluRIIA abundance between *ΔI-IIA* and control, we cannot exclude other changes in postsynaptic receptor fields. However, given that *I-IIA* excision primarily affects the relative abundance of I-IIA and I-IIB cac in the presynaptic AZ but not mean channel number, given that postsynaptic VGCCs in muscle are encoded by the Drosophila *Ca_v1* and *Ca_v3* homologs, and given that cac channels localize to axon terminal AZs, we consider altered properties of different cac isoforms a possible explanation for altered EPSC properties upon *I-IIA* excision. During repetitive firing, the median increase of EPSC amplitude by ~10 % is potentially counteracted by the significant decrease in EPSC half amplitude width by ~25 %, so that neither paired pulse ratios, nor synaptic depression show significant differences between control and *ΔI-IIA*. Even for stimulus trains that mimic intraburst motoneuron activity as observed during restrained crawling in semi-intact preparations (Kadas et al. 2017), there is no difference in charge transfer from the motoneuron axon terminal to the postsynaptic muscle cell between *ΔI-IIA* and control. Surprisingly, crawling is significantly affected by the removal of *I-IIA*, in that the animals show a significantly increased mean crawling speed but no significant change in the number of stops. Given that the presynaptic function at the NMJ is not strongly altered upon *I-IIA* excision, and that *I-IIA* likely mediates also cac functions outside presynaptic AZs (see above) and in other neuron types than motoneurons, and that the muscle calcium current is mediated by *Ca_v1* and *Ca_v3*, the effects of *I-IIA* excision of increasing crawling speed is unlikely caused by altered pre-or postsynaptic function at the NMJ. We judge it more likely that excision of *I-IIA* has multiple effects on sensory and pre-motor processing, but identification of these functions is beyond the scope of this study.

Removal of *I-IIB* (*ΔI-IIB*) leaves 10 cac isoforms that contain I-IIA. This does not affect presynaptic AZ localization of cac or the proximity to the AZ scaffold protein brp (Kittel et al. 2006), but it significantly reduces P_r by ~ 50 %. This bisection in P_r is correlated with a 50 % reduction in the number of cac channels in AZs from about 10 to about 5, as determined by tagged cac fluorescence intensity measurement in fixed specimen and by live sptPALM counting of cac^{mEOS4b} (Heck et al. 2019; Ghelani et al. 2023). These data suggest that P_r is nearly linearly related to the number of VGCCs in the presynaptic AZ, at least at 0.5 mM external calcium which we mainly used for this study. Please note that the relation between external calcium and P_r at the Drosophila NMJ has been reported non-linear at external calcium concentrations above 1.5 mM, but linear between 0.5 and 1.5 mM (Weyhersmüller et al. 2011). Accordingly, at 1.5 mM external calcium a linear correlation between P_r and tagged cac channel fluorescence intensity has recently been reported (Medeiros et al. 2024). This also corresponds to observations at the mammalian calyx of Held, where the number of AZ VGCCs correlates linearly with P_r, and moreover, influences whether subsequent release is depressed or facilitated (Sheng et al. 2012). Similarly, in synapses with fewer cac channels upon *I-IIB* excision, we find a significant decrease in P_r along with a significant reduction in paired pulse ratio (PPR). The effects on PPR can by fully attributed to reduced channel numbers in presynaptic AZs upon *I-IIB* excision, because they can be fully rescued by triturating the external calcium concentration so that the first pulse amplitude matches that of controls with normal P_r. Therefore, regulation of VGCC number in presynaptic AZs may be a conserved mechanism to tune P_r and short-term plasticity from flies to mammals.

At the Drosophila NMJ a steep gradient of synaptic transmission amplitude exists along the motoneuron axons over their target muscle fibers, with the highest presynaptic Ca^{2+} influx in most distal presynaptic sites along the axon. This has been interpreted as gradient control of P_r along the axon of the same neuron (Guerrero et al. 2005), which is at least in part regulated by

the balance of different release enhancing and suppressing proteins at proximal versus distal release sites, such as complexin (Newman et al. 2022). Another potential means to regulate P_r at different release sites of the same neuron could be uneven ratios of I-IIA and I-IIB cac isoforms, which requires additional analysis. The prediction would be that the more distal the release site the more I-IIB channels are expressed. Given that these have a highly conserved Ca_β binding motif, targeting to distal release sites might be promoted in comparison to I-IIA channels with a less conserved Ca_β binding motif (Smith et al. 1998).

The reduction in AZ cac number upon removal of *I-IIB* has three additional important functional consequences. First, reduced P_r and charge transfer across the NMJ during crawling-like motoneuron bursting patterns are reflected in a significant decrease in mean crawling speed and a highly significant increase in the number of stops, whereas maximum crawling speed is not affected. Unaffected maximum speed at significantly reduced P_r indicates that the charge transfer at high motoneuron intrabust firing frequencies is above the one needed for maximum muscle contraction. Moreover, mean speed is significantly but just slightly decreased upon removal of *I-IIB* and a highly significant reduction in P_r, whereas the number of stops is increased highly significantly by ~50 %. It seems likely that large effects on the continuation of motor behavior but only mild effects on the speed are caused not only by effects on synaptic transmission at the NMJ but also by effects on other neuronal compartments or on other neurons in sensory or premotor circuitry. This interpretation would be in accordance with the finding that cac currents are also measured from the somatodendritic domain of pupal and adult Drosophila (this study) and that larval Drosophila motoneuron excitability as measured by I/F relationships are altered upon *cac*-RNAi (Worrell, Levine, 2008). Second, removal of *I-IIB* increases the variability of paired pulse ratio and the time course of synaptic depression, but this is solely due to reduced channel numbers upon *I-II* excision, because the effect is rescued by increasing the external calcium concentration. It seems plausible that mechanism with probabilistic features, such as cac activation/inactivation/de-inactivation as well as Ca_v2 channel mobility in AZs (Heck et al. 2019; Ghelani et al. 2023) exert a higher impact with fewer channels. Therefore, increasing variability of presynaptic function might be another consequence of reduced AZ cac number upon *I-IIB* excision. And third, removal of *I-IIB* abolished the ability of both initiation and maintenance of presynaptic homeostatic potentiation (PHP), which in turn, requires an upregulation of the number of cac and of brp molecules in the presynaptic AZ (Ghelani et al. 2023; Gratz et al. 2019). Similarly, PHP is also blocked in cac hypomorphic mutants which also reduce EPSC amplitude, likely due to reduced calcium influx (Frank et al., 2006), thus indicating that fast PHP induction might not be possible with reduced calcium conductance in AZs. Similarly, increased calcium influx into the presynaptic AZ after induction of PHP (Müller, Davis 2012; 2015) fits with an increase in cac channel number. Increasing the number of $cac^{I\text{-}IIA}$ in AZs as a compensatory response to reduced postsynaptic receptor function seems not likely with reduced Ca_β binding affinity, or in the face of fewer channels to start with, or for additional reasons, which will require additional studies.

In summary, our study suggests mutually exclusive splicing at two *cac* splice sites, that do not exist in mammals, as an alternative strategy to increase functional heterogeneity at the presynaptic AZ of fast chemical synapses, so that the Drosophila *Ca_v2* homolog *cacophony* may portrait some of the functional heterogeneity that arises in mammals from the combinatorial usage of $Ca_v2.1$, $Ca_v2.2$, and $Ca_v2.3$. Splicing at the first Drosophila mutually exclusive site directs cac to different subcellular compartments and tunes cac biophysical properties. Splicing at the second mutually exclusive site does not direct cac to different subcellular compartments, but it fine tunes multiple aspects of presynaptic function by changing presynaptic AZ channel numbers or ratios between cac splice variants.

Methods

Generation of CRISPR flies

Exon excision was performed via the CRISPR/Cas9 method (Doudna and Charpentier, 2014; Sternberg and Doudna, 2015). Cacophony is located on the X-chromosome in Drosophila. Cac^{sfGFP} exon out flies were generated by crossing female virgin flies expressing super folder GFP (sfGFP)-tagged cac (C cac^{sfGFP}, Gratz et al. 2019) channels along with the Cas9 enzyme under the control of the germ line active *nanos*-promoter (*nos-cas9*, Bloomington stock center #78781) to male flies expressing a *gRNA* transgene under the control of the germ line active *U6*-promoter. The *gRNA* sequences were designed such to specifically target sequences flanking the exon to be excised (see **table 1**). CRISPR events take place as soon as both *nos-cas9* as well as *U6-gRNA* transgenes are present in the same fly, no matter whether these flies are male or female. For simplicity, for excision of exons *IS4A*, *I-IIA*, and *I-IIB*, male progeny were collected as such flies are hemizygous vital, whereas for excision of *IS4B*, females were collected because removal of *IS4B* is lethal. Flies were then back-crossed into suitable balancer strains to keep the X-chromosome with the putative cac exon excision and to be able to follow out-crossing of *nos-cas9* or *U6-gRNA* transgenes. Successful exon excision was confirmed with single fly genomic PCR with suitable primers and Taq DNA polymerase (New England Biolabs, #M0267S) (for cycler (Biorad T100 thermo cycler) settings and primers see **tables 2** and **3**) and subsequent 1% agarose gel electrophoresis. Gene sequence around the excision was confirmed with next generation sequencing (StarSeq, University of Mainz Campus with the exon out verification primers, see **table 3**). Gels were run at 100 V for 45 minutes. Primers were obtained from Integrated DNA Technologies, Germany. To minimize contamination of exon out fly stocks, successful excision mutants were cantonized for at least 5 generations to enhance the likelihood of outcrossing of undesired mutations due to CRISPR off-target events. To clean up the X-chromosome itself on which the desired CRISPR event took place, flies were subjected to recombination with Canton S flies. Lack of the desired exon was then re-confirmed by PCR again.

Generation of gRNA transgenic flies

First, the eligibility for Cas9 cleavage was assessed, core properties are the protospacer adjacent motif (PAM) NGG flanking the 20 bp *gRNA* (see **table 1**) to facilitate site recognition, and a 5' G as the vector used for *gRNA* expression later used the *U6*-promoter. Moreover, CRISPR sites must not disrupt recognition sites for the splicing machinery. For this, online tools were used (CRISPR target finder: Gratz et al. 2014, *http://targetfinder.flycrispr.neuro.brown.edu/index.php* and Cas9 target finder: *https://shigen.nig.ac.jp/fly/nigfly/cas9/cas9TargetFinder.jsp*). Sites for double strand breaks were picked at a distance from the intron/exon borders to not affect splice acceptor sites. Furthermore, sites known to impact splice efficiency (Blanchette et al. 2005; Brooks et al. 2011) were avoided. In addition, sites for minimal loss of total genomic region were determined and the *gRNA* sequences with as few as possible predicted off-target cleavage sites were selected.

Fly rearing

Flies were kept at 25°C in 25 mm diameter plastic vials with mite proof foam stoppers on a cornmeal, yeast, agar, glucose diet on a 12 hr light/dark regimen. Wandering L3 larvae were collected directly from food vials. 2-day old adult flies were collected from their food vials and placed on ice in pre-chilled empty food vials for no more than 1 minute prior to dissection (for patch clamp recordings).

target exon	pre-exon	post exon
IS4A	**cca**atatcacctatg|tttaagtc	gttgctac|taccaaaaacct**agg**
IS4B	**ccg**aaactatagagt|gactgacc	gtggcaca|tgattgtcgtgg**agg**
I-IIA	gctacgtg|catgtgcataca**cgg**	**cca**agtaaactgcca|taatcaac
I-IIB	**cca**gtaaatgatttc|gactttct	**ccc**ccatatgttcat|ccacatcc

Table 1

gRNA sequences used for cas9 target site.

Vertical lines depict intended break points. Bold and underlined nucleotides indicated PAM (protospacer adjacent motif) sequences.

Table 2

Cycler settings for exon out verification.

Step	temperature		duration
1	95°C		3:00 min
2	95°C		0:30 min
3	57°C	-1°C per cycle	0:45 min
4	68°C		1:30 min
5	Go to step 2	10x	
6	95°C		0:30 min
7	52°C		0:45 min
8	68°C		1:30 min
9	Go to step 6	24x	
10	68°C		5:00 min
11	4°C		∞

Table 3

Exon out verification primers

excised exon	forward primer	reverse primer	expected band size with/without exon
IS4A	CACGCCGTGCAAGCATTATC	CCTAAATTCGTGGCTACCAC	988 bp/482 bp
IS4B	CTGTGTGTGATTCTCGCGAC	CCGTTCCGATTCGATCCAG	1305 bp/340 bp
I-IIA	GCCACTTCTACACCAGTTCAC	GAACTCTTTGTAGCCGGG	951 bp/571 bp
I-IIB	CTCATTGAAGGTTCCCGTC	GGAGAGGGATGCTAAGAATG	954 bp/446 bp

Flies

For electrophysiological recordings as well as for immunohistochemical labeling, sfGFP-tagged cac flies were used. First, validity of sfGFP-tagged cac channel flies was confirmed by comparing w^+ TI{TI}$cac^{sfGFP-N}$ flies with the wildtype strain Canton special (Canton S). After that, the control strain for all sfGFP-tagged exon out flies was w^+ TI{TI}$cac^{sfGFP-N}$

Exon out flies were w^+ TI{TI}$cac^{sfGFP-N\ \Delta IS4A}$, w^+ TI{TI}$cac^{sfGFP-N\ \Delta IS4B}$/FM7c P{2x Tb-RFP}, w^+ TI{TI}$cac^{sfGFP-N\ \Delta I-IIA}$, w^+ TI{TI}$cac^{sfGFP-N\ \Delta I-IIB}$. All CRISPR fly strains were originally white mutant. To reduce the likelihood of accumulation of off-target effects resulting from CRISPR events, we replaced the mutant white gene on the X-chromosome (on which *cacophony* is also located) by a Canton S derived wildtype white gene from our Canton S lab stock that we also used as control (see above). In addition, after CRISPR events, flies were crossed to remove nos-Cas9 and gRNA transgenes on the 2^{nd} chromosome and replaced these chromosomes by ones without transgenes or other known mutations. This first removed transgenes that were needed for CRISPR induction and second, this also removed possible off target events on the 2^{nd} chromosome. In the process, 3^{rd} and 4^{th} chromosomes were replaced automatically as well. We back crossed with Canton S strains for at least 5 generations. Thus, off-target chromosomal aberrations were minimized by recombination on the X-chromosome and by replacement of all other chromosomes by out-crossing.

For channel counting and for assessment of cac^{I-IIA} and cac^{I-IIB} expression in AZs (both see below), we used exon out flies that carried mEOS4b endogenously directly after the start codon of *cacophony* (Ghelani et al. 2023). mEOS4b-tagged exon out fly strains were: w* TI{TI}$cac^{mEOS4b-N}$ w* TI{TI}$cac^{mEOS4b-N\ \Delta I/IIA}$, w* TI{TI}$cac^{mEOS4b-N\ \Delta I/IIB}$. All mEOS4b-tagged fly strains were white mutant.

For GluRIIA immunohistochemistry, transgenic flies expressing $GluRIIA^{GFP}$ under a native promoter were used (Rasse et al. 2005).

Western Blots

For proof of protein expression after exon excision, Western Blots were performed with detection of the N-terminal sfGFP tag (due to lack of cacophony antibodies). As loading control, β-actin was used. Cacophony bands were expected above 250 kDa (cacophony plus GFP) and actin was expected at 42 kDa. For viable exon excision mutants (cac^{sfGFP} as control, $cac^{sfGFP\ \Delta IS4A}$, $cac^{sfGFP\ \Delta I-IIA}$, $cac^{sfGFP\ \Delta I-IIB}$), 10 adult male brains per lane were prepared, for lethal exon excisions (Canton S as control, cac^{sfGFP}/+, $cac^{sfGFP\ \Delta IS4B}$/+), 20 adult female brains of heterozygous animals were used. Brains were dissected with forceps one by one and collected in 23 µl squishing buffer (composition below) in 0.5 ml low bind sample tubes on ice. When 10 or 20 brains, respectively, were collected, samples were squished with a sterile pestle using a motorized squishing device. After squishing, 3 µl sample buffer (composition below) were added to the homogenized samples, which were subsequently boiled at 95°C for 5 min. Samples were then stored at –30°C until use. For loading, samples were taken out of the freezer, boiled for 3 minutes at 95°C and directly loaded into a 10 well Mini-Protean TGX Precast Gel with a 4-15% polyacrylamide gel gradient with 50 µl volume per well (Biorad, Cat#456-1084). The gel was run in running buffer (composition below) for 2h 40 minutes at 80 V. As protein marker, 8 µl Spectra Multicolor High Range Ladder (Thermo Scientific, Cat# 26625) was used. Transfer was done in transfer buffer (composition below) on nitrocellulose membrane overnight at 35 V with a cool block and the setup sitting in an ice box. Next day, the nitrocellulose membrane was washed with TBS-Tween20 and then subjected to blocking with Intercept T20 Antibody Diluent (LI-COR, Cat#927-65001) diluted 1:1 with 0.1M PBS for 2 hrs. Then the nitrocellulose membrane was cut horizontally to subject the pieces with the expected cacophony bands and the expected loading control (β-actin) separately to antibody labeling. This was followed by primary antibody incubation with 1:500 polyclonal rabbit anti-GFP

antibody (Thermo Fisher Scientific, Cat# A11122) or 1:10,000 monoclonal mouse anti-actin (DSHB, JLA20) diluted in Intercept T20 Antibody Diluent (see above), first for 2 hrs at room temperature and then for two nights at 4°C. Then antibody solution was removed and membrane washed 3× 15 minutes with TBS-Tween20. This was followed by incubation with secondary antibodies diluted in Intercept T20 Antibody Diluent for 2 hrs at room temperature in the dark with IRDye 680 donkey anti-rabbit (LI-COR, Cat# 926-68073) at 1:10,000 to detect GFP-tagged cacophony bands, or IRDye 800 donkey anti-mouse 1:10,000 to detect β-actin, respectively. This was followed by 2× 15 minutes washes with TBS-Tween20 and then 1× 15 minutes with 0.1M PBS to reduce background. Bands were detected with a LI-COR Odyssey Fc Imaging System with 30 second or 2 minutes exposure times.

Western Blot solutions

Lyse buffer: 25 ml 4xTris-HCl/SDS pH 6.8, 20 ml glycerol, 4 g SDS, 1 mg bromophenol blue.

6x sample buffer (10 ml): 0.3 M Tris-HCl pH 6.8, 8% SDS, 50% glycerol, 0.25% bromophenol blue. 8% mercapto-ethanol was added fresh directly before use.

10x SDS running buffer: 30 g Tris Base (pH 8.3), 150 g glycine, 10 g SDS. Add ddH_2O to 1000 ml total volume.

Transfer buffer: 15.5 g Tris Base, 72 g glycine, 1000 ml methanol, 5000 ml ddH_2O.

Dissection for electrophysiology and immunohistochemical labeling

Third instar larvae were dissected in HL3.1 saline (composition below). Larvae were fixed dorsal side up to a Sylgard (Sylgard 184, DowCorning) coated lid of a 35 mm Falcon dish with two insect minuten pins through the mouth hook and through the tail. After covering the larva with saline (composition below), the body wall was cut along the dorsal midline. To obtain a filet preparation, the body wall was spread laterally and fixed with two minuten pins on each side. Gut and trachea were removed as well as the ventral nerve cord. For electrophysiology from the larval NMJ (see below: electrophysiology), the motor nerves were left long, for immunohistochemical labeling (see below: immunohistochemistry), the motor nerves were cut very short.

Adult flies were dissected in normal saline (composition below – but calcium current recordings were performed with different external solution – composition and electrophysiology see below). Adult two-day old female flies were anaesthetized briefly on ice in pre-chilled empty fly rearing vials. Then legs and wings were removed and the fly fixed dorsal side up in a Sylgard coated lid of a 35 mm Falcon dish with two insect minute pins through the head and through the tip of the abdomen. After covering the fly with saline (composition below), the cuticle was cut along the dorsal midline. To expose the ventral nerve cord with the motoneurons, the thoracic cuticle with the cut wing depressor muscle (DLM) was spread laterally and pinned down with one minuten pin on either side. After removal of gut, esophagus, and salivary glands, the ventral nerve cord was exposed.

Electrophysiology

All electrophysiological recordings were carried out at room temperature (~ 22°C). For TEVC recording microelectrodes were pulled with a Sutter Flaming Brown P97 microelectrode puller from borosilicate glass capillaries with filament, with inner diameter of 0.5 mm, and an outer diameter of 1 mm (Sutter BF100-50-10 or World Precision Instruments 1B100F-4). Patch pipettes were pulled with a Narishige PC10 electrode puller from borosilicate glass capillaries without filament, with an inner diameter of 1 mm, and an outer diameter of 1.5 mm (World Precision Instruments PG52151-4).

TEVC of muscle 6 or muscle 12 in the larval body wall

For two electrode voltage clamp (TEVC) recordings, dissected third instar larvae (see dissection) were placed on an upright Olympus BX51WI fixed stage microscope with a 20x water dipping lens (Zeiss LD A-Plan). The motor nerves of either segment A2 or A3 on the left or the right side was sucked into a glass microelectrode filled with saline with an individually broken tip. After placing the recording electrodes filled with 3 M potassium chloride (KCl) and the ground wire (chlorinated silver) into the recording solution (HL3.1 saline, composition see below), both electrodes were nulled against the ground electrode (bridge mode) using an Axoclamp 2B intracellular amplifier (Molecular Devices). Then the muscle (M6 or M12) cell was first impaled with the larger tip current passing glass microelectrode (~8 – 13 MΩ) directly followed at a small distance by the smaller tip recording electrode (~20 – 30 MΩ). If both electrodes recorded a membrane potential of at least –50 mV without differing by more than 3 mV, RMP balance was adjusted and then TEVC established by pressing the respective knob on the amplifier. Gain was set between 8 and 25. Anti-alias filter was set to ½ the sampling rate to minimize noise. Then the desired command potential was set, mostly at –70 mV. Holding current needed to keep the membrane potential at the desired –70 mV had to be below 4 nA, otherwise recordings were discarded. Data were digitized at 50 kHz (Digidata 1550B, Molecular Devices) and recorded with pClamp 11.1.0.23 software package (Molecular Devices). Data were filtered offline with a lowpass Gaussian Filter with a –3 dB cutoff frequency of 360 Hz.

The suction electrode with the motor nerve was connected to a pulse generator (A-M Systems Model 2100) to deliver low voltage (up to 10 V) 0.1 ms duration stimulations at varying patterns. Stimulation voltage was adjusted slowly to be sure that both motor axons innervating the recorded muscles were stimulated. This was determined unequivocally by the transmission amplitude, which is distinctly smaller if just one motor axon is stimulated as compared to stimulation of both motor axons.

For recordings of miniature excitatory postsynaptic currents (mEPSCs), spontaneous occurrence of mEPSCs was recorded for one minute without stimulation. For single evoked excitatory postsynaptic currents (EPSCs), the motor nerve was stimulated at 0.1 Hz frequency for 50 seconds and the amplitude was recorded. Mean quantal content was determined by dividing the mean amplitude of several EPSCs of one recording by the mean amplitude of several mEPSC of the same recording. For short term plasticity, paired pulses (PPs) were recorded by stimulation of the motor nerve twice with varying interspike intervals (IPIs) of 10 ms, 15 ms, 20 ms, 25 ms, 30 ms, 50 ms, and 100 ms (applied in that order with intersweep intervals of 10 s). Paired pulse ratios (PPRs) were calculated by dividing the amplitude of the second pulse by that of the first pulse. Mean PPR values are based on the PPRs of each sweep and then averaged and also by first averaging the amplitudes of all first and all second pulses separately, to then divide the mean of the second by the mean of the first amplitude. In contrast to work on pyramidal neurons (Kim and Alger 2001) in our data PPRs not different depending on these two analysis schemes. Short term facilitation or short term depression were induced by 60 s stimulation at 1 Hz or by 1s stimulation at 10 Hz or by 200 ms stimulation at 60 Hz and 120 Hz stimulation frequency. For each animal the amplitudes of all subsequent EPSCs in each train were plotted over time and fitted with a single exponential. For depression at 1 and 10 Hz, we used one train per animal, and 5-6 animals per genotype. Motoneuron burst firing as occurring during crawling (Kadas et al. 2017) was simulated by higher frequency stimulation for 200 ms at 60 Hz and 120 Hz.

Presynaptic homeostatic potentiation (PHP) was induced either acutely by application of the bee wolf toxin Philanthotoxin 433 or by using animals carrying a null mutation in the GluRIIA glutamate receptor that is expressed in the muscle membrane. PhTx (10 µM) is applied in calcium-free HL3.1 saline (composition see below) after dissection but before mounting the preparation on the microscope stage. For the toxin to work properly, it must be applied after cutting the animal open along its dorsal midline but prior to spreading the larval body wall laterally (see dissection).

The larva must be fixed with two minuten pins through the mouth hooks and the tail but without stretching the animal and without removing any inner organs yet. The preparation is bathed in the toxin solution for 10 minutes. After rinsing the preparation with HL3.1 saline, the body wall is spread laterally and dissected as described above (see dissection), and the specimen is mounted on the microscope stage ready for recording.

Synaptic transmission on muscle M6 in segment A2 and A3 was assessed in male animals carrying excisions of either *IS4A*, *I-IIA*, or *I-IIB* in cac on their only X-chromosome. Animals lacking exon *IS4B* are homozygous lethal. Thus, we used heterozygous females that expressed cac with *IS4B* excision on one X-chromosome over a $cac^{FLPStop}$ construct which contains a tdTomato reporter followed by a stop codon within the open reading frame of all cac variants upon expression of a flipase transgene. Briefly, a reverse stop cassette followed by UAS-tdTomato flanked by canonical FRT sites of opposing orientation is inserted within a MiMIC residing in an intron of the Drosophila cac channel gene *cacophony*. Presence of canonical flipase turns the entire FlpStop-tdTomato cassette around and-re-inserts it in frame, which leads to pre-mature termination of cac transcription that is reported by tdTomato (Fisher et al. 2017). We expressed UAS-flipase under the control of the OK6 (Rapgap1)-GAL4 driver (Sanyal 2009), that drives expression of UAS-transgenes also in larval crawling motoneurons.

However, in our hands, flp events happen in a more or less stochastic manner. Flp events in motoneurons on M6 are less reliable as compared to Flp events on M12. As it is necessary that the FlpStop technique works in all motoneurons that innervate a target muscle to investigate the role of the IS4B exon for synaptic transmission, we used M12 (left and right) in A3 for this experiment rather than M6.

Whole cell voltage clamp recordings

To investigate calcium currents that remain upon excision of IS4B, we used the same FlpStop approach as for synaptic transmission at the larval NMJ. UAS-flipase was expressed under the control of a DLM (dorsal longitudinal muscle) motoneuron Split-GAL4 fly strain that targets mainly the 5 wing depressor motoneurons (MN1-5) on each side of the body (10 neurons total, Hürkey et al. 2023). Expression of UAS-flipase under the control of this Split-GAL4 driver reliably led to expression of tdTomato in these motoneurons. In addition these flies are flight-less.

Adult MN patch clamp experiment were carried out as previously reported (Ryglewski et al. 2012). After dissection, the fly was positioned under a 40x water dipping lens (Zeiss, W Apochromat 40x/1.0 DIC VIS-IR ∞/0) on a fixed stage Zeiss AxioExaminer A1 upright fluorescence microscope. MN5 is situated on the dorsal surface of the ventral nerve cord in the mesothoracic neuromere. For whole cell voltage clamp recordings from MN5, protease was applied focally by alternating positive and negative pressure applied through a broken patch pipette to clean the membrane of the MN5 soma to facilitate seal formation. After cleaning, the preparation was perfused constantly with fresh saline (composition below). Voltage gated potassium channels were blocked by TEA, 4-AP and cesium in the recording solution (composition below). Tetrodotoxin (TTX, 10^{-7} M) to block voltage gated sodium channels was applied directly to the recording chamber while perfusion was halted for 3 minutes before approaching the cell with the patch pipette. Then perfusion resumed. Patch pipettes were filled with internal patch solution (composition below) and had resistances of ~ 3.5 – 4 MΩ with this combination of internal and external solution. Recordings were carried out with an Axopatch 200B patch clamp amplifier (Molecular Devices). Data were digitized at 50 kHz (Digidata 1440, Molecular Devices) and filtered at 5 kHz through a lowpass Bessel filter. Data were recorded with pClamp 10.7.0.3 software package (Molecular Devices). After giga seal formation, whole cell configuration was achieved by a brief application of negative pressure to the patch pipette. We allowed 2 minutes for solution exchange with the cell interior and stabilization of the recording before adjusting whole cell capacitance and series resistance compensations and setting prediction at around 80% and

correction at around 45%. Holding potential was –70 mV between voltage clamp protocols. Voltage gated calcium currents were elicited by voltage command steps to +20 mV in 10 mV increments from a holding potential of –90 mV. Leak was subtracted offline.

Dissection and electrophysiology salines

Adult dissection saline [mM]: NaCl 128, KCl 2, $CaCl_2$ 1.8, $MgCl_2$ 4, HEPES 5, Sucrose ~35.5. Osmolality was adjusted to 300 mOsM/kg with sucrose. pH was adjusted to 7.24 with 1N NaOH.

Larval dissection saline HL3.1 calcium free [mM]: NaCl 70, KCl 5, $MgCl_2$ 4, $NaHCO_3$ 10, trehalose 5, sucrose 115, HEPES 5. Osmolality was adjusted to 300 mOsM/kg with sucrose. pH was adjusted to 7.24 with 1N NaOH.

TEVC recording saline HL3.1 [mM]: NaCl 70, KCl 5, $CaCl_2$ 0.5, $MgCl_2$ 4, $NaHCO_3$ 10, trehalose 5, sucrose 115, HEPES 5. Osmolality was adjusted to 300 mOsM/kg with sucrose. pH was adjusted to 7.24 with 1N NaOH.

Whole cell voltage clamp saline [mM]: NaCl 93.2, KCl 5, $MgCl_2$ 4, $CaCl_2$ 1.8, $BaCl_2$ 1.8, Tetraethylammonium (TEA) Cl 30, 4-aminopyridine (4-AP) 2, HEPES 5, sucrose ~35.5. Osmolality was adjusted to 300 mOsM/kg with sucrose. pH was adjusted to 7.24 with 1N NaOH.

Tetrodotoxin (10^{-7}M) in normal saline was applied directly to the recording chamber.

Whole cell voltage clamp intracellular solution [mM]: CsCl 144, $CaCl_2$ 0.5, EGTA 5, HEPES 10, TEA-Br 20, 4-AP 0.5, Mg-ATP 2. Osmolality was adjusted to 300 mOsm/kg with glucose. pH was adjusted to 7.24 with 1N CsOH.

mEOS4b-tagged cac channel counting

The calculation of cac channel splice form numbers in individual AZs of the NMJ are based on the photoconversion of the fluorescent tag mEOS4b fused to the N-terminus of the cac channel (cac::mEOS4b-N; Ghelani et al. 2023). Third instar larvae were used for a body wall dissection. This preparation was suitable to image individual AZs within single boutons of an NMJ. We focused on muscle 6/7 on large type Ib boutons (Jia et al. 1993). Experiments were conducted at 25°C with HL3.1 solution (composition see above). We used a TIRF setup based on an inverted microscope (Nikon Eclipse Ti) equipped with a 60x 1.49 NA oil immersion objective (Nikon). Image series of up to 5000 frames were acquired at a frame rate of 20 Hz, using a sCMOS camera (Hamamatsu, Orca flash 4.0) controlled by the NIS-Element acquisition software (Nikon). Labelling of the NMJ with an anti-HRP antibody (diluted 1:1000) directly tagged with Alexa-488 for 5 min was used to have an initial landmark for NMJs within the preparation. During imaging of cac channels, we use a 1.5 magnification lens to reduce the effective pixel size to 71 x 71 nm. The used illumination protocol started with an initial continuous illumination with a 561 nm laser (80 % of initial laser power of 100 mW) for 250 frames to reduce the autofluorescent background. Afterward, we triggered the photoconversion of mEOS4b by switching on the photoconversion with a 405 nm UV-laser (5% of initial laser power of 100 mW) in addition to the 561 nm laser. The UV-excitation was sufficient to convert the majority of mEOS4b molecules into the red fluorescent state that was read out by the 561 nm laser. With the dual excitation of 405 nm and 561 nm, synapses were imaged until complete bleaching of the cac::mEOS4b-N population. The ability of the TIRF setup to adjust the laser beam orientation in the specimen was used to obtain an oblique illumination profile that limited the contribution of out of focus fluorescence. The number of channels was calculated as ratio of the maximal fluorescent intensity shortly after starting the photoconversion and the fluorescence of single mEOS4b molecules, which occurred as stochastic blinking events in the second half of the illumination sequence (see **Fig. 4G**, Ghelani et al. 2023). Two-dimensional x-y movements of the NMJ was corrected by using the NanoJ-Core drift correction from the NanoJ-Plugin for ImageJ/Fiji (Laine et al. 2019). After background

subtraction, regions of 5×5 pixels were used to read out the fluorescence intensity profile of individual AZs. At least 30 AZs per ROI and larva were analyzed. For plotting the data and statistical calculations, we used Igor Pro 8 and GraphPad Prism 10.2.3.

Immunohistochemistry

For cacophony immunohistochemistry, L3 larvae were dissected as described above and the VNC along with the motor nerves were removed. The specimen was then fixed for 7 minutes in ice cold (−30°C) 100% ethanol. For this, the saline was replaced by ice cold ethanol and rinsed a few times to assure cooling down of the specimen. Then the preparation was kept in the freezer at –30°C for 7minutes. Afterwards, the specimen was treated with PBS 0.1M with 0.3 % TritonX (PBS-Tx) at room temperature for 3×10 minutes, rocking.

cac^{sfGFP} (Gratz et al. 2019) localization (**Figs. 2** and **3**): Primary antibodies (α-brp nc-82, 1:400, DSHB; α-HRP rabbit, 1:500, Jackson Immunoresearch Cat# 323-005-021) were applied in PBS-Tx 0.3 % overnight at 4°C, rocking. Next day, primary antibody solution was removed, the preparation rinsed a few times with PBS-Tx 0.3 % and then washed 3×10 minutes with PBS-Tx 0.3 % at room temperature, rocking. 2 hour application of α-GFP nanobody (Fluotag X4 α-GFP Alexa 647, Nanotag Biotechnologies, Germany, Cat# N0304-AF647) and secondary antibodies donkey α-mouse Alexa 555 (Jackson Immunoresearch, Cat# 715-165-151) and donkey α-rabbit Alexa 488 (Jackson Immunoresearch, Cat# 711-545-152), all at a concentration of 1:500 at room temperature.

Assessment of ΔI-IIA and ΔI-IIB channel expression: Primary antibodies (α-brp nc-82, 1:400, DSHB; α-mEOS rabbit, 1:500, Badrilla, Cat# A010-mEOS2) were applied in PBS-Tx 0.3 % overnight at 4°C, rocking. Next day, primary antibody solution was removed, the preparation rinsed a few times with PBS-Tx 0.3 % and then washed 3×10 minutes with PBS-Tx 0.3 % at room temperature, rocking. 2 hour application of α-GFP nanobody (Fluotag X4 α-GFP Abberior Star Red, Nanotag Biotechnologies, Germany, Cat# N0304-ABRED) and secondary antibodies donkey α-mouse Alexa 555 (Jackson Immunoresearch, Cat# 715-165-151) and donkey α-rabbit Alexa 488 (Jackson Immunoresearch, Cat# 711-545-152), all at a concentration of 1:500 at room temperature.

For $GluRIIA^{GFP}$ immunostaining, L3 larvae were fixed for 5 minutes in Bouin's solution at room temperature. Then 3×10 minute washed were performed with 0.3% PBS-Tx at room temperature. This was followed by primary antibody incubation with α-brp (nc-82, 1:400, DSHB) overnight-After 3 more 10 minute washes with PBS-Tx 0.3%, specimen were incubated with α-GFP nanobody (Fluotag X4 α-GFP Abberior Star Red, Nanotag Biotechnologies, Germany, Cat# N0304-ABRED) and secondary donkey α-mouse Alexa 555 antibody (Jackson Immunoresearch, Cat# 715-165-151) for 3 hours at room temperature, covered to protect from light.

All immunolabel: Preparations were covered to prevent bleaching of fluorophores. Then, antibodies were removed, the preparations were rinsed a few times, which was followed by 3×10 minutes PBS (no Tx). Then an ascending ethanol series with 10 minues each with 50, 70, 90, 100 % ethanol was applied at room temperature, rocking. Preparations were then mounted in methylsalicylate, covered with a high precision cover slip that was sealed with clear nail polish. Preparations were kept in the dark until scanning with a Leica TSC SP8 upright confocal laser scanning microscope with a 40x oil NA 1.3 oil lens. Overviews were scanned without zoom at 1 µm z-step size. Magnifications were scanned with a 3.5 zoom with z-steps of 0.3 µm. All scans were done with a 3x line average.

Assessment of fluorescence intensity

For fluorescence intensity measurement of sfGFP tagged cac channels in larval AZs, immunohistochemical labeling was carried out as for localization of cac channels. The only difference was that each round contained animals of all genotypes that were assessed. Animals

were treated in the identical dish at the same time to ensure identical treatment. Confocal images were acquired with identical settings (lasers, detectors, scanning speed).

Fluorescence intensity was compared between genotypes by employing a custom Python script (available at doi://10.5281/zenodo.11299005) in which we used brp labeling (nc-82 antibody, DSHB) as a mask and asked for cac intensity within this mask. Intensity was then normalized to control. brp intensity was assessed identically.

GluRIIA fluorescence intensity was assessed identically, but as GluRIIA fields are larger than brp, we inflated the brp mask to encompass GluRIIA label. We then used the aforementioned python script to quantify intensity. For GluRIIA label we used flies that expressed a $GluRIIA^{GFP}$ transgene that was previously shown to exhibit native GluRIIA expression levels (Rasse et al. 2005)

Colocalization of cac and brp scaffold protein

To determine the Pearson's correlation coefficient and the Manders co-occurrence coefficients of cac and brp stainings using the Costes' threshold calculation (Manders et al. 1993; Costes et al. 2004) a custom Python script was utilized (available at doi://10.5281/zenodo.11299005).

In image stacks triple stained for cac, brp and HRP that had been deconvolved with the software Huygens, HRP staining served as a mask in which the desired coefficients were calculated for cac and brp.

Super resolution microscopy (STED) and deconvolution

STED images were acquired at a Leica Stellaris 8 STED system (*Leica microsystems*) equipped with a pulsed white light laser (WLL) for excitation ranging from 440 to 790 nm and a 775 nm pulsed laser for depletion. Samples were imaged with a 93x glycerol objective (*Leica,* HC APO 93x/1.30 GLYC motCORR). For excitation of the respective channels the WLL was set to 640 nm for FluoTag-X4 anti-GFP Atto647N (NanoTag Biotechnologies, Cat# N0304-At647N) or 580 nm for Abberior Star 580 conjugated FluoTag-X2 anti-mouse antibody (NanoTag Biotechnologies, Cat# N2702-Ab580). Emission were detected in between 650-710 nm for Atto647N and in between 590-640 nm for Abberior Star 580. STED was attained by using the 775 nm laser for both channels. Additionally a 3rd confocal channel was acquired (HRP, not shown, labeled with rabbit α-HRP antibody, Jackson Immunoresearch Cat# 323-005-021) by using 488 nm light for excitation of Alexa488 (Jackson Immunoresearch, Cat# 711-545-152) and an emission band of 500 – 530nm. Scanning properties were set to a format of 1024×1024 pixels, optical zoom factor to 5 (x/y=24.44 nm, z=191.69 nm) and scanning speed to 400 lines per second. Detectors were operated in in photon counting mode for both channels by 3 times line accumulation. For $_{gated}$STED, detector time gates were set to 0.5-6 ns for both channels.

Deconvolution of STED stacks was done with Huygens Essential (*Scientific Volume Imaging, The Netherlands, http://svi.nl*). Within the *Deconvolution wizard*, images were subjected to background correction. *Signal-to-noise ratio* was set to 20*. The Optimized iteration mode of the CMLE* was applied by using 40 Iterations.

Behavioral experiments

Wandering L3 larvae were selected off vial walls for crawling experiments and starved in empty vials for 5 minutes. Afterwards, they were placed in the middle of a plasticine square on an agarose gel (1% in H_2O) using a brush. This square itself was placed on a tracking table with an acrylic glass plate. Usually, 10 larvae of the same genotype were recorded at a time. Occasionally, less than 10 larvae were available, in which case fewer larvae were recorded. Dishes were freshly poured each day before starting experiments. To prevent the larvae from escaping the boundary, an electrically charged wire was placed inside the square boundaries. Crawling pictures were

obtained with a camera (Basler acA2040-90µm) from below the glass plate at a frame rate of 4 Hz for 5 minutes via pylon viewer (Version 6). Since few larvae were able to dig into the gel through small holes, only larvae that stayed inside the arena for 5 minutes were included into analysis. Tracking data of larval crawling were analyzed via the free software FIMtrack (University of Münster, Germany). Parameters that were read out included (but were not limited to) number of stops, average and maximum speed. The full list of data that were read out is available (doi://10.5281/zenodo.11299005). For explanation of read-out parameters, consult the FIMtrack manual (University of Münster website).

Statistics and figure generation

Statistical analysis was performed with GraphPad Prism 10.2.1 (395). Data were tested for normal distribution using the Shapiro Wilk test. Normally distributed data were compared using either Student's T-test (for two groups) or one-way ANOVA (for more than two groups) with subsequent Sidak's Test post-hoc test for multiple comparisons or Dunnett's test for each test group against control (planned comparisons). For non-normally distributed data either Mann-Whitney U-test (for two groups) or Kruskal Wallis Anova (with more than two groups) with subsequent Dunn's post-hoc test for multiple comparisons or for test groups against control (planned comparisons) were used.

Differences were considered significant if $p \leq 0.05$ *, $p \leq 0.01$ **, $p \leq 0.001$ ***, $P \leq 0.0001$ ****.

Diagrams were generated with GraphPad Prism 10.2.1 (395) or Microsoft Excel 365. Figures with immunohistochemical images were generated with LasX software (Leica Microsystems, Wetzlar, Germany), with Fiji (*www.Fiji.sc*), or with Amira (version 6.5, Thermo Scientific). Images and diagrams were imported into CorelDraw Graphics Suite 2022 (Corel Corporation) either as Tiff images or as enhanced meta files (.emf) for figure production. Final figures were exported as .tif files.

All data and script is available at doi://10.5281/zenodo.11383963. Cacophony exon out flies will be sent to the Drosophila Bloomington Stock Center upon publication.

Acknowledgements

We thank Kerstin Birod for performing Western Blots, Kate O'Connor-Giles for providing cacophony^{mEOS4b} flies, Tayfun Göncü for participating in gathering STED data, Susanne Hornig for confocal recordings of co-expressed cacophony exon out variants and Jan Werner for GluRIIA immunohistochemistry. This work was supported by a DFG research grant to S. Ryglewski (RY117/3-2) and to the Johannes Gutenberg Light Microscopy Core facility (Leica Stellaris STED, DFG INST 247/1004-1 FUGG).

Supplementary Figures

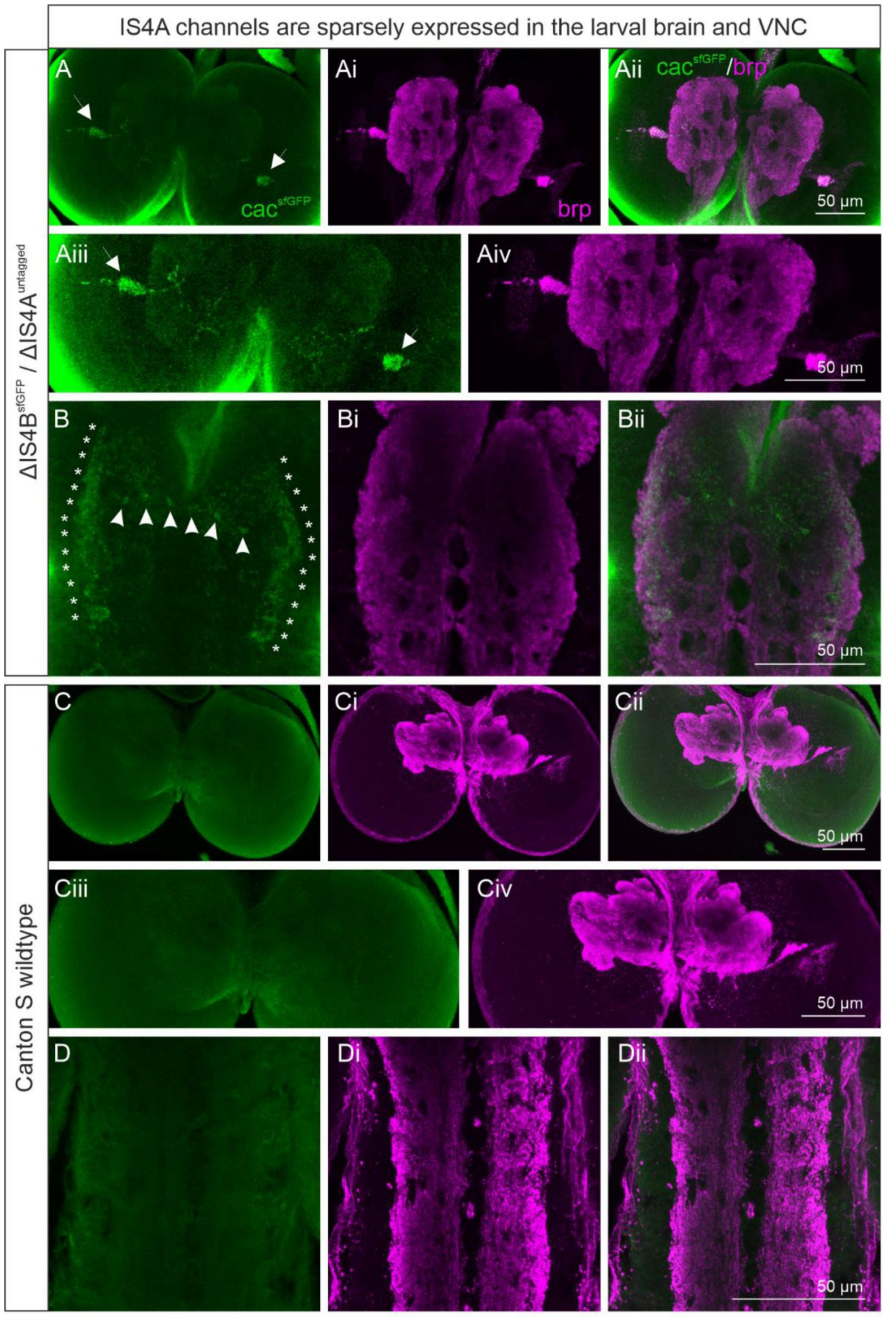

Supplementary Figure 1.

Cacophony^{IS4A} channels are sparsely expressed in the larval brain and ventral nerve cord.

(A, B) Antibody labeling of GFP-tagged cacophony channels lacking exon IS4B (*ΔIS4B^{sfGFP}*) reveals sparse cac label in the larval brain (green, **A-Aiv**, see arrows in **Aiii**) and the larval ventral nerve cord (green, **B-Bii**, see asterisks and arrow heads in B). Label was conducted in transheterozygous animals expressing cac$^{sfGFP\ IS4A}$ over untagged cac^{IS4B} (*ΔIS4B^{sfGFP}/ΔIS4A$^{no\ tag}$*) to avoid expression of untagged IS4A channels. This likely increases labeling intensity. Cac label co-incides with AZ label as indicated by brp label (magenta, **Ai**, **Aiv**; **Bi**, **Bii**). **(C, D)** To exclude the possibility that cac label is misinterpreted due to overlap of with brp channel, antibody label was repeated in untagged Canton S wildtype animals **(C-CiV, D-Dii)**. Even strong brp label does not show in the green channel **(C, Ciii, D)**, thus indicating that cac^{IS4A} channels are indeed made and expressed. Images are maximum projections off F 13 single images, **(B)** 7 single images, **(C)** 10 single images, **(D)** 8 single images, z-size is 1 µm.

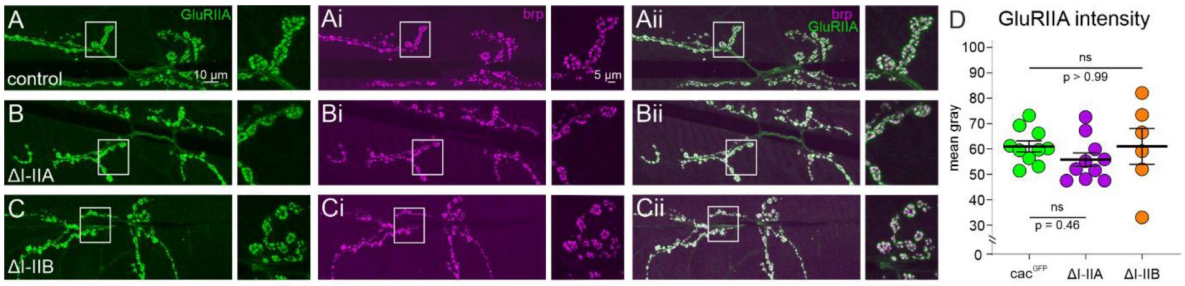

Supplementary Figure 2.

GluRIIA intensity across the NMJ is not altered upon excision of I-IIA or I-IIB.

(**A-C**) GluRIIA is expressed in all NMJs independent of cacophony I-II exon excision (green; **A, Aii**: control, **B, Bii**: *ΔI-IIA*, **C, Cii**: *ΔI-IIB*, see overlap of GluRIIA and brp in **Aii-Cii**). The AZ scaffold protein brp (**Ai-Ci**) was used as mask to assess GluRIIA labeling intensity (**D**). Quantification of GluRIIA labeling intensity is shown as mean gray value and shows no difference between genotypes (**D**, cac^{sfGFP} control green, *ΔI-IIA^{sfGFP}* purple, *ΔI-IIB^{sfGFP}* orange, ANOVA with Dunn's pairwise comparison).

References

1. Atwood HL, Karunanithi S (2002) **Diversification of synaptic strength: Presynaptic elements** *Nat. Rev. Neurosci* **3**:497–516

2. Bezanilla F (2002) **Voltage sensor movements** *J Gen Physiol* **120**:465–73

3. Blanchette M, Green RE, Brenner SE, Rio DC (2005) **Global analysis of positive and negative pre-mRNA splicing regulators in Drosophila** *Genes Dev* **19**:1306–14

4. Bourinet E, Soong TW, Sutton K, Slaymaker S, Mathews E, Monteil A, Zamponi GW, Nargeot J, Snutch TP (1999) **Splicing of alpha 1A subunit gene generates phenotypic variants of P– and Q-type calcium channels** *Nat Neurosci* **2**:407–15

5. Brooks AN, Aspden JL, Podgornaia AI, Rio DC, Brenner SE (2011) **Identification and experimental validation of splicing regulatory elements in Drosophila melanogaster reveals functionally conserved splicing enhancers in metazoans** *RNA* **17**:1884–94

6. Costes S, Daelemans D, Cho EH, Dobbin Z, Pavlakis G, Lockett S (2004) **Automatic and quantitative measurement of protein-protein colocalization in live cells** *Biophysical Journal* **86**:3993–4003

7. Davis GW, Müller M (2012) **Transsynaptic Control of Presynaptic Ca2+ Influx Achieves Homeostatic Potentiation of Neurotransmitter Release** *Curr Biol* **22**:1102–8

8. Davis GW, Müller M (2015) **Homeostatic control of presynaptic neurotransmitter release** *Annu Rev Physiol* **77**:251–70

9. Dietrich D, Kirschstein T, Kukley M, Pereverzev A, von der Brelie C, Schneider T, et al. (2003) **Functional specialization of presynaptic Cav2.3 Ca2+ channels** *Neuron* **39**:483–496

10. Dittman JS, Ryan TA (2019) **The control of release probability at nerve terminals** *Nat Rev Neurosci* **20**:177–186

11. Dolphin AC (2009) **Calcium channel diversity: multiple roles of calcium channel subunits** *Curr Opin Neurobiol* **19**:237–44

12. Dolphin AC, Lee A (2020) **Presynaptic calcium channels: specialized control of synaptic neurotransmitter release** *Nat Rev Neurosci* **21**:213–229

13. Doudna JA, Charpentier E (2014) **Genome editing. The new frontier of genome engineering with CRISPR-Cas9** *Science* **346**

14. Eggermann E, Bucurenciu I, Goswami SP, Jonas P (2011) **Nanodomain coupling between Ca^{2+} channels and sensors of exocytosis at fast mammalian synapses** *Nat Rev Neurosci* **13**:7–21

15. Emperador-MeleroKit Kaeser PS (2020) **Assembly of the presynaptic active zone** *Curr Opin Neurobiol* **63**:95–103

16. Fioravante D, Regehr WG (2011) **Short-term forms of presynaptic plasticity** *Curr Opin Neurobiol* **21**:269–74

17. Frank CA, Kennedy MJ, Goold CP, Marek KW, Davis GW (2006) **Mechanisms underlying the rapid induction and sustained expression of synaptic homeostasis** *Neuron* **52**:663–77

18. Fisher YE, Yang HH, Isaacman-Beck J, Xie M, Gohl DM, Clandinin TR (2017) **FlpStop, a tool for conditional gene control in Drosophila** *eLife* **6**

19. Ghelani T *et al.* (2023) **Interactive nanocluster compaction of the ELKS scaffold and Cacophony Ca2+ channels drives sustained active zone potentiation** *Sci Adv* **9**

20. Gratz SJ, Ukken FP, Rubinstein CD, Thiede G, Donohue LK, Cummings AM, O'Connor-Giles KM (2014) **Highly specific and efficient CRISPR/Cas9-catalyzed homology-directed repair in Drosophila** *Genetics* **196**:961–71

21. Gratz SJ, Goel P, Bruckner JJ, Hernandez RX, Khateeb K, Macleod GT, Dickman D, O'Connor-Giles KM (2019) **Endogenous Tagging Reveals Differential Regulation of Ca2+ Channels at Single Active Zones during Presynaptic Homeostatic Potentiation and Depression** *J Neurosci* **39**:2416–2429

22. Guerrero G, Reiff DF, Agarwal G, Ball RW, Borst A, Goodman CS, Isacoff EY (2005) **Heterogeneity in synaptic transmission along a Drosophila larval motor axon** *Nat Neurosci* **8**:1188–96

23. Guo Y *et al.* (2016) **Transmembrane channel-like (tmc) gene regulates Drosophila larval locomotion** *PNAS* **113**:7243–8

24. Harris KP, Littleton JT (2015) **Transmission, Development, and Plasticity of Synapses** *Genetics* **201**:345–375

25. Heck J, Parutto P, Ciuraszkiewicz A, Bikbaev A, Freund R, Mitlöhner J, Andres-Alonso M, Fejtova A, Holcman D, Heine M (2019) **Transient Confinement of CaV2.1 Ca2+-Channel Splice Variants Shapes Synaptic Short-Term Plasticity** *Neuron* **103**:66–79

26. Herlitze S, Hockerman GH, Scheuer T, Catterall WA (1997) **Molecular determinants of inactivation and G protein modulation in the intracellular loop connecting domains I and II of the calcium channel alpha1A subunit** *PNAS* **94**:1512–6

27. James TD, Zwiefelhofer DJ, Frank CA (2019) **Maintenance of homeostatic plasticity at the Drosophila neuromuscular synapse requires continuous IP3-directed signaling** *Elife* **8**

28. Jia XX, Gorczyca M, Budnik V (1993) **Ultrastructure of neuromuscular junctions in Drosophila: comparison of wild type and mutants with increased excitability** *J Neurobiol* **24**:1025–1044

29. Kadas D, Klein A, Krick N, Worrell JW, Ryglewski S, Duch C (2017) **Dendritic and Axonal L-Type Calcium Channels Cooperate to Enhance Motoneuron Firing Output during Drosophila Larval Locomotion** *J Neurosci* **37**:10971–10982

30. Kawasaki F, Collins SC, Ordway RW (2002) **Synaptic calcium-channel function in Drosophila: analysis and transformation rescue of temperature-sensitive paralytic and lethal mutations of cacophony** *J Neurosci* **22**:5856–64

31. Kawasaki F, Zou B, Xu X, Ordway RW (2004) **Active zone localization of presynaptic calcium channels encoded by the cacophony locus of Drosophila** *J Neurosci* **24**:282–5

32. Kim J, Alger BE (2001) **Random response fluctuations lead to spurious paired-pulse facilitation** *J Neurosci* **21**:9608–18

33. Kittel RJ *et al.* (2006) **Bruchpilot promotes active zone assembly, Ca2+ channel clustering, and vesicle release** *Science* **312**:1051–4

34. Krick N, Ryglewski S, Pichler A, Bikbaev A, Götz T, Kobler O, Heine M, Thomas U, Duch C (2021) **Separation of presynaptic Cav2 and Cav1 channel function in synaptic vesicle exo- and endocytosis by the membrane anchored Ca2+ pump PMCA** *PNAS* **118**

35. Laine RF *et al.* (2019) **NanoJ: a high-performance open-source super-resolution microscopy toolbox** *J Phys D Appl Phys* **52**

36. Li L, Bischofberger J, Berger J (2007) **Differential gating and recruitment of P/Q-, N-, and R-type Ca2+ channels in hippocampal mossy fiber boutons** *J Neurosci* **27**:13420–13429

37. Littleton JT, Ganetzky B (2000) **Ion channels and synaptic organization: analysis of the Drosophila genome** *Neuron* **26**:35–43

38. Liu Y, Hasegawa E, Nose A, Zwart MF, Kohsaja H (2023) **Synchronous multi-segmental activity between metachronal waves controls locomotion speed in Drosophila larvae** *Elife* **12**

39. Manders EMM, Verbeek FJ, Aten JA (1993) **Measurement of co-localization of objects in dual-colour confocal images** *Journal of Microscopy* **169**:375–382

40. Medeiros AT, Gratz SJ, Delgado A, Ritt JT, O'Connor-Giles KM (2024) **Ca2+ channel and active zone protein abundance intersects with input-specific synapse organization to shape functional synaptic diversity** *eLife* **12**

41. Moser T, Karagulyan N, Neef J, Jaime Tobón LM (2023) **Diversity matters – extending sound intensity coding by inner hair cells via heterogeneous synapses** *EMBO* **42**

42. Moser T, Grabner CP, Schmitz F (2020) **Sensory Processing at Ribbon Synapses in the Retina and the Cochlea** *Physiol Rev* **100**:103–144

43. Mukaka MM (2012) **A guide to appropriate use of Correlation coefficient in medical research** *Malawi Med J* **24**:69–71

44. Newman ZL *et al.* (2022) **Determinants of synapse diversity revealed by super-resolution quantal transmission and active zone imaging** *Nat Comm* **13**

45. Nicoll RA, Schmitz D (2005) **Synaptic plasticity at hippocampal mossy fibre synapses** *Nat Rev Neurosci* **6**:863–76

46. Pan P-Y, Tian J-H, Sheng Z-H (2009) **Snapin facilitates the synchronization of synaptic vesicle fusion** *Neuron* **61**:412–24

47. Ralowicz AJ, Hokeness S, Hoppa MB (2024) **Frequency of Spontaneous Neurotransmission at Individual Boutons Corresponds to the Size of the Readily Releasable Pool of Vesicles** *J Neurosci* **44**

48. Rasse TM *et al.* (2005) **Glutamate receptor dynamics organizing synapse formation in vivo** *Nat Neurosci* **8**:898–905

49. Rebola N, Reva M, Kirizs T, Szoboszlay M, Lőrincz A, Moneron G, Nusser Z, DiGregorio DA (2019) **Distinct Nanoscale Calcium Channel and Synaptic Vesicle Topographies Contribute to the Diversity of Synaptic Function** *Neuron* **104**:693–710

50. Ryglewski S, Lance K, Levine RB, Duch C (2012) **Ca(v)2 channels mediate low and high voltage-activated calcium currents in Drosophila motoneurons** *J Physiol* **590**:809–25

51. Ryglewski S, Kilo L, Duch C (2014) **Sequential acquisition of cacophony calcium currents, sodium channels and voltage-dependent potassium currents affects spike shape and dendrite growth during postembryonic maturation of an identified Drosophila motoneuron** *Eur J Neurosci* **39**:1572–85

52. Ryglewski S, Kadas D, Hutchinson K, Schuetzler N, Vonhoff F, Duch C (2014) **Dendrites are dispensable for basic motoneuron function but essential for fine tuning of behavior** *PNAS* **111**:18049–54

53. Sanyal S (2009) **Genomic mapping and expression patterns of C380, OK6 and D42 enhancer trap lines in the larval nervous system of Drosophila** *Gene Expr Patterns* **9**:371–80

54. Sheng J, He L, Zheng H, Xue L, Luo F, Shin W, et al. (2012) **Calcium-channel number critically influences synaptic strength and plasticity at the active zone** *Nat. Neurosci* **15**:998–1006

55. Smith LA, Wang X, Peixoto AA, Neumann EK, Hall LM, Hall JC (1996) **A Drosophila calcium channel alpha1 subunit gene maps to a genetic locus associated with behavioral and visual defects** *J Neurosci* **16**:7868–7879

56. Smith LA, Peixoto AA, Kramer EM, Villella A, Hall JC (1998) **Courtship and visual defects of cacophony mutants reveal functional complexity of a calcium-channel alpha1 subunit in Drosophila** *Genetics* **149**:1407–1426

57. Sternberg SH, Doudna JA (2015) **Expanding the Biologist's Toolkit with CRISPR-Cas9** *Mol Cell* **58**:568–74

58. Südhof TC (2012) **Calcium control of neurotransmitter release** *Cold Spring Harb Perspect Biol* **4**

59. Südhof TC (2013) **Neurotransmitter release: the last millisecond in the life of a synaptic vesicle** *Neuron* **80**:675–90

60. Südhof TC (2014) **The molecular machinery of neurotransmitter release (Nobel lecture)** *Angew Chem Int Ed Engl* **53**:12696–717

61. Takahashi T, Momiyama A (1993) **Different types of calcium channels mediate central synaptic transmission** *Nature* **366**:156–158

62. Turrigiano GG (2008) **The self-tuning neuron: synaptic scaling of excitatory synapses** *Cell* **135**:422–35

63. Van Vactor D, Sigrist SJ (2017) **Presynaptic morphogenesis, active zone organization and structural plasticity in Drosophila** *Curr Opin Neurobiol* **43**:119–129

64. Wheeler DB, Randall A, Tsien RW (1994) **Roles of N-type and Q-type Ca2+ channels in supporting hippocampal synaptic transmission** *Science* **264**:107–111

65. Wang JW, Sylwester AW, Reed D, Wu DA, Soll DR, Wu CF (1997) **Morphometric Description of the Wandering Behavior in Drosophila Larvae: Aberrant Locomotion in Na+ and K+ Channel Mutants Revealed by Computer-Assisted Motion Analysis** *J Neurogenet* **11**:231–54

66. Worrell JW, Levine RB (2008) **Characterization of voltage-dependent Ca2+ currents in identified Drosophila motoneurons in situ** *J Neurophysiol* **100**:868–78

67. Wu LG, Borst JG, Sakmann B (1998) **R-type Ca2+ currents evoke transmitter release at a rat central synapse** *PNAS* **95**:4720–4725

68. Zhang W, Jiang HH, Luo F (2022) **Diverse organization of voltage-gated calcium channels at presynaptic active zones** *Front Synaptic Neurosci* **14**

Author information

Christopher Bell*
Johannes Gutenberg University Mainz, Institute of Developmental Biology and Neurobiology, Biocenter 1, Mainz, Germany

*these authors contributed equally

Lukas Kilo*
RWTH Aachen University, Aachen, Germany

*these authors contributed equally

Daniel Gottschalk
Johannes Gutenberg University Mainz, Institute of Developmental Biology and Neurobiology, Biocenter 1, Mainz, Germany

Jashar Arian
Johannes Gutenberg University Mainz, Institute of Developmental Biology and Neurobiology, Biocenter 1, Mainz, Germany

Lea Deneke
Johannes Gutenberg University Mainz, Institute of Developmental Biology and Neurobiology, Biocenter 1, Mainz, Germany

Hanna Kern
Johannes Gutenberg University Mainz, Institute of Developmental Biology and Neurobiology, Biocenter 1, Mainz, Germany

Christof Rickert
Johannes Gutenberg University Mainz, Institute of Developmental Biology and Neurobiology, Biocenter 1, Mainz, Germany

Oliver Kobler
Leibniz Institute for Neurobiology Magdeburg, Combinatorial NeuroImaging Core Facility, Magdeburg, Germany
ORCID iD: 0000-0001-7173-9919

Julia Strauß
Johannes Gutenberg University Mainz, Institute of Developmental Biology and Neurobiology, Biocenter 1, Mainz, Germany

Martin Heine
Johannes Gutenberg University Mainz, Institute of Developmental Biology and Neurobiology, Biocenter 1, Mainz, Germany

Carsten Duch
Johannes Gutenberg University Mainz, Institute of Developmental Biology and Neurobiology, Biocenter 1, Mainz, Germany
ORCID iD: 0000-0002-6962-6023

Stefanie Ryglewski
Johannes Gutenberg University Mainz, Institute of Developmental Biology and Neurobiology, Biocenter 1, Mainz, Germany
ORCID iD: 0000-0002-3066-6298

For correspondence: ryglewsk@uni-mainz.de

Editors

Reviewing Editor
Dion Dickman
University of Southern California, Los Angeles, United States of America

Senior Editor
Albert Cardona
University of Cambridge, Cambridge, United Kingdom

Reviewer #2 (Public review):

This study by Bell et al. focuses on understanding the roles of two alternatively spliced exons in the single Drosophila Cav2 gene cac. The authors generate a series of cac alleles in which one or the other mutually exclusive exons are deleted to determine the functional consequences at the neuromuscular junction. They find alternative splicing at one exon encoding part of the voltage sensor impacts the activation voltage as well as localization to the active zone. In contrast, splicing at the second exon pair does not impact Cav2 channel localization, but it appears to determine the abundance of the channel at active zones. Together, the authors propose that alternative splicing at the Cac locus enables diversity in Cav2 function generated through isoform diversity generated at the single Cav2 alpha subunit gene encoded in Drosophila.

Overall this is an excellent, rigorously validated study that defines unanticipated functions for alternative splicing in Cav2 channels. The authors have generated an important toolkit of mutually exclusive Cac splice isoforms that will be of broad utility for the field, and show convincing evidence for distinct consequences of alternative splicing of this single Cav2

channel at synapses. Importantly, the authors use electrophysiology and quantitative live sptPALM imaging to determine the impacts of Cac alternative splicing on synaptic function. There remain some questions regarding the mechanisms underlying the changes in Cac localization to somatodendritic compartments. Nonetheless, this is a compelling investigation of alternative splicing in Cav2 channels that should be of interest to many researchers.

https://doi.org/10.7554/eLife.100394.2.sa2

Reviewer #3 (Public review):

Summary:

Bell and colleagues studied how different splice isoforms of voltage-gated CaV2 calcium channels affect channel expression, localization, function, synaptic transmission, and locomotor behavior at the larval Drosophila neuromuscular junction. They reveal that one mutually exclusive exon located in the fourth transmembrane domain encoding the voltage sensor is essential for calcium channel expression, function, active zone localization, and synaptic transmission. Furthermore, a second mutually exclusive exon residing in an intracellular loop containing the binding sites for Caβ and G-protein βγ subunits promotes the expression and synaptic localization of around ~50% of CaV2 channels, thereby contributing to ~50% of synaptic transmission. This isoform enhances release probability, as evident from increased short-term depression, is vital for homeostatic potentiation of neurotransmitter release induced by glutamate receptor impairment, and promotes locomotion. The roles of the two other tested isoforms remain less clear.

Strengths:

The study is based on solid data that was obtained with a diverse set of approaches. Moreover, it generated valuable transgenic flies that will facilitate future research on the role of calcium channel splice isoforms in neural function.

Weaknesses:

Comments on revisions:

The authors addressed most points. However, from my point of view, the new data (somatodendritic cac currents in adult motoneurons of IS4B mutants without the pre-pulse, and localization of IS4A channels in the larval brain) do not strongly support that the IS4B exon is required for cacophony localization. According to their definition of localization, IS4B is required for cacophony channels to enter motoneuron boutons and to localize to active zones. In case of a true localization defect (without degradation, as they claim), IS4A channels should mislocalize to the soma, axon, or dendrite. However, they do not find them in motoneurons of IS4B mutants. Furthermore, I find the interpretation of the voltage clamp data in flight motoneurons rather difficult. On the one hand, sustained HVA cac currents are strongly attenuated/absent in IS4B mutants. On the other hand, total cac currents (without the -50 mV pre-pulse, not shown in the original submission) are less affected in IS4B mutants. Based on these data, they conclude that IS4B is required for sustained HVA cac currents and that IS4A channel isoforms are expressed and functional. How does this relate to a localization defect at the NMJ? Finally, detecting IS4A channels in other cell types and regions is not a strong argument for a localization defect at the NMJ. I, therefore, suggest toning down the conclusions regarding a localization defect in IS4B mutants/a role for the IS4B exon in cac localization. It should be also discussed how a splice isoform in S4 may result in no detectable cac channels at the NMJ or regulate subcellular channel localization.

I have a few additional points, mainly related to the responses to my previous points:

(1) The authors state "active zones at the NMJ contain only cac isoforms with the IS4B exon. Nevertheless, the small representative EPSC remaining in IS4B mutants suggests that there is synchronous release in the absence of IS4B (Fig. 3B). Are the small EPSCs in dIS4B (Fig. 3B) indeed different from noise/indicative of evoked release? If yes, which cac channels may drive these EPSCs? IS4A channels?
(2) (Related to previous point 4) The authors argue that EPSC amplitudes are not statistically different between Canton S and IS4A mutants (Fig. 2F). However, the Canton S group appears undersampled, thus precluding conclusions based on statistics. Moreover, the effect size Canton S vs. dIS4A looks similar to the one of Canton S vs. dIS4A/dIS4B.
(3) (Related to previous point 11): Can they cite a paper relating calcium channel inactivation to EPSC half width/decay kinetics to support their speculation that "decreased EPSC half width could be caused by significantly faster channel inactivation kinetics" (p. 42, l.42). In addition, many papers have demonstrated that mini decay kinetics provide valuable insights into GluR subunit composition at the Drosophila NMJ (e.g., Schmid et al., 2008 https://doi.org/10.1038/nn.2122). Thus, the statement "Mini decay kinetic analysis because this depends strongly on the distance of the recording electrode to the actual site of transmission in these large muscle cells" is not valid and should be revised.

https://doi.org/10.7554/eLife.100394.2.sa1

Author response:

The following is the authors' response to the original reviews.

> ***Public Reviews:***
>
> ***Reviewer #1 (Public Review):***
>
> *Summary:*
>
> *The manuscript by Bell et. al. describes an analysis of the effects of removing one of two mutually exclusive splice exons at two distinct sites in the Drosophila CaV2 calcium channel Cacophony (Cac). The authors perform imaging and electrophysiology, along with some behavioral analysis of larval locomotion, to determine whether these alternatively spliced variants have the potential to diversify Cac function in presynaptic output at larval neuromuscular junctions. The author provided valuable insights into how alternative splicing at two sites in the calcium channel alters its function.*
>
> *Strengths:*
>
> *The authors find that both of the second alternatively spliced exons (I-IIA and I-IIB) that are found in the intracellular loop between the 1st and second set of transmembrane domains can support Cac function. However, loss of the I-IIB isoform (predicted to alter potential beta subunit interactions) results in 50% fewer channels at active zones and a decrease in neurotransmitter release and the ability to support presynaptic homeostatic potentiation. Overall, the study provides new insights into Cac diversity at two alternatively spliced sites within the protein, adding to our understanding of how regulation of presynaptic calcium channel function can be regulated by splicing.*
>
> *Weaknesses:*
>
> *The authors find that one splice isoform (IS4B) in the first S4 voltage sensor is essential for the protein's function in promoting neurotransmitter release, while the other isoform (IS4A) is dispensable. The authors conclude that IS4B is required to localize Cac channels to active zones. However, I find it more likely that IS4B is required for channel stability*

> *and leads to the protein being degraded, rather than any effect on active zone localization. More analysis would be required to establish that as the mechanism for the unique requirement for IS4B.*

(1) We thank the reviewer for this important point. In fact, all three reviewers raised the same question, and the reviewing editor pointed out that caution or additional experiments were required to distinguish between IS4 splicing being important for cac channel localization versus channel stability/degradation. We provide multiple sets of experiments as well as text and figure revisions to strengthen our claim that the IS4B exon is required for cacophony channels to enter motoneuron presynaptic boutons and localize to active zones.

a. If IS4B was indeed required for cac channel stability (and not for localization to active zones) IS4A channels should be instable wherever they are. This is not the case because we have recorded somatodendritic cacophony currents from IS4A expressing adult motoneurons that were devoid of cac channels with the IS4B exon. Therefore, IS4A cac channels are not instable but underlie somatodendritic voltage dependent calcium currents in these motoneurons. These new data are now shown in the revised figure 3C and referred to in the text on page 7, line 42 to page 8 line 9.

b. Similarly, if IS4B was required for channel stability, it should not be present anywhere in the nervous system. We tested this by immunohistochemistry for GFP tagged IS4A channels in the larval CNS. Although IS4A channels are sparsely expressed, which is consistent with low expression levels seen in the Western blots (Fig. 1E), there are always defined and reproducible patterns of IS4A label in the larval brain lobes as well as in the anterior part of the VNC. This again shows that the absence of IS4A from presynaptic active zones is not caused by channel instability, because the channel is expressed in other parts of the nervous system. These data are shown in the new supplementary figure 1 and referred to in the text on page 15, lines 3 to 8.

c. As suggested in a similar context by reviewers 1 and 2, we now show enlargements of the presence of IS4B channels in presynaptic active zones as well as enlargements of the absence of IS4A channels in presynaptic active zones in the revised figures 2A-C and 3A. In these images, no IS4A label is detectable in active zones or anywhere else throughout the axon terminals, thus indicating that IS4B is required for expressing cac channels in the axon terminal boutons and localizing it to active zones. Text and figure legends have been adjusted accordingly.

d. Related to this, reviewer 1 also recommended to quantify the IS4A and ISB4 channel intensity and co-localization with the active zone marker brp (recommendation for authors). After following the reviewers' suggestion to adjust the background values in IS4A and IS4B immunolabels to identical (revised Figs. 2A-C), it becomes obvious that IS4A channel are not detectable above background in presynaptic terminals or active zones, thus intensity is close to zero. We still calculated the Pearsons co-localization coefficient for both IS4 variants with the active zone marker brp. For IS4B channels the Pearson's correlation coefficient is control like, just above 0.6, whereas for IS4A channels we do not find colocalization with brp (Pearson's below 0.25). These new analyses are now shown in the revised figure 2D and referred to on page 6, lines 33 to 38.

e. Consistent with our finding that IS4B is required for cac channel localization to presynaptic active zones, upon removal of IS4B we find no evoked synaptic transmission (Fig. 2 in initial submission, now Fig. 3B).

Together these data are in line with a unique requirement of IS4B at presynaptic active zones (not excluding additional functions of IS4B), whereas IS4A containing cac isoforms are not found in presynaptic active zones and mediate different functions.

Reviewer #2 (Public Review):

This study by Bell et al. focuses on understanding the roles of two alternatively spliced exons in the single Drosophila Cav2 gene cac. The authors generate a series of cac alleles in which one or the other mutually exclusive exons are deleted to determine the functional consequences at the neuromuscular junction. They find alternative splicing at one exon encoding part of the voltage sensor impacts the activation voltage as well as localization to the active zone. In contrast, splicing at the second exon pair does not impact Cav2 channel localization, but it appears to determine the abundance of the channel at active zones.

Together, the authors propose that alternative splicing at the Cac locus enables diversity in Cav2 function generated through isoform diversity generated at the single Cav2 alpha subunit gene encoded in Drosophila.

Overall this is an excellent, rigorously validated study that defines unanticipated functions for alternative splicing in Cav2 channels. The authors have generated an important toolkit of mutually exclusive Cac splice isoforms that will be of broad utility for the field, and show convincing evidence for distinct consequences of alternative splicing of this single Cav2 channel at synapses. Importantly, the authors use electrophysiology and quantitative live sptPALM imaging to determine the impacts of Cac alternative splicing on synaptic function. There are some outstanding questions regarding the mechanisms underlying the changes in Cac localization and function, and some additional suggestions are listed below for the authors to consider in strengthening this study. Nonetheless, this is a compelling investigation of alternative splicing in Cav2 channels that should be of interest to many researchers.

(2) We believe that the additional data on cac IS4A isoform localization and function as detailed above (response to public review 1) has strengthened the manuscript and answered some of the remaining questions the reviewer refers to. We are also grateful for the specific additional reviewer suggestions which we have addressed point-by-point and refer to below (section recommendations for authors).

Reviewer #3 (Public Review):

Summary:

Bell and colleagues studied how different splice isoforms of voltage-gated CaV2 calcium channels affect channel expression, localization, function, synaptic transmission, and locomotor behavior at the larval Drosophila neuromuscular junction. They reveal that one mutually exclusive exon located in the fourth transmembrane domain encoding the voltage sensor is essential for calcium channel expression, function, active zone localization, and synaptic transmission. Furthermore, a second mutually exclusive exon residing in an intracellular loop containing the binding sites for Caβ and G-protein βγ subunits promotes the expression and synaptic localization of around ~50% of CaV2 channels, thereby contributing to ~50% of synaptic transmission. This isoform enhances release probability, as evident from increased short-term depression, is vital for homeostatic potentiation of neurotransmitter release induced by glutamate receptor impairment, and promotes locomotion. The roles of the two other tested isoforms remain less clear.

Strengths:

The study is based on solid data that was obtained with a diverse set of approaches. Moreover, it generated valuable transgenic flies that will facilitate future research on the role of calcium channel splice isoforms in neural function.

> *Weaknesses:*
>
> *(1) Based on the data shown in Figures 2A-C, and 2H, it is difficult to judge the localization of the cac isoforms. Could they analyze cac localization with regard to Brp localization (similar to Figure 3; the term "co-localization" should be avoided for confocal data), as well as cac and Brp fluorescence intensity in the different genotypes for the experiments shown in Figure 2 and 3 (Brp intensity appears lower in the dI-IIA example shown in Figure 3G)? Furthermore, heterozygous dIS4B imaging data (Figure 2C) should be quantified and compared to heterozygous cacsfGFP/+.*

According to the reviewer's suggestion, we have quantified cac localization relative to brp localization by computing the Pearson's correlation coefficient for controls and IS4A as well as IS4B animals. These new data are shown in the revised Fig. 2D and referred to on page 6, lines 33-38. Furthermore, we now confirm control-like Pearson's correlation coefficients for all exon out variants except *ΔIS4B* and show Pearson's correlation coefficients for all genotypes side-by-side in the revised Fig. 4D (legend has been adjusted accordingly). In addition, in response to the recommendations to authors, we now provide selective enlargements for the co-labeling of Brp and each exon out variant in the revised figures 2-4. We have also adjusted the background in Fig. 2C (*ΔIS4B*) to match that in Figs. 2A and B (control and *ΔIS4A*). This allows a fair comparison of cac intensities following excision of *IS4B* versus excision of *IS4A* and control (see also Fig 3). Together, this demonstrates the absence of IS4A label in presynaptic active zones much clearer. As suggested, we have also quantified brp puncta intensity on m6/7 across homozygous exon excision mutants and found no differences (this is now stated for IS4A/IS4B in the results text on page 6, lines 37/38 and for I-IIA/I-IIB on page 8, lines 42-44.). We did not quantify the intensity of cacophony puncta upon excision of *IS4B* because the label revealed no significant difference from background (which can be seen much better in the images now), but the brp intensities remained control-like even upon excision of *IS4B*.

> *(2) They conclude that I-II splicing is not required for cac localization (p. 13). However, cac channel number is reduced in dI-IIB. Could the channels be mis-localized (e.g., in the soma/axon)? What is their definition of localization? Could cac be also mis-localized in dIS4B? Furthermore, the Western Blots indicate a prominent decrease in cac levels in dIS4B/+ and dI-IIB (Figure 1D). How do the decreased protein levels seen in both genotypes fit to a "localization" defect? Could decreased cac expression levels explain the phenotypes alone?*

We have now precisely defined what we mean by cac localization, namely the selective label of cac channels in presynaptic active zones that are defined as brp puncta, but no cac label elsewhere in the presynaptic bouton (page 6, lines 18 to 20). On the level of CLSM microscopy this corresponds to overlapping cac puncta and brp puncta, but no cac label elsewhere in the bouton. Based on the additional analysis and data sets outlined in our response 1 (see above) we conclude that excision of *IS4B* does not cause channel mislocalization because we find reproducible expression patterns elsewhere in the nervous system as well as somatodendritic cac current in *ΔIS4B* (for detail see above). Therefore, the isoforms containing the mutually exclusive *IS4A* exon are expressed and mediate other functions, but cannot substitute *IS4B* containing isoforms at the presynaptic AZ. In fact, our Western blots are in line with reduced cac expression if all isoforms that mediate evoked release are missing, again indicating that the presynapse specific cac isoforms cannot be replaced by other cac isoforms. This is also in line with the sparse expression of IS4A throughout the CNS as seen in the new supplementary figure 1 (for detail see above).

> *(3) Cac-IS4B is required for Cav2 expression, active zone localization, and synaptic transmission. Similarly, loss of cac-I-IIB reduces calcium channel expression and number.*

> *Hence, the major phenotype of the tested splice isoforms is the loss of/a reduction in Cav2 channel number. What is the physiological role of these isoforms? Is the idea that channel numbers can be regulated by splicing? Is there any data from other systems relating channel number regulation to splicing (vs. transcription or post-transcriptional regulation)?*

Our data are not consistent with the idea that splicing regulates channel numbers. Rather, splicing can be used to generate channels with specific properties that match the demand at the site of expression. For the *IS4* exon pair we find differences in activation voltage between IS4A and IS4B channels (revised Fig. 3C), with IS4B being required for sustained HVA current. IS4A does not localize to presynaptic active zones at the NMJ and is only sparsely expressed elsewhere in the NS (new supplementary Fig. 1). By contrast, IS4B is abundantly expressed in many neuropils. Therefore, taking out *IS4B* takes out the more abundant IS4 isoform. This is consistent with different expression levels for IS4 isoforms that have different functions, but we do not find evidence for splicing regulating expression levels *per se*.

Similarly, the *I-II* mutually exclusive exon pair differs markedly in the presence or absence of G-protein βγ binding sites that play a role in acute channel regulation as well the conservation of the sequence for β-subunit binding (see page 5, lines 9-17). Channel number reduction in active zones occurs specifically if expression of the cac channels with the $G_{\beta\gamma}$-binding site as well as the more conserved β-subunit binding is prohibited by excision of the *I-IIB* exon (see Fig. 5F). *Vice versa*, excision of *I-IIA* does not result in reduced channel numbers. This scenario is consistent with the hypothesis that conserved β-subunit binding affects channel number in the active zone (see page 17, lines 3 to 6 and lines 33-36), but we have no evidence that I-II splicing *per se* affects channel number.

> *(4) Although not supported by statistics, and as appreciated by the authors (p. 14), there is a slight increase in PSC amplitude in dIS4A mutants (Figure 2). Similarly, PSC amplitudes appear slightly larger (Figure 3J), and cac fluorescence intensity is slightly higher (Figure 3H) in dI-IIA mutants. Furthermore, cac intensity and PSC amplitude distributions appear larger in dI-IIA mutants (Figures 3H, J), suggesting a correlation between cac levels and release. Can they exclude that IS4A and/or I-IIA negatively regulate release? I suggest increasing the sample size for Canton S to assess whether dIS4A mutant PSCs differ from controls (Figure 2E). Experiments at lower extracellular calcium may help reveal potential increases in PSC amplitude in the two genotypes (but are not required). A potential increase in PSC amplitude in either isoform would be very interesting because it would suggest that cac splicing could negatively regulate release.*

There are several possibilities to explain this, but as none of the effects is statistically significant, we prefer to not investigate this in further depth. However, given that we cannot find IS4A in presynaptic active zones (revised figures 2C and 3A plus the new enlargements 2Ci and 3Ai, revised text page 6, lines 22 to 24 and 29 to 31, and page 7, second paragraph, same as public response 1D) IS4A channels cannot have a direct negative effect on release probability. Nonetheless, given that IS4A containing cac isoforms mediate functions in other neuronal compartments (see revised Fig. 3C) it may regulate release indirectly by affecting e.g. action potential shape. Moreover, in response to the more detailed suggestions to authors we provide new data that give additional insight.

> *(5) They provide compelling evidence that IS4A is required for the amplitude of somatic sustained HVA calcium currents. However, the evidence for effects on biophysical properties and activation voltage (p. 13) is less convincing. Is the phenotype confined to the sustained phase, or are other aspects of the current also affected (Figure 2J)? Could they also show the quantification of further parameters, such as CaV2 peak current density, charge density, as well as inactivation kinetics for the two genotypes? I also*

> *suggest plotting peaknormalized HVA current density and conductance (G/Gmax) as a function of Vm. Could a decrease in current density due to decreased channel expression be the only phenotype? How would changes in the sustained phase translate into altered synaptic transmission in response to AP stimulation?*

Most importantly, sustained HVA current is abolished upon excision of *IS4B* (not *IS4A*, we think the reviewer accidentally mixed up the genotype) and presynaptic active zones at the NMJ contain only cac isoforms with the *IS4B* exon. This indicates that the cac isoforms that mediate evoked release encode HVA channels. The somatodendritic currents shown in the revised figure 3C (previously 2J) that remain upon excision of *IS4B* are mediated by IS4A containing cac isoforms. Please note that these never localize to the presynaptic active zone, and thus do not contribute to evoked release. Therefore, the interpretation is that specifically sustained HVA current encoded by IS4B cac isoforms is required for synaptic transmission. Reduced cac current density due to decreased channel expression is not the cause for impaired evoked release upon IS4B excision, but instead, the cause is the absence of any cac channels in active zones. IS4B-containing cac isoforms encode sustained HVA current, and we speculate that this might be a well suited current to minimize cacophony channel inactivation in the presynaptic active zone. Given that HVA current shows fast voltage dependent activation and fast inactivation upon repolarization, it is useful at large intraburst firing frequencies as observed during crawling (Kadas et al., 2017) without excessive cac inactivation (see page 15, Kadas, lines 16 to 20).

However, we agree with the reviewer that a deeper electrophysiological analysis of splice isoform specific cac currents will be instructive. We have now added traces of control and *ΔIS4B* from a holding potential of -90 mv (revised Fig. 3C, bottom traces and revised text on page 7, line 43 to page 8, lines 1 to 10), and these are also consistent with IS4B mediating sustained HVA cac current. However, further analysis of activation and inactivation voltages and kinetics suffers form space clamp issues in recordings from the somata of such complex neurons (DLM motoneurons of the adult fly contain roughly 6000 µm of dendrites with over 4000 branches, Ryglewski et al., 2017, Neuron 93(3):632-645). Therefore, we will analyze the currents in a heterologous expression system and present these data to the scientific community as a separate study at a later time point.

> *(6) Why was the STED data analysis confined to the same optical section, and not to max. intensity z-projections? How many and which optical sections were considered for each active zone? What were the criteria for choosing the optical sections? Was synapse orientation considered for the nearest neighbor Cac - Brp cluster distance analysis? How do the nearest-neighbor distances compare between "planar" and "side-view" Brp puncta?*

Maximum intensity z-projections would be imprecise because they can artificially suggest close proximity of label that is close by in x and y but far away in z. Therefore, the analysis was executed in xy-direction of various planes of entire 3D image stacks. We considered active zones of different orientations (Figs. 5C, D) to account for all planes. In fact, we searched the entire z-stacks until we found active zones of all orientations within the same boutons, as shown in figures 5C1-C6. The same active zone orientations were analyzed for all exon-out mutants with cac localization in active zones. The distance between cac and brp did not change if viewed from the side or any other orientation. We now explain this in more clarity in the results text on page 9, lines 23/24.

> *(7) Cac clusters localize to the Brp center (e.g., Liu et al., 2011). They conclude that Cav2 localization within Brp is not affected in the cac variants (p. 8). However, their analysis is not informative regarding a potential offset between the central cac cluster and the Brp*

> *"ring". Did they/could they analyze cac localization with regard to Brp ring center localization of planar synapses, as well as Brp-ring dimensions?*

In the top views (planar) we did not find any clear offset in cac orientation to brp between genotypes. In such planar synapses (top views, Fig. 5D, left row) we did not find any difference in Brp ring dimensions. We did not quantify brp ring dimensions rigorously, because this study focusses on cac splice isoform-specific localization and function. Possible effects of different cac isoforms on brp-ring dimensions or other aspects of scaffold structure are not central to our study, in particular given that brp puncta are clearly present even if cac is absent from the synapse (Fig. 3A), indicating that cac is not instructive for the formation of the brp scaffold.

> *(8) Given the accelerated PSC decay/ decreased half width in dI-IIA (Fig. 5Q), I recommend reporting PSC charge in Figure 3, and PPR charge in Figures 5A-D. The charge-based PPRs of dI-IIA mutants likely resemble WT more closely than the amplitude-based PPR. In addition, miniature PSC decay kinetics should be reported, as they may contribute to altered decay kinetics. How could faster cac inactivation kinetics in response to single AP stimulation result in a decreased PSC half-width? Is there any evidence for an effect of calcium current inactivation on PSC kinetics? On a similar note, is there any evidence that AP waveform changes accelerate PSC kinetics? PSC decay kinetics are mainly determined by GluR decay kinetics/desensitization. The arguments supporting the role of cac splice isoforms in PSC kinetics outlined in the discussion section are not convincing and should be revised.*

We agree that reporting charge in figure 3 is informative and do so in the revised text. Since the result (no significant difference in the PSCs between between CS, cac^{GFP}, $^{\Delta I\text{-}IIA}$, and transheterozygous *I-IIA/I-IIB*, but significantly smaller values in *ΔI-IIB*) remained unchanged no matter whether charge or amplitude were analyzed, we decided to leave the figure as is and report the additional analysis in the text (page 8, lines 40 to 42). This way, both types of analysis are reported. Please note that EPSC amplitude is slightly but not significantly increased upon excision of I-IIA (Fig. 4J), whereas EPSC half amplitude width is significantly smaller (Fig. 5Q, now revised Fig 6R). Together, a tendency of increased EPSC amplitudes and smaller half amplitude width result in statistically insignificant changes in EPSC in ΔI-IIA (now discussed on page 15, lines 37 to 40). We also understand the reviewer's concern attributing altered EPSC kinetics to presynaptic cac channel properties. We have toned down our interpretation in the discussion and list possible alterations in presynaptic AP shape or cac channel kinetics as alternative explanations (not conclusions; see revised discussion on page 15, line 40 to page 16, line 2). Moreover, we have quantified postsynaptic GluRIIA abundance to test whether altered PSC kinetics are caused by altered GluRIIA expression. In our opinion, the latter is more instructive than mini decay kinetic analysis because this depends strongly on the distance of the recording electrode to the actual site of transmission in these large muscle cells. Although we find no difference in GluRIIA expression levels we now clearly state that we cannot exclude other changes in GluR receptor fields, which of course, could also explain altered PSC kinetics. We have updated the discussion on page 16, lines 2/3 accordingly.

> *(9) Paired-pulse ratios (PPRs): On how many sweeps are the PPRs based? In which sequence were the intervals applied? Are PPR values based on the average of the second over the first PSC amplitudes of all sweeps, or on the PPRs of each sweep and then averaged? The latter calculation may result in spurious facilitation, and thus to the large PPRs seen in dI-IIB mutants (Kim & Alger, 2001; doi: 10.1523/JNEUROSCI.21-2409608.2001).*

We agree that the PP protocol and analyses had to be described more precisely in the methods and have done so on page 23, lines 31 to 37 in the methods. Mean PPR values are based on the PPRs of each sweep and then averaged. We are aware of the study of Kim and Alger 2001 and have re-analyzed the PP data in both ways outlined by the reviewer. We get identical results with either analyses method. Spurious facilitation is thus not an issue in our data. We now explain this in the methods section along with the PPR protocol. The large spread seen in dI-IIB is indeed caused by reduced calcium influx into active zones with fewer channels, as anticipated by the reviewer (see next point).

> *(10) Could the dI-IIB phenotype be simply explained by a decrease in channel number/ release probability? To test this, I propose investigating PPRs and short-term dynamics during train stimulation at lower extracellular Ca2+ concentration in WT. The Ca2+ concentration could be titrated such that the first PSC amplitude is similar between WT and dI-IIB mutants. This experiment would test if the increased PPR/depression variability is a secondary consequence of a decrease in Ca2+ influx, or specific to the splice isoform.*

In fact, the interpretation that decreased PSC amplitude upon I-IIB excision is caused mainly by reduced channel number is precisely our interpretation (see discussion page 14, last paragraph to page 15, first paragraph in the original submission, now page 16, second paragraph paragraph). In addition, we are grateful for the reviewer's suggestion to triturate the external calcium such that the first PSC amplitude in matches in ΔI-IIB and control. This experiment tests whether altered short term plasticity is solely a function of altered channel number or whether additional causes, such as altered channel properties, also play into this. We triturated the first pulse amplitude in *ΔI-IIB* to match control and find that paired pulse ratio and the variance thereof are not different anymore. Therefore, the differences observed in identical external calcium can be fully explained by altered channel numbers. This additional dataset is shown in the revised figures 6D and E and referred to in the results section on page 10, lines 14 to 25 and the discussion on page16, lines 36 to 38.

> *(11) How were the depression kinetics analyzed? How many trains were used for each cell, and how do the tau values depend on the first PSC amplitude? Time constants in the range of a few (5-10) milliseconds are not informative for train stimulations with a frequency of 1 or 10 Hz (the unit is missing in Figure 5H). Also, the data shown in Figures 5E-K suggest slower time constants than 5-10 ms. Together, are the data indeed consistent with the idea that dIIIB does not only affect cac channel number, but also PPR/depression variability (p. 9)?*

For each animal the amplitudes of all subsequent PSCs in each train were plotted over time and fitted with a single exponential. For depression at 1 and 10 Hz, we used one train per animal, and 5-6 animals per genotype (as reflected in the data points in Figs. 6I, M). This is now explained in more detail in the revised methods section (page 23, lines 39 to 41). The tau values are not affected by the amplitude of the first PSC. First, we carefully re-fitted new and previously presented depression data and find that the taus for depression at low stimulation frequencies (1 and 10Hz) are not affected by exon excisions at the I-II site. We thank the reviewer for detecting our error in units and tau values in the previous figure panels 5H and L (this has now been corrected in the revised figure panels 6I and M). Given that PSC amplitude upon I-IIB excision is significantly smaller than in controls and following I-IIA excision, we suspected that the time course of depression at low stimulation frequency is not significantly affected by the amount of calcium influx during the first PSC. To further test this, we followed the reviewer 's suggestion and re-measured depression at 1 and 10 Hz for cac-GFP controls and for delta I-IIB in a higher external calcium concentration (1.8 mM), so that the first PSC was increased in amplitude in both genotypes (1.8 mM external calcium

triturates the PSC amplitude in delta I-IIB to match that of controls measured in 0.5 mM external calcium, see revised Figs. 6H, L). Neither in control, nor in delta I-IIB did this affect the time course of synaptic depression (see revised Figs. 6I, M). This indicates that at low stimulation frequencies (1 and 10Hz) the time course of depression is not affected by mean quantal content. This is consistent with the paired pulse ratio at 100 ms interpulse interval shown in figures 6A-D. However, for synaptic depression at 1 Hz stimulation the variability of the data is higher for delta I-IIB (independent of external calcium concentration, see rev. Fig. 6I), which might also be due to reduced channel number in this genotype. Taken together, the data are in line with the idea that altered cac channel numbers in active zones are sufficient to explain all effects that we observe upon I-IIB excision on PPRs and synaptic depression at low stimulation frequencies. This is now clarified in the revised text on page 12, lines 3 to 7.

> *(12) The GFP-tagged I-IIA and mEOS4b-tagged I-IIB cac puncta shown in Figure 6N appear larger than the Brp puncta. Endogenously tagged cac puncta are typically smaller than Brp puncta (Gratz et al., 2019). Also, the I-IIA and I-IIB fluorescence sometimes appear to be partially non-overlapping. First, I suggest adding panels that show all three channels merged. Second, could they analyze the area and area overlap of I-IIA and I-IIB with regard to each other and to Brp, and compare it to cac-GFP? Any speculation as to how the different tags could affect localization? Finally, I recommend moving the dI-IIA and dI-IIB localization data shown in Figure 6N to an earlier figure (Figure 1 or Figure 3).*

We now show panels with the two I-II cac isoforms merged in the revised figure 7H (previously 6N). We also tested merging all three labels as suggested, but found this not instructive for the reader. We thank the reviewer for pointing out that the Brp puncta appeared smaller than the cac puncta in some panels. We carefully went through the data and found that the Brp puncta are not systematically smaller than the cac puncta. Please note that punctum size can appear quite differently, depending on different staining qualities as well as different laser intensities and different point spread in different imaging channels. The purpose of this figure was not to analyze punctum size and labeling intensity, but instead, to demonstrate that I-IIA and I-IIB are both present in most active zones, but some active zones show only I-IIB labeling, as quantified in figure 7I. We did not follow the suggestion to conduct additional co-localization analyses and compare it with cac-GFP controls, because Pearson co-localization coefficients for cac-GFP and all exon-out variants analyzed, including delta I-IIA and delta I-IIB are presented in the revised figure 4D. Moreover, delta I-IIA and delta I-IIB show similar Manders 1 and 2 co-localization coefficients with Brp (see Figs. 4E, F). We do not want to speculate whether the different tags have any effect on localization precision. Artificial differences in localization precision can also be suggested by different antibodies, but we know from our STED analyses with identical tags and antibodies for all isoforms that I-IIA and I-IIB co-localize identically with Brp (see Figs. 5A-E). Finally, we prefer to not move the figure because we believe it is informative to show our finding that active zones usually contain both splice I-II variants together with the finding that only I-IIB is required for PHP.

> ***Recommendations for the authors:***
>
> ***Reviewing Editor Comments:***
>
> *We thank you for your submission. All three reviewers urge caution in interpreting the S4 splice variant playing a role specifically in Cac localization, as opposed to just leading to instability and degradation. There are other issues with the electrophysiological experiments, a need for improved imaging and analyses, and some areas of interpretation detailed in the reviews.*

We agree that additional data was required to conclude that IS4 splicing plays a specific role in cac channel localization and is not just leading to channel instability and degradation. As outlined in detail in our response to reviewer 1, comment 1, we conducted several sets of experiments to support our interpretation. First, electrophysiological experiments show that upon removal of IS4B, which eliminates synaptic transmission at the larval NMJ and cac positive label in presynaptic active zones, somatodendritic cac current is reliably recorded (new data in revised figure 3C). This is not in line with a channel instability or degradation effect, but instead with IS4B containing isoforms being required and sufficient for evoked release from NMJ motor terminals, whereas IS4A isoforms are not sufficient for evoked release from axon terminals, but IS4A isoforms alone can mediate a distinct component of somatodendritic calcium current. Second, immunohostochemical analyses reveal that IS4A, which is not present in NMJ presynaptic active zones, is expressed sparsely, but in reproducible patterns in the larval brain lobes and in specific regions of the anterior VNC parts (new supplementary figure 1). Again, the absence of a IS4A-containing cac isoform from presynaptic active zones but their simultaneous presence in other parts of the nervous system is in accord with isoform specific localization, but not with general channel isoform instability. Third, enlargements of NMJ boutons with brp positive presynaptic active zones confirm the absence of IS4A and the presence of IS4B in active zones (these enlargements are now shown in the revised figures 2A-C, 3A, and 4A-C). Fourth, as suggested we have quantified the Pearson co-localization of IS4 isoforms with Brp in presynaptic active zones (revised Fig. 2D). This confirms quantitatively similar co-localization of IS4B and control with Brp, but no co-localization of IS4A with Brp. In fact, the labeling intensity of IS4A in presynaptic active zones is quantitatively not significantly different from background, no IS4A label is detected anywhere in the axon terminals at the NMJ, but we find IS4 label in the CNS. Together, these data strongly support our interpretation that the IS4 splice site plays a distinct role in cac channel localization. Figure legends as well as results and discussion section have been modified accordingly (the respective page and line numbers are listed in our-point-by-point responses).

In addition, we have carefully addressed all other public comments as well as all other recommendations for authors by providing multiple new data sets, new image analyses, and revising text. Addressing the insightful comments of all three reviewers and the reviewing editor has greatly helped to make the manuscript better.

> ***Reviewer #1 (Recommendations For The Authors):***
>
> *The conclusion that the IS4B exon controls Cac localization to active zones versus simply being required for channel abundance is not well supported. The authors need to either mention both possibilities or provide stronger support for the active zone localization model if they want to emphasize this point.*

We agree and have included several additional data sets as outlined in our response to point 1 of reviewer 1 and to the reviewing editor (see above). These new data strongly support our interpretation that the IS4B exon controls Cac localization to active zones and is not simply required for channel abundance. The additions to the figures and accompanying text (including the respective figure panel, page, and line numbers) are listed in the point-bypoint responses to the reviewers' public suggestions.

> *Figure 2C staining for Cac localization in the delta 4B line is difficult to compare to the others, as the background staining is so high (muscles are green for example). As such, it is hard to determine whether the arrows in C are just background.*

We had over-emphasized the green label to show that there really is no cacophony label in active zones. However, we agree that this hampered image interpretation. Thus, we have

adjusted brightness such that it matches the other genotypes (see new figure panel 2C, and figure 3A, bottom). Revising the figure as suggested by the reviewer shows much more clearly that IS4B puncta are detected exclusively in presynaptic active zones, whereas IS4A channels are not detectable in active zones or anywhere else in the axon terminal boutons. Quantification of IS4A label in brp positive active zones confirms that labeling intensity is not significantly above background (page 6, lines 29 to 31 and page 7, lines 19 to 21). Therefore, IS4A is not detectable in active zones at the NMJ.

> *It seems more likely that the removal of the 4B exon simply destabilizes the protein and causes it to be degraded (as suggested by the Western), rather than mislocalizing it away from active zones. It's hard to imagine how some residue changes in the S4 voltage sensor would control active zone localization to begin with. The authors should note that the alternative explanation is that the protein is just degraded when the 4B exon is removed.*

Based on additional data and analyses, we disagree with the interpretation that removal of IS4B disrupts protein integrity and present multiple lines of evidence that support sparse expression of IS4A channels (ΔIS4B). As outlined in our response to reviewer 1 and to the reviewing editor, we show (1) in new immunohistochemical stainings (new supplementary figure 1) that upon removal of IS4B, sparse label is detectable in the VNC and the brain lobes (for detail see above). (2) In our new figure 3C, we show cacophony-mediated somatodendritic calcium currents recorded from adult flight motoneurons in a control situation and upon removal of IS4B that leaves only IS4A channels. This clearly demonstrates that IS4A underlies a substantial component of the HVA somatodendritic calcium current, although it is absence from axon terminals. This is in line with isoform specific functions at different locations, but not with IS4A instability/degradation. (3) We do not agree with the reviewer's interpretation of the Western Blot data in figure 1E (formerly figure 1D). Together with our immunohistochemical data that show sparse cacophony IS4A expression, we think that the faint band upon removal of IS4B in a heterozygous background (that reduces labeled channels even further) reflects the sparseness of IS4A expression. This sparseness is not due to channel instability, but to IS4A functions that are less abundant than the ubiquitously expressed cac^{IS4B} channels at presynaptic active zones of fast chemical synapses (see page 15, lines 24 to 29).

> *If they really want to claim the 4B exon governs active zone localization, much higher quality imaging is required (with enlarged views of individual boutons and their AZs, rather than the low-quality full NMJ imaging provided). Similarly, higher resolution imaging of Cac localization at Muscle 12 (Figure 2H) boutons would be very useful, as the current images are blurry and hard to interpret. Figure 6N shows beautiful high-resolution Cac and Brp imaging in single boutons for the I-II exon manipulations - the authors should do the same for the 4B line. For all immuno in Figure 2, it is important to quantify Cac intensity as well. There is no quantification provided, just a sample image. The authors should provide quantification as they do for the delta I-II exons in Figure 3.*

We did as suggested and added figure panels to figure 2A-C and to new figures 3A (formerly part of figure 2 and 4A-C (formerly figure 3) showing magnified label at the NMJ AZs to better judge on cacophony expression after exon excision. These data are now referred to in the results section on page 6, lines 22 to 24, page 7, lines 18 to 21 and page 8, lines 17/18.

As suggested, we now also provide quantification of co-localization with brp puncta as Pearson's correlation coefficient for control, IS4B, and IS4A in the new figure panel 2D (text on page 6, lines 34 to 38). This further underscores control-like active zone localization of IS4B but no significant active zone localization of IS4A. As suggested, we quantified now also the intensity of IS4B label in active zones, and it was not different from control (see revised

figure 4H and text on page 8, lines 38/39). We did not quantify the intensity of IS4A label, because it was not over background (text, page 6, lines 30/31).

> ***Reviewer #2 (Recommendations For The Authors):***
>
> *(1a) Questions about the engineered Cac splice isoform alleles:*
>
> *The authors using CRISPR gene editing to selectively remove the entire alternatively spliced exons of interest. Do the authors know what happens to the cac transcript with the deleted exon? Is the deleted exon just skipped and spliced to the next exon? Or does the transcript instead undergo nonsense-mediated decay?*

We do not believe that there is nonsense mediated mRNA decay, because for all exon excisions the respective mRNA and protein are made. Protein has been detected on the level of Western blotting and immunocytochemistry. Therefore, we are certain that the mRNA is viable for each exon excision (and we have confirmed this for low abundance cac protein isoforms by rt-PCR), but only subsets of cac isoforms can be made from mRNAs that are lacking specific exons. However, we can not make any statements as to whether the lack of specific protein isoforms exerts feedback on mRNA stability, the rate of transcription and translation, or other unknown effects.

> *(1b) While it is clear that the IS4 exons encode part of the voltage sensor in the first repeat, are there studies in Drosophila to support the putative Ca-beta and G-protein beta-gamma binding sites in the I-II loop? Or are these inferred from Mammalian studies?*

To the best of our knowledge, there are no studies in Drosophila that unambiguously show Caβ and Gβγ binding sites in the I-II loop of cacophony. However, sequence analysis strongly suggests that I-IIB contains both, a Caβ as well as a Gβγ binding site (AID: α-interacting domain) because the binding motif QXXER is present. In mouse Cav2.1 and $Ca_v2.2$ channels the sequence is QQIER, while in Drosophila cacophony I-IIB it is QQLER. In the alternative IIIA, this motif is not present, strongly suggesting that $G_{\beta\gamma}$ subunits cannot interact at the AID. However, as already suggested by Smith et al. (1998), based on sequence analysis, Ca_β should still be able to bind, although possibly with a lower affinity. We agree that this information should be given to the reader and have revised the text accordingly on page 5, lines 9 to 17.

> *(1c) The authors assert that splicing of Cav2/cac in flies is a means to encode diversity, as mammals obviously have 4 Cav2 genes vs 1 in flies. However, as the authors likely know, mammalian Cav2 channels also have various splice isoforms encoded in each of the 4 Cav2 genes. The authors should discuss in more detail what is known about the splicing of individual mammalian Cav2 channels and whether there are any homologous properties in mammalian channels controlled by alternative splicing.*

We agree and now provide a more comprehensive discussion of vertebrate Ca_v2 splicing and its impact on channel function. In line to what we report in Drosophila, properties like $G_{\beta\gamma}$ binding and activation voltage can also be affected by alternative splicing in vertebrate Ca_v2 channel, through the exon patterns are quite different from Drosophila. We integrated this part on page 14, first paragraph) in the revised discussion. The respective text is below for the reviewer's convenience:

"However, alternative splicing increases functional diversity also in mammalian Ca_v2 channels. Although the mutually exclusive splice site in the S4 segment of the first homologous repeat (IS4) is not present in vertebrate Cav channels, alternative splicing in the extracellular linker region between S3 and S4 is at a position to potentially change voltage sensor properties (Bezanilla 2002). Alternative splice sites in rat $Ca_v2.1$ exon 24 (homologous

repeat III) and in exon 31 (homologous repeat IV) within the S3-S4 loop modulate channel pharmacology, such as differences in the sensitivity of $Ca_v2.1$ to Agatoxin. Alternative splicing is thus a potential cause for the different pharmacological profiles of P- and Q-channels (both $Ca_v2.1$; Bourinet et al. 1999). Moreover, the intracellular loop connecting homologous repeats I and II is encoded by 3-5 exons and provides strong interaction with $G_{\beta\gamma}$-subunits (Herlitze et al. 1996). In $Ca_v2.1$ channels, binding to $G_{\beta\gamma}$ subunits is potentially modulated by alternative splicing of exon 10 (Bourinet et al. 1999). Moreover, whole cell currents of splice forms α1A-a (no Valine at position 421) and α1A-b (with Valine) represent alternative variants for the I-II intracellular loop in rat $Ca_v2.1$ and $Ca_v2.2$ channels. While α1A-a exhibits fast inactivation and more negative activation, α1A-b has delayed inactivation and a positive shift in the IV-curve (Bourinet et al. 1999). This is phenotypically similar to what we find for the mutually exclusive exons at the IS4 site, in which IS4B mediates high voltage activated cacophony currents while IS4A channels activate at more negative potentials and show transient current (Fig. 3; see also Ryglewski et al. 2012). Furthermore, altered Ca_β interaction have been shown for splice isoforms in loop III (Bourinet et al. 1999), similar to what we suspect for the I-II site in cacophony. Finally, in mammalian VGCCs, the C-terminus presents a large splicing hub affecting channel function as well as coupling distance to other proteins. Taken together, Ca_v2 channel diversity is greatly enhanced by alternative splicing also in vertebrates, but the specific two mutually exclusive exon pairs investigated here are not present in vertebrate *Ca_v2* genes."

> *(1d) In Figure 1, it would be helpful to see the entire cac genomic locus with all introns/exons and the 4 specific exons targeted for deletion.*

We agree and have changed figure 1 accordingly.

> *(2a) Cav2.IS4B deletion alleles:*
>
> *More work is necessary to explain the localization of Cac controlled by the IS4B exon. First, can the authors determine whether actual Cac channels are present at NMJ boutons? The authors seem to indicate that in the IS4B deletion mutants, some Cac (GFP) signal remains in a diffuse pattern across NMJ boutons. However, from the imaging of wild-type Cac-GFP (and previous studies), there is no Cac signal outside of active zones defined by the BRP signal. It would benefit the study to a) take additional, higher resolution images of the remaining Cac signal at NMJs in IS4B deletion mutants, and b) comment on whether the apparent remaining signal in these mutants is only observed in the absence of IS4Bcontaining Cac channels, or if the IS4A-positive channels are normally observed (but perhaps mis-localized?).*

We have conducted additional analyses to show convincingly that IS4A channels (that remain upon IS4B deletion) are absent from presynaptic active zone. Please see also responses to reviewers 1 and 3. By adjusting the background values in of CLSM images to identical values in control, delta IS4A, and delta IS4B, as well as by providing selective enlargements as suggested, the figure panels 2C, Ci and 3A now show much clearer, that upon deletion of IS4B no cac label remains in active zones or anywhere else in the axon terminal boutons (see text on page 6, lines 22 to 24). This is further confirmed by quantification showing the in IS4B mutants cac labeling intensity in active zones is not above background (see text on page 6, lines 27 to 31). We never intended to indicate that there was cac signal outside of active zones defined by the brp signal, and we now carefully went through the text to not indicate this possibility unintentionally anywhere in the manuscript.

> *(2b) Do the authors know whether any presynaptic Ca2+ influx is contributed by IS4Apositive Cac channels at boutons, given the potential diffuse localization? There are*

> *various approaches for doing presynaptic Ca2+ imaging that could provide insight into this question.*

We agree that this is an interesting question. However, based on the revisions made, we now show with more clarity that IS4A channels are absent from the presynaptic terminal at the NMJ. IS4A labeling intensities within active zones and anywhere else in the axon terminals are not different from background (see text on page 6, lines 27 to 31 and revised Figs. 2C, Ci, and 3A with new selective enlargements in response to comments of both other reviewers). This is in line with our finding that evoked synaptic transmission from NMJ axon terminals to muscle cells is mostly absent upon excision of IS4B (see Fig. 3B). The very small amplitude EPSC (below 5 % of the normal amplitude of evoked EPSCs) that can still be recorded in the absence of *IS4B* is similar to what is observed in *cac null* mutant junctions and is mediated by calcium influx through another voltage gated calcium channels, a Ca_V1 homolog named Dmca1D, as we have previously published (Krick et al., 2021, PNAS 118(28):e2106621118. Gathering additional support for the absence of IS4A from presynaptic terminals by calcium imaging experiments would suffer significantly from the presence of additional types of VGCCs in presynaptic terminals (for sure Dmca1D (Krick et al., 2021) and potentially also the Ca_V3 homolog DmαG or Dm-α1T). Such experiments would require mosaic null mutants for *cac* and *DmαG* channels in a mosaic *IS4B* excision mutant, which, if feasible at all, would be very hard and time consuming to generate. In the light of the additional clarification that IS4A is not located in NMJ axon terminal boutons, as shown by additional labeling intensity analysis, revised figures with selective enlargement, and revised text, we feel confident to state that IS4A is not sufficient for evoked SV release.

> *(2c) Mechanistically, how are amino acid changes in one of the voltage sensing domains in Cac related to trafficking/stabilization/localization of Cac to AZs?*

This is an exciting question that has occupied our discussions a lot. Some sorting mechanism must exist that recognizes the correct protein isoforms, just as sorting and transport mechanisms exist that transport other synaptic proteins to the synapse. We do not think that the few amino acid changes in the voltage sensor are directly involved in protein targeting. We rather believe that the cacophony variants that happen to contain this specific voltage sensor are selected for transport out to the synapse. There are possibilities to achieve this cell biological, but we have not further addressed potential mechanisms because we do not want enter the realms of speculation.

> *(3) How are auxiliary subunits impacted in the Cac isoform mutants?*
>
> *Recent work by Kate O'Connor-Giles has shown that both Stj and Ca-Beta subunits localize to active zones along with Cac at the Drosophila NMJ. Endogenously tagged Stj and CaBeta alleles are now available, so it would be of interest to determine if Stj and particular Cabeta levels or localization change in the various Cac isoform alleles. This would be particularly interesting given the putative binding site for Ca-beta encoded in the I-II linker.*

We agree that the synthesis of the work of Kate O'Connor-Giles group and our study open up new avenues to explore exciting hypotheses about differential coupling of specific cacophony splice isoforms with distinct accessory proteins such as Caβ and $\alpha_2\delta$ subunits. However, this requires numerous full sets of additional experiments and is beyond the scope of this study.

> *(4a) Interpretation of short-term plasticity in the I-IIB exon deletion:*
>
> *The changes in short-term plasticity presented in Figure 5 are interpreted as an additional phenotype due to the loss of the I-IIB exon, but it seems this might be entirely explained simply due to the reduced Cac levels. Reduced Cac levels at active zones will*

> *obviously reduce Ca2+ influx and neurotransmitter release. This may be really the only phenotype/function of the I-IIB exon. Hence, to determine whether loss of the I-IIB exon encodes any functions in short-term plasticity, separate from reduced Cac levels, the authors should compare short-term plasticity in I-IIB loss alleles compared to wild type with starting EPSC amplitudes are equal (for example by reducing extracellular Ca2+ levels in wild type to achieve the same levels at in Cac I-IIB exon deleted alleles). Reduced release probability, simply by reduced Ca2+ influx (either by reduced Cac abundance or extracellular Ca2+) should result in more variability in transmission, so I am not sure there is any particular function of the I-IIB exon in maintaining transmission variability beyond controlling Cac abundance at active zones.*

For two reasons we are particularly grateful for this comment. First, it shows us that we needed to explain much clearer that our interpretation is that changes in paired pulse ratios (PPRs) and in depression at low stimulation frequencies are a causal consequence of lower channel numbers upon I-IIB exon deletion, precisely as pointed out by the reviewer. We have carefully revised the text accordingly on page 10, lines 14-25, page 11, lines 3-7 and 22-28; page 16, lines 36-38. Second, the experiment suggested by the reviewer is superb to provide additional evidence that the cause of altered PPRs is in fact reduced channel number, but not altered channel properties. Accordingly, we have conducted additional TEVC recordings in elevated external calcium (1.8 mM) so that the single PSC amplitudes in *I-IIB* excision animals match those of controls in 0.5 mM extracellular calcium. This makes the amplitudes and the variance of PPR for all interpulse intervals tested control-like (see revised Figs. 6D, E). This strongly indicates that differences observed in PPRs as well as the variance thereof were caused by the amount of calcium influx during the first EPSC, and thus by different channel numbers in active zones.

> *(4b) Another point about the data in Figure 5: If "behaviorally relevant" motor neuron stimulation and recordings are the goal, the authors should also record under physiological Ca2+ conditions (1.8 mM), rather than the highly reduced Ca2+ levels (0.5 mM) they are using in their protocols.*

Although we doubt that the effective extracellular calcium concentration that determines the electromotoric force for calcium to enter the ensheathed motoneuron terminals *in vivo* during crawling is known, we followed the reviewer's suggestion partly and have repeated the high frequency stimulation trains for *ΔI-IIB* in 1.8 mM calcium. As for short-term plasticity this brings the charge conducted to values as observed in control and in *ΔI-IIA* in 0.5 mM calcium. Therefore, all difference observed in previous figure 5 (now revised figure 6) can be accounted to different channel numbers in presynaptic active zones. This is now explained on page 11, lines 19-28. For controls recordings at high frequency stimulation in higher external calcium (e.g. 2 mM) have previously been published and show significant synaptic depression (e.g. Krick et al., 2021, PNAS). Given that in the exon out variants we do not expect any differences except from those caused by different channel numbers, we did not repeat these experiments for control and *ΔI-IIA*.

> *(5a) Mechanism of Cac's role in PHP :*
>
> *As the authors likely know, mutations in Cac were previously reported to disrupt PHP expression (see Frank et al., 2006 Neuron). Inexplicably, this finding and publication were not cited anywhere in this manuscript (this paper should also be cited when introducing PhTx, as it was the first to characterize PhTx as a means of acutely inducing PHP). In the Frank et al. paper (and in several subsequent studies), PHP was shown to be blocked in mutations in Cac, namely the CacS allele. This allele, like the I-IIB excision allele, reduces baseline transmission presumably due to reduced Ca2+ influx through Cac. The authors*

> *should at a minimum discuss these previous findings and how they relate to what they find in Figure 6 regarding the block in PHP in the Cac I-IIB excision allele.*

We thank the reviewer for pointing this out and apologize for this oversight. We agree that it is imperative to cite the 2006 paper by Frank et al. when introducing PhTx mediated PHP as well as when discussing cac the effects of cac mutants on PHP together with other published work. We have revised the text accordingly on page 12, lines 9-11 and 21-23 and on page 17, lines 29-33.

> *In terms of data presentation in Fig. 6, as is typical in the field, the authors should normalize their mEPSC/QC data as a percentage of baseline (+PhTx/-PhTx). This makes it easier to see the reduction in mEPSC values (the "homeostatic pressure" on the system) and then the homeostatic enhancement in QC. Similarly, in Fig. 6M, the authors should show both mEPSC and QC as a percentage of baseline (wild type or non-GluRIIA mutant background).*

We agree and have changed figure presentation accordingly. Figure 7 (formerly figure 6) was updated as was the accompanying results text on page 12, lines 23-40.

> *(6) Cac I-IIA and I-IIB excision allele colocalization at AZs:*
>
> *These are very nice and important experiments shown in Figures 6N and O, which I suggest the authors consider analyzing in further detail. Most significantly:*
>
> *(6i) The authors nicely show that most AZs have a mix of both Cac IIA and IIB isoforms. Using simple intensity analysis, can the authors say anything about whether there is a consistent stoichiometric ratio of IIA vs IIB at single AZs? It is difficult to extract actual numbers of IIA vs IIB at individual AZs without having both isoforms labeled mEOS4b, but as a rough estimate can the authors say whether the immunofluorescence intensity of IIA:IIB is similar across each AZ? Or is there broad heterogeneity, with some AZs having low vs high ratios of each isoform (as the authors suggest across proximal to distal NMJ AZs)?*

We agree and have conducted experiments and analyses to provide these data. We measured the cac puncta fluorescence intensities for heterozygous cac^{sfGFP}/cac, cacIIIA^{sfGFP}/cacI-IIB, and cacI-IIB^{sfGFP}/cacI-IIA animals. We preferred this strategy, because intensity was always measured from cac puncta with the same GFP tag. Next, we normalized all values to the intensities obtained in active zones from heterozygous cac^{sfGFP}/cac controls and then plotted the intensities of I-IIA versus I-IIB containing active zones side by side. Across junctions and animals, we find a consistent ratio 2:1 in the relative intensities of I-IIB and I-IIA, thus indicating on average roughly twice as many I-IIB as compared to I-IIA channels across active zones. This is consistent with the counts in our STED analysis (see Fig. 5F). These new data are shown in the new figure panel 7J and referred to on page 13, lines 10-16 in the revised text.

> *(6ii) Intensity analysis of Cac IIA vs IIB after PHP: Previous studies have shown Cac abundance increases at NMJ AZs after PHP. Can the authors determine whether both Cac IIA vs IIB isoforms increase after PHP or whether just one isoform is targeted for this enhancement?*

We already show that PHP is not possible in the absence of I-IIB channels (see figure 7). However, we agree that it is an interesting question to test whether I-IIA channel are added in the presence of I-IIB channels during PHP, but we consider this a detail beyond the scope of this study.

> *Minor points:*

> *(1) Including line numbers in the manuscript would help to make reviewing easier.*

We agree and now provide line numbers.

> *(2) Several typos (abstract "The By contrast", etc).*

We carefully double checked for typos.

> *(3) Throughout the manuscript, the authors refer to Cac alleles and channels as "Cav2", which is unconventional in the field. Unless there is a compelling reason to deviate, I suggest the authors stick to referring to "Cac" (i.e. cacdIS4B, etc) rather than Cav2. The authors make clear in the introduction that Cac is the sole fly Cav2 channel, so there shouldn't be a need to constantly reinforce that cac=Cav2.*

We agree and have changed all fly Ca_V2 reference to cac.

> *(4) In some figures/text the authors use "PSC" to refer to "postsynaptic current", while in others (i.e. Figure 6) they switch to the more conventional terms of mEPSC or EPSC. I suggest the authors stick to a common convention (mEPSC and EPSC).*

We have changed PSC to EPSC throughout.

> ***Reviewer #3 (Recommendations For The Authors):***
>
> *(1) The abstract could focus more on the results at the expense of the background.*

We agree and have deleted the second introductory background sentence and added information on PPRs and depression during low frequency stimulation.

> *(2) What does "strict" active zone localization refer to? Could they please define the term strict?*

Strict active zone localization means that cac puncta are detected in active zones but no cac label above background is found anywhere else throughout the presynaptic terminal, now defined on page 6, lines 27-29.

> *(3) Single boutons/zoomed versions of the confocal images shown in Figures 2A-C, 2H, and 3A-C would be very helpful.*

We have provided these panels as suggested (see above and revised figures 2-4). Figure 3 is now figure 4.

> *(4) The authors cite Ghelani et al. (2023) for increased cac levels during homeostatic plasticity. I recommend citing earlier work making similar observations (Gratz et al., 2019; DOI: 10.1523/JNEUROSCI.3068-18.2019), and linking them to increased presynaptic calcium influx (Müller & Davis, 2012; DOI: 10.1016/j.cub.2012.04.018).*

We agree and have added Gratz et al. 2019 and Davis and Müller 2012 to the results section on page 12, lines 17/18 and lines 21-23, in the discussion on page 17, lines 29-33.

> *(5) The data shown in Figure 3 does not directly support the conclusion of altered release probability in dI-IIB. I therefore suggest changing the legend's title.*

We have reworded to “Excisions at the I-II exon do not affect active zone cacophony localization but can alter cacsfGFP label intensity in active zones and PSC amplitude” as this is reflecting the data shown in the figure panels more directly.

> *(6) It would be helpful to specify "adult flight muscle" in Figure 2J.*

We agree that it is helpful to specify in the figure (now revised figure 3C) that the voltage clamp recordings of somatodendritic calcium current were conducted in adult flight motoneurons and have revised the headline of figure panel 3C and the legend accordingly. Please note, these are not muscle cells but central neurons.

> *(7) Do dIS4B/Cav2null MNs indeed show an inward or outward current at -90 to -70 mV/-40 and -50 mV, or is this an analysis artifact?*

No, this is due to baseline fluctuations as typical for voltage clamp in central neurons with more than 6000 µm dendritic length and more than 4000 dendritic branches.

> *(8) Loss of several presynaptic proteins, including Brp (Kittel et al., 2006), and RBP (Liu et al., 2011), induce changes in GluR field size (without apparent changes in miniature amplitude). The statement regarding the Cav2 isoform and possible effects on GluR number (p. 8) should be revised accordingly.*

We understand and have done two things. First, we measured the intensity of GluRIIA immunolabel in *ΔI-IIA*, *ΔI-IIB*, and controls and found no differences. Second, we reworded the statement. It now reads on page 9, lines 1-6: “It seems unlikely that presynaptic cac channel isoform type affects glutamate receptor types or numbers, because the amplitude of spontaneous miniature postsynaptic currents (mEPSCs, Fig. 4K) and the labeling intensity of postsynaptic GluRIIA receptors are not significantly different between controls, I-IIA, and I-IIB junctions (see suppl. Fig. 2, p = 0.48, ordinary one-way ANOVA, mean and SD intensity values are 61.0 ± 6.9 (control), 55.8 ± 8.5 (*ΔI-IIA*), 61.1 ± 17.3 (*ΔI-IIB*)). However, we cannot exclude altered GluRIIB numbers and have not quantified GluR receptor field sizes.”

> *(9) The statement relating miniature frequency to RRP size is unclear (p. 8). Is there any evidence for a correlation between miniature frequency to RRP size? Could the authors please clarify?*

We agree that this statement requires caution. Although there is some published evidence for a correlation of RRP size and mini frequency (Neuron, 2009 61(3):412-24. doi: 10.1016/j.neuron.2008.12.029 and Journal of Neuroscience 44 (18) e1253232024; doi: 10.1523/JNEUROSCI.1253-23.2024), which we now refer to on page 9, it is not clear whether this is true for all synapses and how linear such a relationship may be. Therefore, we have revised the text on page 9, lines 6-9. It now reads: “Similarly, the frequency of miniature postsynaptic currents (mEPSCs) remains unaltered. Since mEPSCs frequency has been related to RRP size at some synapses (Pan et al., 2009; Ralowicz et al., 2024) this indicates unaltered RRP size upon I-IIB excision, but we have not directly measured RRP size.”

> *(10) Please define the "strict top view" of synapses (p. 8).*

Top view is what this reviewer referred to as “planar view” in the public review points 6 and 7. In our responses to these public review points we now also define “strict top view”, see page 9, lines 17-19.

> *(11) Two papers are cited regarding a linear relationship between calcium channel number and release probability (p. 15). Many more papers could be cited to demonstrate a supralinear relationship (e.g., Dodge & Rahaminoff, 1967; Weyhersmüller et al., 2011 doi: 10.1523/JNEUROSCI.6698-10.2011). The data of the present study were collected at an extracellular calcium concentration of 0.5 mM, whereas Meideiros et al. (2023) used 1.5 mM. The relationship between calcium and release is supra-linear around 0.5 mM extracellular calcium (Weyhersmüller et al. 2011). This should be discussed/the statements be revised. Also, the reference to Meideiros et al. (2023) should be included in the reference list.*

We have now updated the Medeiros reference (updated version of that paper appeared in eLife in 2024) in the text and reference list. We agree that the relationship of the calcium concentration and P_r can also be non-linear and refer to this on page 16, lines 26-32, but the point we want to make is to relate defined changes in calcium channel number (not calcium influx) as assessed by multiple methods (CLSM intensity measures and sptPALM channel counting) to release probability. We now also clearly state that we measured at 0.5 mM external calcium (page 16, lines 27/28) whereas Medeiros et al. 2024 measured at 1.5 mM calcium (page 16, lines 31/32).

> *(12) Figure 6: Quantal content does not have any units - please remove "n vesicles".*

We have revised this figure in response to reviewer 2 (comment 5) and quantal content is now expressed as percent baseline, thus without units (see revised figure 7).

> *(13) Figure 6C should be auto-scaled from zero.*

This has been fixed by revising that figure in response to reviewer 2 (comment 5)

> *(14) The data supporting the statement on impaired motor behavior and reduced vitality of adult IS4A should be either shown, or the statement should be removed (p. 13). Any hypotheses as to why IS4A is important for behavior and or viability?*

As suggested, we have removed that statement.

> *(15) They do not provide any data supporting the statement that changes in PSC decay kinetics "counteract" the increase in PSC amplitude (p. 14). The sentence should be changed accordingly.*

We agree and have down toned. It now reads on page 16, lines 7-9: “During repetitive firing, the median increase of PSC amplitude by ~10 % is potentially counteracted by the significant decrease in PSC half amplitude width by ~25 %...”.

> *(16) How do they explain the net locomotion speed increase in dI -IIA larvae? Although the overall charge transfer is not affected during the stimulus protocols used, could the accelerated PSC decay affect PSP summation (I would actually expect a decrease in summation/slower speed)? Independent of the voltage-clamp data, is muscle input resistance changed in dI-IIA mutants?*

Muscle input resistance is not altered in I-II mutants. We refer to potential causes of the locomotion effects of I-IIA excision in the discussion. On page 16, lines 12 to 21 it reads: “there is no difference in charge transfer from the motoneuron axon terminal to the postsynaptic muscle cell between *ΔI-IIA* and control. Surprisingly, crawling is significantly affected by the removal of *I-IIA*, in that the animals show a significantly increased mean crawling speed but

no significant change in the number of stops. Given that the presynaptic function at the NMJ is not strongly altered upon *I-IIA* excision, and that *I-IIA* likely mediates also Ca_V2 functions outside presynaptic AZs (see above) and in other neuron types than motoneurons, and that the muscle calcium current is mediated by *Ca_V1>/i> and Ca_V3, the effects of I-IIA excision of increasing crawling speed is unlikely caused by altered pre- or postsynaptic function at the NMJ. We judge it more likely that excision of I-IIA has multiple effects on sensory and pre-motor processing, but identification of these functions is beyond the scope of this study."*

https://doi.org/10.7554/eLife.100394.2.sa0